T.C.
ISTANBUL OKAN UNIVERSITY
GRADUATE SCHOOL

PhD THESIS
FOR THE DEGREE OF
BUSINESS ADMINISTRATION

Muhammad Ali FAISAL

THREE ESSAYS ON FOREIGN EXCHANGE'S FUTURES, VOLATILITY, AND INTERACTION WITH STOCK MARKET

THESIS ADVISOR
Prof. Dr. Murat DONDURAN

ISTANBUL, May 2023

T.C.
ISTANBUL OKAN UNIVERSITY
GRADUATE SCHOOL

PhD THESIS
FOR THE DEGREE OF
BUSINESS ADMINISTRATION

Muhammad Ali FAISAL
(172501030)

THREE ESSAYS ON FOREIGN EXCHANGE'S FUTURES, VOLATILITY, AND INTERACTION WITH STOCK MARKET

THESIS ADVISOR
Prof. Dr. Murat DONDURAN

ISTANBUL, May 2023

T.C.
ISTANBUL OKAN UNIVERSITY
GRADUATE SCHOOL

PhD THESIS
FOR THE DEGREE OF
BUSINESS ADMINISTRATION

Muhammad Ali FAISAL
(172501030)

THREE ESSAYS ON FOREIGN EXCHANGE'S FUTURES, VOLATILITY, AND INTERACTION WITH STOCK MARKET

Presentation Date of Thesis: 31/05/2023
Submission Date of Thesis:
Advisor: **Prof. Dr. Murat Donduran** . . . . . .
(Yildiz Technical University)
Jury Members: **Prof. Dr. Mustafa E. Telatar** . . . . . .
(Istanbul Okan University)
Asst. Prof. Bülent Günceler . . . . . .
(Istanbul Okan University)
Prof. Dr. Gökçe Tunç . . . . . .
(Istanbul Okan University)
Asst. Prof. Hasan Karaduman . . . . . .
(Yildiz Technical University)

ISTANBUL, May 2023

PREFACE

The motivation for this dissertation is to contribute to the current literature vis-á-vis financial assets. Studying financial markets is imperative in a highly complex; yet interconnected global system. Any insights from such an endeavor would be of utmost importance to policymakers, investors, and academics.

Our study comprises three separate essays, allowing for different perspectives. In the first chapter, we underline the existing connection among higher moments of currency futures. We identified a gap in the current literature and tried to fulfill it using recently developed statistical approaches within time and frequency domains. Another critical issue related to the Turkish lira gets highlighted in the second chapter. We studied the volatility structure of the lira to understand the inherent variance that encompassed it during the last decade. The third essay takes up the connection between the lira and the Turkish stock market. Our contribution lies in our approach to studying the tail risk dependence between the two assets using a two-step method. Findings derived from this thesis have implications, not only from risk and portfolio management perspectives but also from policy-making standpoints.

All analyses and estimations carried out in this thesis are done using *MATLAB version 9.6.0.1150989 (R2019a) Update 4* (2019), R Core Team's (2021) R Statistical Software (v4.1.2), and Van Rossum and Drake Jr's (1995) Python programming language.

Muhammad Ali FAISAL

May 2023

ACKNOWLEDGEMENTS

I like to extend my sincere gratitude to my advisor Prof. Dr. Murat Donduran for his invaluable insights at every stage of my research. It was a privilege and an honor to work under his supervision. I cannot thank him enough for his feedback, support, and encouragement.

I am indebted to my committee members, Prof. Dr. Mustafa E. Telatar and Asst. Prof. Bülent Günceler, for their extreme cooperation. Their assistance during my study, which also involved a global pandemic, is highly appreciated.

Finally, my admiration goes to my Mum and Dad. Without their unwavering support, I would not have been able to move forward in my journey.

TABLE OF CONTENTS

ÖZET

Döviz piyasalarının farklı yönlerini incelemek için ampirik yöntemler uyguluyoruz.

İlk bölüm, başlıca para birimlerinin vadeli işlemleri arasındaki yayılmaların ayrıntılı bir şekilde araştırılmasını gerektirir. Analizimizi Diebold-Yilmaz (DY) ve Baruník-Krehlík (BK) metodolojileri ile genişleterek, zaman ve frekans alanındaki fiyatların daha yüksek anlarında yayılma etkiler kontrol edilmiştir. Ampirik sonuçlar, zaman alanı içinde oynaklık yayılmalarının çarpıklık ve basıklık yayılmalarından daha yüksek olduğunu göstermektedir. Ancak, kısa vadeli zaman ufuklarında (frekans ayrışımıyla ölçülen), çarpıklık yayılımı daha yüksektir. Genel olarak, euro (EUR) vadeli işlemleri, yüksek anlı yayılmalara göre daha fazla etkiye sahiptir. Bu sonuç her iki dönem için, yani mali kriz öncesi ve sonrası için geçerlidir. Bulgularımız, oynaklığın ani sıçramalar konusunda çarpıklık ve basıklığa göre daha hassas olduğunu göstermektedir.

İkinci bölümde Türk Lirası'nın (TL) volatilite davranışı. TL'nin varyansını modellemek için çok çeşitli istatistiksel yaklaşımlar uygulanmıştır. Bu amaçla lira kurunun günlük log getirilerini, gün içi ve range bazında getirileri incelenmiştir. Ayrıca, daha fazla içgörü için oynaklı ayrıştırılmıştır. Tahminler daha sonra farklı spesifikasyonlar altında destek vektör regresyon (SVR) algoritması kullanılarak analiz edilmiştir. Bulgularımıza göre, şişman kuyruk dağılımları TL'nin oynaklığını daha iyi modellemektedir. Varyans ayrıştırmasından sonra, kısa vadeli oynaklık, ekonomik belirsizliğin neden olduğu uzun vadeli oynaklığa göre daha az kalıcılık göstermiştir. SVR analizimiz, lineer dışındaki çekirdeklerin daha iyi R-kare (R^2) tahminleri ürettiğini ortaya çıkarmıştır. Ayrıca, tahmin sırasında belirli bir özelliğin ağırlığı büyük ölçüde bağımlı değişken olarak kullanılan vekil değişkene bağlıdır.

Son bölüm, 2005'ten 2022'ye Türkiye verilerini kullanarak döviz ve hisse senedi getirileri arasındaki olası bağlantıları analiz etmek için yeni bir yaklaşım kullanmaktadır. Bu amaçla iki aşamalı bir teknik kullanmaktadır. İlk aşama, uyarlanabilir gürültü (CEEMDAN) algoritması ve eksiksiz bir topluluk ampirik mod ayrışımı ile bireysel zaman serisi sinyallerinin ayrı

içsel mod fonksiyonlarına (IMF'ler) ayrıştırılmasıyla başlamaktadır. Ardından, inceden kabaya bir algoritma aracılığıyla yüksek ve düşük frekanslı bileşenler oluşturmak için çıkarılan IMF'leri kullanırız. İkinci aşamada, çapraz-kuantilogram (CQ) yönteminin yardımıyla, orijinal getiri serisinin kuantillerindeki bağımlılığı frekans bileşenleriyle birlikte analiz etmektedir. Sonuçlar, aşağıdaki gibidir: (1) ilgili dönem için hisse senedi getirilerinden döviz kuru getirilerine nispeten daha yüksek bir etki uzanır, (2) getiriler kesin olarak bağlantılı olduğundan kuyruk bağımlılığı açıktır, (3) yüksek frekanslı kompozisyon düşük frekanslı bileşenden daha fazlasını verir (1) ve (2) gibi benzer sonuçlar ve (4) bağımlılık yapısı, analiz edilen örneklem boyunca çoğunlukla sabit kalmıştır.

ABSTRACT

This dissertation consists of three chapters on foreign exchange (FX) rates. We apply empirical methods to study different aspects of currency markets.

The first essay entails a detailed exploration of spillovers among futures of major currencies. We checked for spillover effects in higher moments of prices within the time and frequency domain by extending our analysis through Diebold-Yilmaz (DY) and Baruník-Krehlík (BK) methodologies. Empirical results suggest that within the time domain, volatility spillovers are higher than skewness and kurtosis spillovers. However, in short-term time horizons (measured through frequency decomposition), skewness spillover is higher. Overall, the euro (EUR) futures have more effect in relation to high-moment spillovers. This result applies to both periods, i.e., before and after the financial crisis. Our findings indicate that volatility is more sensitive than skewness and kurtosis concerning sudden jumps.

In the second essay, we studied the volatility behavior of the Turkish Lira (TRY). We applied a wide range of statistical approaches to model the variance of TRY. For this purpose, we considered daily log returns, intraday, and range-based returns of the lira's exchange rate. Moreover, we decomposed volatility for further insights. Estimates were then analyzed using the support vector regression (SVR) algorithm under different specifications. As per our findings, fat tail distributions were better able to model TRY's volatility. After variance decomposition, short-run volatility showed less persistence than long-run volatility driven by economic uncertainty. Our SVR analysis revealed that kernels other than linear produced better R-square (R^2) estimates. Furthermore, weightage for a given feature during estimation depends highly on the proxy used as a dependent variable.

The last essay uses a novel approach to analyze possible connections between FX and stock returns using Turkish financial data from 2005 to 2022. We employ a two-stage technique for this purpose. The first stage begins by decomposing individual time series signals into separate intrinsic mode functions (IMFs) with a complete ensemble empirical mode decomposition with adaptive noise (CEEMDAN) algorithm. Then, we use

extracted IMFs to construct high and low-frequency components through a fine-to-coarse algorithm. In the second phase, with the help of the cross-quantilogram (CQ) method, we analyze dependence in quantiles of the original return series along with frequency components obtained in the previous stage. Results provide the following key insights: (1) a relatively higher effect ran from stock returns to exchange rate returns for the pertinent period, (2) tail dependence is apparent, as returns are unequivocally linked, (3) high-frequency composition gives more analogous results as (1) and (2) than the low-frequency component, and (4) the structure of dependence has stayed mostly constant throughout the sample analyzed.

LIST OF SELECTED SYMBOLS AND NOTATIONS

$(\theta_d)_{j,k}$	generalized variance decomposition on frequency band d
$(\tilde{\theta}_d)_{j,k}$	scaled generalized variance decomposition on frequency band d
$(f(w))_{j,k}$	portion of the spectrum of the j^{th} variable at frequency w due to shocks in the k^{th} variable
$C_d^{\mathscr{F}}$	frequency connectedness
$C^{\mathscr{F}}_{\hat{A}.\leftarrow k}(d)$	spillovers received by market j from markets k
$C^{\mathscr{F}}_{k\leftarrow\hat{A}.}(d)$	spillovers received by market k from markets j
RV	realized volatility
RS	realized skewness
RK	realized kurtosis
$F_i(\cdot)$	distribution function
$K_{i,j}(t)$	IMF's j^{th} component at the i^{th} time
RV^M_{t-1}	monthly realized volatility at time $t-1$
RV^W_{t-1}	weekly realized volatility at time $t-1$
$S^g(H)$	total spillovers
$S^g_i(H)$	net spillovers
$S^g_{.i}(H)$	directional spillovers transmitted by market i to all other markets j
$S^g_{i,j}(H)$	net pairwise spillovers
$S^g_{i.}(H)$	directional spillovers received by market i from all markets j
S_t	positive definite scaling matrix at time t
$S_x(w)$	spectral density of x_t at frequency w
$Tr(.)$	trace operator

$\Gamma_j(w)$	frequency share of the variance of the j^{th} variable at frequency w
RQ	realized quarticity
TPQ	tripower quarticity
BPV	bipower variation
$MASR$	moving average of lagged squared returns
$\Psi(e^{-iw})$	Fourier transform of the coefficients
ε_t	error at time t
$\hat{Q}_\beta^p$	Box-Ljung portmanteau test
$\hat{\rho}_\beta(k)$	sample cross quantilogram
$\hat{q}_1(\beta_1)$	unconditional quantile function
$\hat{q}_2(\beta_2)$	unconditional quantile function
$\mathbb{R}$	real numbers
$\mathbb{R}^+$	positive real numbers
$\mathscr{B}(x,y)$	beta function
∇_t	score of density function
$\rho_\beta(k)$	cross correlation of quantile exceedance process
$\theta(\cdot)$	nonlinear transformation
$\theta_{i,j}^g(H)$	H-step ahead forecast error variance decompositions
θ_t	vector containing time varying parameters
$\tilde{\beta}$	range of quantiles which is Cartesian product
$\varphi_k(w1,w2)$	weighting scheme with weights $w1$ and $w2$
RR	range return
ξ_i^*	prediction error parameter
$f_i(\cdot)$	density function
$fm(t)$	local mean
$ln(p_t)$	natural log of price at time t
$n_j(t)$	noise component
$p(\cdot)$	density function
$q_i(B_i)$	quantile function
$y_t\|\mathscr{Q}_{t-1}$	vector containing y_t upto $t-1$

LIST OF ABBREVIATIONS AND ACRONYMS

ACD	Autoregressive Conditional Duration
ADF	Augmented Dickey-Fuller
AIC	Akaike information criterion
ald	the asymmetric laplace distribution
ALLGARCH	all nested GARCH
ANN	artificial neural network
APARCH	asymmetric power ARCH
ARCH	AutoRegressive Conditional Heteroskedastic
ARDL	autoregressive distributive lag
ast	the asymmetric student-t with two tail decay parameters
ast1	the asymmetric student-t with one tail decay parameter
AUD	the Australian dollar
AVGARCH	absolute value GARCH
BEKK	Baba, Engle, Kraft, and Kroner
BIC	Bayesian information criterion
BIST	Borsa Istanbul
BK	Baruník-Krehlík
CAD	the Canadian dollar
CARR	Conditional AutoRegressive Range
CCARR	Component CARR
CEEMDAN	complete ensemble empirical mode decomposition with adaptive noise
CGARCH	component GARCH
CHAR	continuous HAR
CHARQ	CHAR quarticity
CHF	the Swiss franc

CQ	cross-quantilogram
DCS	dynamic conditional score
DY	Diebold-Yilmaz
EEMD	ensemble empirical mode decomposition
EGARCH	exponential GARCH
EMD	empirical mode decomposition
EUR	the euro
FX	foreign exchange
GARCH	Generalized ARCH
MIDAS	mixed data sampling
GAS	generalized autoregressive score
GBP	the British pound
GFC	global financial crisis
GFEVD	generalized forecast error variance decomposition
GJRGARCH	Glosten, Jagannathan, and Runkle's (1993) GARCH
HAR	heterogeneous autoregressive
HARJ	HAR with jump
HARQ	HAR quarticity
HARQJ	HAR quarticity with jump
HHT	Hilbert-Huang transform
HQIC	Hannan–Quinn information criterion
IMFs	intrinsic mode functions
IRFs	impulse response functions
JB	Jarque-Bera
JPY	the Japanese yen
jsu	Johnson's SU distribution
KPPS	Koop, Pesaran, and Potter (1996) and Pesaran and Shin (1998)
LHAR	log HAR
LLH	log-likelihood
KKT	Karush-Kunh-Tucker
MA	moving average
MCMC	Markov chain Monte Carlo

ML	machine learning
NAGARCH	nonlinear asymmetric GARCH
NARDL	nonlinear ARDL
NGARCH	nonlinear GARCH
norm	the normal distribution
NPWS	net pairwise spillovers
PP	Phillips–Perron
RBF	radial basis function
snorm	the skewed normal distribution
sstd	the skewed student-t distribution
std	the student-t distribution
SV	stochastic volatility
SVL	SV with leverage
SVM	support vector machine
SVR	support vector regression
SVT	SV with student-t errors
SVTL	SV with student-t errors and leverage
TEFUI	the Turkish Economic and Financial Uncertainty Index
TGARCH	threshold GARCH
TL	the Turkish lira
TRY	the Turkish lira
USD	the United States dollar
VAR	vector autoregression
WRS	Wilcoxon rank sum

List of Figures

List of Tables

CHAPTER 1

HOW MUCH CONNECTION EXISTS IN CURRENCY FUTURES? AN EMPIRICAL DIVE INTO HIGHER MOMENTS

1.1 INTRODUCTION

Currency markets do possess a linkage among each other; however, the nature and dynamics of this linkage are opaque. Understanding this connection is vital for researchers, traders, portfolio managers, multinational corporations, and policymakers. Two main reasons for this significance are to improve forecasting abilities and generate better policy coordination (Ciner, 2011). In addition, this linkage can facilitate managers to create better strategies regarding risk mitigation (S. Kumar, 2016). Based on these premises, we attempt to uncover the dynamics underlying associations among currency futures. Our analysis starts by checking for spillovers in realized volatility (RV), realized skewness (RS), and realized kurtosis (RK) within time and frequency domains. We use Diebold-Yilmaz (DY) and Baruník-Krehlík (BK) methods to construct the overall spillover index and frequency bands. We then conduct a rolling window analysis to check for dynamics over the total period. Our sample spans over 20 years, within which world markets witnessed a global financial crisis (GFC). We incorporate this factor to check the effect of a stressful event on foreign exchange (FX) futures.

Engle III, Ito, and Lin (1988) tested meteor shower (volatility spillovers) and heat wave (country-specific autocorrelation) hypotheses for the Yen/Dollar exchange rate to find evidence in favor of meteor showers, thereby rejecting the market dexterity hypothesis (a form of market efficiency). Another study concerning information transmission among currency futures by Fung and Patterson (1999) argues that with linkages at different levels,

information-flow effects are similar regardless of trading hours. Ciner (2011) investigated return and volatility spillovers in major European currency futures and found informational dependencies among the tested sample. S. Kumar (2016) made a similar empirical attempt to check spillovers within the first two moments of Indian currency futures prices and found significant spillovers in both returns and volatility. Asimakopoulos, Ayling, and Mahmood (2000) studied the nonlinear causality among currency futures. They found that a unidirectional relationship exists among returns of major currencies. However, after volatility filtering, connections became weaker. It is also important to note that the nature of spillovers varies in stressful periods. Greenwood-Nimmo, Nguyen, and Rafferty (2016) analyzed G10 currencies and concluded that intensity increases among higher moment linkages of currencies. To capture asymmetries encircling volatility linkages, Barunik, Kocenda, and Vacha (2017) used a vector autoregression (VAR) based approach to conclude that distinctive nonuniformity exists among all major quotes. In addition to overall irregularities in the connectedness, the spillovers among currencies could vary in magnitude depending on their source. For instance, McMillan and Speight (2010) checked for return and volatility spillovers in three exchange rates. Their results showed that the US dollar dominated flows asymmetrically.

Practitioners have used various methods to examine potential connections among financial assets. These include; copula-based models (Mensi, Hammoudeh, Shahzad, Al-Yahyaee, & Shahbaz, 2017; Ji, Liu, & Fan, 2019; Hoesli & Reka, 2013), Generalized ARCH (GARCH) (Fedorova & Saleem, 2009; A. S. Kumar & Anandarao, 2019; Dedi & Yavas, 2016; Sehgal, Ahmad, & Deisting, 2015), VAR-BEKK-GARCH (Vardar & Aydogan, 2019; Lin, Chang, & Hsiao, 2019; L. Yu, Zha, Stafylas, He, & Liu, 2020; Wen, Wang, Ma, & Zhang, 2020), and cointegration (MacDonald & Marsh, 2004; AuYong, Gan, & Treepongkaruna, 2004), among other techniques. Even though studies of currency futures have taken different perspectives, most papers have checked for links within the first two moments. The contribution of this essay is multifold in that sense. Firstly, our analysis dives into exploring currency futures which hasn't been addressed much, especially in the recent literature. Secondly, we extend understanding by studying spillover effects in higher moments. Generally, spillover tests among financial assets exist within the mean and variance perspective. We also expand our analysis into different period frequencies in addition to testing for overall time dependence

through two relatively novel statistical approaches. This approach helps in differentiating between the short and long-term linkages. We also present our findings concerning the nature of spillovers before and after the GFC. Considering all these factors, such analysis could be of great importance to investors, portfolio managers, hedgers, and policymakers alike.

The arrangement of this essay is as follows: In subsection 1.2, we put forward the models used for empirical testing. Subsection 1.3 describes data and its descriptive statistics, along with our base models' results and their extensions. Subsection 1.4 concludes the chapter by suggesting the policy implications and discussing our analysis.

1.2 METHODOLOGY

1.2.1 DY Model

Diebold and Yilmaz (2009) relied on n-variable VAR variance decomposition. One drawback of this technique is that results are order-dependent and driven by Cholesky factor orthogonalization. To eliminate this issue, Diebold and Yilmaz (2012) removed dependency on order by measuring directional spillovers:

$$x_t = \sum_{i=1}^{P} \phi_i x_{t-i} + \varepsilon_t \tag{1.1}$$

where $\varepsilon \backsim (0, \Sigma)$ i.i.d. disturbances vector. Moving average (MA) representation is:

$$x_t = \sum_{i=0}^{\infty} A_i \varepsilon_{t-i} \tag{1.2}$$

where $A_i = N \times N$ coefficient matrix. $A_i = \phi_1 A_{i-1} + \phi_2 A_{i-2} + \ldots + \phi_p A_{i-p}$ with A_0 being an $N \times N$ identity matrix with $A_i = 0$ for $i < 0$. MA coefficients, impulse response functions (IRFs), or variance decompositions are key to this system. Koop et al.'s (1996) & Pesaran and Shin's (1998) (KPPS) method is used to navigate the order-dependent result problem. For own variance shares, fractions of H-step ahead error variances in forecasting x_i are due to shocks to x_i for i = 1,2,...,N, whereas for cross variance shares (spillovers) fractions of H-step ahead error variances in forecasting x_i are due to shocks to x_j for i = 1,2,...,N such that $i \neq j$. KPPS H-step ahead

forecast error variance decompositions denoted by $\theta^g_{i,j}(H)$ for H = 1,2,...,N:

$$\theta^g_{i,j}(H) = \frac{\sigma^{-1}_{j,j} \sum_{h=0}^{H-1} (e^{'} A_h \Sigma e_j)^2}{\sum_{h=0}^{H-1} (e^{'}_i A_h \Sigma A^{'}_h e_i)} \tag{1.3}$$

where Σ = variance matrix for the error vector ε, $\sigma_{j,j}$ = standard deviation of the error term for the j^{th} equation, e_i = selection vector with 1 as i^{th} element and 0 otherwise.[1] Normalization of each entry of the variance decomposition matrix by the row sum is done as:

$$\tilde{\theta}^g_{i,j}(H) = \frac{\theta^g_{i,j}(H)}{\sum_{j=1}^{N} \theta^g_{i,j}(H)} \tag{1.4}$$

Note that by construction, $\sum_{j=1}^{N} \tilde{\theta}^g_{i,j}(H) = 1$ and $\sum_{i,j=1}^{N} \tilde{\theta}^g_{i,j}(H) = N$. Moving on to total spillovers:

$$S^g(H) = \frac{\sum_{\substack{i,j=1 \\ i \neq j}}^{N} \tilde{\theta}^g_{ij}(H)}{N} * 100 \tag{1.5}$$

This is the analog KPPS of the Cholesky factor-based measure used by Diebold and Yilmaz (2009). The total spillover index measures the contribution of spillovers of volatility shocks across four asset classes to the total forecast error variance. Directional spillovers received by market i from all markets j are given by:

$$S^g_{i.}(H) = \frac{\sum_{\substack{j=1 \\ j \neq i}}^{N} \tilde{\theta}^g_{i,j}(H)}{N} * 100 \tag{1.6}$$

Directional spillovers transmitted by market i to all other markets j are obtained as:

$$S^g_{.i}(H) = \frac{\sum_{\substack{j=1 \\ j \neq i}}^{N} \tilde{\theta}^g_{j,i}(H)}{N} * 100 \tag{1.7}$$

Net spillovers are computed simply by taking the difference:

$$S^g_i(H) = S^g_{.i}(H) - S^g_{i.}(H) \tag{1.8}$$

[1] It should be noted that sum of the row elements in variance decomposition table is not equal to 1 ($\sum_{j=1}^{N} \theta^g_{j,j}(H) \neq 1$).

Net pairwise spillovers (NPWS) can be taken as:

$$\begin{aligned} S^{g}_{i,j}(H) &= \left(\frac{\tilde{\theta}^{g}_{j,i}(H)}{\sum_{i,k=1}^{N} \tilde{\theta}^{g}_{i,k}(H)} - \frac{\tilde{\theta}^{g}_{i,j}(H)}{\sum_{j,k=1}^{N} \tilde{\theta}^{g}_{j,k}(H)} \right) * 100 \\ &= \frac{\tilde{\theta}^{g}_{j,i}(H) - \tilde{\theta}^{g}_{i,j}(H)}{N} * 100 \end{aligned} \tag{1.9}$$

The NPWS between markets i and j is simply the difference between the gross volatility shocks transmitted from market i to market j.

1.2.2 BK Model

Baruník and Křehlík (2018) expanded the DY approach into the frequency domain by using spectral decomposition. The spectral density of x_t at frequency w can be conveniently defined as Fourier transform of MA (∞) filtered as:

$$S_x(w) = \sum_{h=-\infty}^{\infty} E(x_t x_{t-h}^{'}) e^{-iwh} = \Psi(e^{-iw}) \Sigma \Psi^{'}(e^{+iw}) \tag{1.10}$$

where $\Psi(e^{-iw}) = \Sigma_h e^{-iwh} \Psi_h$ which is obtained as a Fourier transform of the coefficients Ψ_h with $i = \sqrt{-1}$. To obtain generalized forecast error variance decomposition (GFEVD) of frequency w, a derivation is done as:

$$(f(w))_{j,k} = \frac{\sigma_{k,k}^{-1} |(\Psi(e^{-iw})\Sigma)_{j,k}|^2}{(\Psi(e^{-iw})\Sigma\Psi'(e^{+iw}))_{j,j}} \tag{1.11}$$

$(f(w))_{j,k}$ represents the portion of the spectrum of the j^{th} variable at a given frequency w due to shocks in the k^{th} variable. To obtain a natural decomposition of variance decompositions to frequencies, we can weight the $(f(w))_{j,k}$ by the frequency share of the variance of the j^{th} variable, which is defined as:

$$\Gamma_j(w) = \frac{(\Psi(e^{-iw})\Sigma\Psi'(e^{+iw}))_{j,j}}{\frac{1}{2\pi}\int_{-\pi}^{\pi} (\Psi(e^{-i\lambda})\Sigma\Psi'(e^{+i\lambda}))_{j,j} d\lambda} \tag{1.12}$$

Frequency band $d = (a,b)$ where $a,b \in (-\pi,\pi), a < b$. The generalized variance decomposition on frequency band d as:

$$(\theta_d)_{j,k} = \frac{1}{2\pi} \int_{-\pi}^{\pi} \Gamma_j(w)(f(w))_{j,k} dw \tag{1.13}$$

For scaled GFEVD:

$$(\tilde{\theta}_d)_{j,k} = \frac{(\theta_d)_{j,k}}{\sum_k (\theta_\infty)_{j,k}} \tag{1.14}$$

Total directional connectedness along with spillovers flowing 'from' and 'towards' the markets are obtained similarly as in the DY approach. Frequency connectedness is obtained by:

$$C_d^{\mathscr{F}} = \left(\frac{\Sigma \tilde{\theta}_d}{\Sigma \tilde{\theta}_\infty} - \frac{Tr(\tilde{\theta}_d)}{\Sigma \tilde{\theta}_\infty} \right) * 100 \tag{1.15}$$

where $Tr(.)$ is the trace operator. Spillovers received by market j from markets k is given by :

$$C^{\mathscr{F}}_{\hat{A}.\leftarrow k}(d) = \frac{\sum_{\substack{j=1 \\ j \neq k}}^{N} \tilde{\theta}_{j,k}(d)}{N} * 100 \tag{1.16}$$

whereas spillover from the opposite direction is taken as:

$$C^{\mathscr{F}}_{k\leftarrow \hat{A}.}(d) = \frac{\sum_{\substack{j=1 \\ j \neq k}}^{N} \tilde{\theta}_{k,j}(d)}{N} * 100 \tag{1.17}$$

1.3 ESTIMATION

1.3.1 Data

The data consists of the futures of six exchange rates, the euro (EUR), the Japanese yen (JPY), the British pound (GBP), the Australian dollar (AUD), the Canadian dollar (CAD), and the Swiss franc (CHF). The United States dollar (USD) is the base currency. The data sample starts in January 2001 and ends in September 2021 (excluding weekends).[2] In the initial stage, we conduct our analysis for the whole period. Then we split the sample into two sections. This approach helps in underlining the behavior before and after the GFC. It's worth noting that GFC emerged in developed markets due to the housing market bubble.[3] For a trading day t, return r_t is computed as:

[2]Missing points in the data are imputed using the Kalman filter.

[3]The splitting period for the data was selected as September 2008, when Lehman Brothers filed for bankruptcy.

$$r_t = ln(p_t) - ln(p_{t-1}) \tag{1.18}$$

where p_t is the futures contract price at time t. For each value of RV_t (monthly), the squares of all daily returns are summed:

$$RV_t = \sum_{i=1}^{T} r_{t,i}^2 \tag{1.19}$$

where T is the total number of daily returns observed in the month. To obtain RS_t, which measures the asymmetry underlying the distribution of asset returns, the following expression is used:

$$RS_t = \frac{\sqrt{T}\sum_{i=1}^{T} r_{t,i}^3}{RV_t^{\frac{3}{2}}} \tag{1.20}$$

To get RK_t signaling tail properties of the asset return distribution, the equation is constructed as:

$$RK_t = \frac{T\sum_{i=1}^{T} r_{t,i}^4}{RV_t^2} \tag{1.21}$$

Since our methodology is based on an estimation within the VAR framework, to ensure stationarity, we used Augmented Dickey-Fuller (ADF) and Phillips–Perron (PP) tests to check for a unit root in all series. Results suggest that all series possess stationarity at levels. Summary statistics for all series are presented in Table A.1.1 whereas Figures A.2.1, A.2.2, and A.2.3 plot full sample *RV*, *RS*, and *RK* respectively.

1.3.2 Results

We analyzed spillovers in higher moments of exchange rate futures within the time and frequency domain. In this section, we present our findings in three steps. First, we render results obtained after analyzing complete data by DY and BK methods. Then, we give rolling window spillovers for all three higher moments. Finally, we provide results from our analysis after breaking the whole sample into pre and post-GFC periods.

1.3.2.1 Spillover Analysis

For VAR estimation of the system, we select lag one based on the Akaike information criterion (AIC) with a maximum of five lags. Results are reported through Tables A.1.2-A.1.5. Forecast error variance, explained in the previous subsection, from market j to market i, is represented by each ij^{th} entry in the tables. The last row, 'To' shows directional spillovers from each asset to other assets, whereas the last column, 'From' gives spillover from all other assets combined to each exchange rate.[4] Total volatility spillover is in the lowest right corner.

Let's focus on the DY results in the table A.1.2. Overall spillovers are highest for *RV* (40.14%), followed by *RS* (37.85%) and *RK* (9.46%). Within *RV*, CAD is the highest contributor to the system (11.91%), whereas, within *RS* and *RK*, EUR has the highest contribution. Now let's move on to the frequency domain. Spillovers within short (1-6 months), medium (6-12 months), and long (12-∞) term frequencies are presented for *RV*, *RS*, and *RK* in Tables A.1.3, A.1.4, and A.1.5 respectively. As suggested by (Baruník & Křehlík, 2018), for variance decomposition, we set the forecast horizon (H) at 100. It is interesting to note that within the short-term horizon, skewness spillover (31.13%) is higher than volatility spillover (15.23%). Within mid and long-term frequencies, the second moment's spillover is higher than the third and fourth moments. Volatility spillovers in the short term get the highest contribution from CAD. This result is consistent with the results obtained for overall time domain analysis. However, in mid and long-term horizons, the most significant givers to the system are AUD and EUR. Skewness and kurtosis spillovers in all time horizons get the most contribution from EUR.

Since it is insufficient to analyze spillovers of one asset to another from the given tables, we provide a more intuitive analysis through plots of pairwise contribution for *RV*, *RS*, and *RK* within time and frequency domains from Figures A.2.4 (a)-A.2.6 (d) respectively. The strength of the connection between pairs moves through shades from lighter (weak) to darker (strong) lines. For *RV*, GBP receives strong spillovers from EUR. The same is the case within *RS* spillovers. Interestingly enough, for *RK*, it is evident that EUR is mainly on the receiving end, as far as spillover from other currencies is concerned.

[4] 'From-ABS' in case of tables for BK method.

1.3.2.2 Dynamic Moving Window Analysis

Possibly, spillover analysis missed potential cyclical movements. To cover this issue, we also conducted a dynamic rolling window analysis. Three moving windows are analyzed using 36, 48, and 60 months, separately. As was done in the previous step, we use a 100-period ahead forecast horizon (H). It can be seen from time domain examination (black line in Figures A.2.7 (a)-A.2.9 (c)), that for *RV*, *RS*, and *RK*, there is no clear trend. However, within all three moments, sudden spikes are prominent. Spillovers are on the relatively higher side post-2007. Volatility mostly stays between 40% and 80%, with occasional spikes over 80%. An interesting fact that can be seen is that volatility jumps are less smooth than skewness and kurtosis plots. Within RV spillovers, short and long-term horizons seem to have more sensitive jumps, contrary to midterm spans. Short-term spillover in *RS* and *RK* is greater (with no drastic upward or downward trend) than mid and long-term horizons.

1.3.2.3 Crisis Factor

In this section, we split our complete sample into two subsamples to re-estimate the models. One potential benefit of including a break is that it helps to avoid the overlapping that may have arisen in the dynamics of moving average window analysis (D. Zhang & Broadstock, 2020). Our sample break date is September 2008, consistent with the triggering point related to GFC.[5] For subsamples, we observed a similar pattern to overall spillovers. For instance, in *RV* pairs for currency futures, GBP mainly receives from EUR. Especially after the crisis period, the magnitude of spillover was greater. Second-moment spillovers for EUR moved in the same direction among futures before and after the crisis in the overall sample, with numerically minute differences. However, the nature and magnitude of spillovers changed among other currencies. The highest contribution in overall spillovers was seen from EUR. However, after adding a sample break, CHF was found to be contributing to JPY with a significant magnitude pre-crisis, whereas the post-crisis sample revealed EUR and AUD to be major senders within time and frequency domains. In *RK*, it was evident from complete sample analysis that CAD was a major contributor to the system. Sample break analysis reveals that CAD's magnitude of contribution increased after the crisis pe-

[5]To save space, tables and plots for results in this section are not reported. They can be made available upon request.

riod. Pre-crisis era scan shows that EUR and CHF were major connectors in both models.

1.4 DISCUSSION & CONCLUSION

We can derive several implications through our empirical analysis. Our purpose was to uncover the high-moment linkages in currency futures. Results suggest that spillovers exist in higher moments among currency futures with varying degrees. Overall, spillovers in the second moment get transferred quicker than in the third and fourth moments. However, within short horizons, skewness gets spilled more swiftly than in other moments. Currency futures, most significant to the connected system, are CAD, EUR, and AUD. These findings could play a vital role in defining risk mitigation strategies not only for traders but also for risk managers of multinationals. For instance, if a portfolio holds currency futures, managers should consider diversification strategies based on the spillovers that emerge through sudden price jumps. Currencies exert spillovers towards each other with asymmetries underlying short, medium, and long-term frequencies. Also, the dynamics differ based on the period that may exhale extra stress toward global markets. Overall, EUR seems to have high spillovers on other currencies. With inclusive policy coordination, synchronized fiscal architectures, and efficient regulations, the linkages among FX futures can provide aid in achieving monetary stability.

In this essay, we dived into the higher moments' connectivity within the context of the currency futures market. We conducted our analysis using time and frequency domain tests for spillovers in RV, RS, and RK. Our data covered a period of almost 21 years involving a major crisis that affected global financial markets. In the time domain, we found that most spillover happens in the second moment, with CAD being the highest contributor. In the third and fourth moments, Euro also plays a critical role as a contributor. Frequency domain results suggest that volatility spillovers are greater in mid and long-term horizons. In shorter frequencies, skewness spills more rapidly than volatility and kurtosis. EUR, CAD, and AUD are the most important currencies to watch in a connected system. Our moving window analysis revealed that spillovers are less smooth in volatility. Skewness and kurtosis move in a manner where sudden jumps are less frequent with no clear trend. When we split our sample into pre- and post-financial crisis periods,

we found that even though CHF contributed to the system before the crisis, post-crisis analyses were similar to overall sample results.

CHAPTER 2

TURKISH LIRA'S VOLATILITY: A NOVEL PERSPECTIVE

2.1 INTRODUCTION

A key aspect of growth within an economy is a stable exchange rate. Competitive exchange rates determine the success of macroeconomic indicators (Sabri, Abdul Rahman, Meero, Abro, & AsadUllah, 2022). In 1973, to calculate currency values, a new system was adopted by global markets. This framework allowed the value of a particular currency to be determined through transactions based on demand and supply, thus ending the Bretton Woods fixed rate regime. But, this also increased the general volatility in the FX markets. Since then, academics have been keen on understanding the volatility dynamics of exchange rates. Producing decent volatility forecasts of exchange rates carries equal importance for policymakers, investors, central banks, domestic firms, multinational corporations, and other participants. Therefore, the influence of this volatility is not just on the micro level but on a macro level as well since it dictates capital flows within a functional economy. Despite its critical value, there has not been any consensus on the econometrical approach to model or predict this volatility. The reason is the same as has been with all financial data. Additionally, unlike prices and returns, which are directly observable, volatility is latent, making it even more challenging for objective analyses.

Over the last decade, the Turkish lira (TRY) has seen relatively turbulent periods. Figure B.3.1 gives us a snapshot of the price of TRY against USD in the previous decade, along with important global and Turkey-specific events. As can be seen, some periods present a different picture enveloping sharp price increases (suggesting a weakened currency) compared to the rest of the

timeline. These increases could be due to several external and internal factors: failed coup attempt, US foreign policy concerning Turkey, and US trade tariffs,[1] US-China trade war, reduction of credit rating, Covid-19 pandemic, and firms' productivity levels. Post-2016 jumps in the price levels were unprecedented. To offset the financial uncertainty, short-term interest rates are a natural choice as a policy instrument. And like other central banks, the Central Bank of the Republic of Turkey (CBRT) used it to control the free fall. Take the one-week repo rate between 2016 and 2018 as an example. It increased from 8% to 16.5% (850 bps) at the beginning of 2018 and eventually reached 24% by September 2018, following a 40% depreciation of the lira in mid-August. However, it got gradually reduced in subsequent announcements. The lira kept receiving shocks, the worst of which came after the global pandemic. On the 20^{th} of December 2021, the lira's nominal value against USD reached an all-time high of 18.4, decreasing to a closing value of 13.5 the next day.[2] In the past, CBRT has not only applied the conventional tool like policy rate adjustments to curb financial instability, but they also used instruments like reserve option mechanism (ROM), required reserve ratio (RRR), and interest rate corridor (IRO), which were only partially successful (Akar & Çiçek, 2016).

Recent studies have analyzed TRY through different empirical perspectives. Some of these analyses include the lira's volatility within the trade paradigm (Vergil, 2002; Nazlioglu, 2013; Bahmani-Oskooee & Durmaz, 2016, 2021), and its link with stocks, interest rate, and other economic/financial variables (Erdem, Arslan, & Sema Erdem, 2005; Kasman, Vardar, & Tunç, 2011; Türkyılmaz & Balıbey, 2013; Mozumder, De Vita, Kyaw, & Larkin, 2015; Bajo-Rubio, Berke, & McMillan, 2017; Mechri, Ben Hamad, de PERETTI, & Charfi, 2018; Sabri et al., 2022). Some findings also highlight the dynamic nature of the volatility encompassing the Turkish lira. Berument, Coskun, and Sahin (2007) suggested that volatility differs during trading days. Akgül and Sayyan (2008) emphasized the benefit of using long-memory GARCH, along with asymmetry and power terms. Their findings also made a case for the skewed and leptokurtic distributions. Another study by Gökbulut and Pekkaya (2014) advocated the presence of similar characteristics in the TRY. Laurini and Mauad (2015) tried to capture the latent volatility through a stochastic volatility (SV) model incorporating the

[1] Especially those related to steel and aluminum imports.

[2] The government announced a scheme on the same day to curb the effects of dollarization. It aims to protect the lira deposits in the banks against fluctuations in FX.

common jump factor. Their model, when applied to real/dollar and lira/dollar series, identified the short and long-term patterns in the volatility for both series. Another dimension was recently presented by Sensoy and Serdengeçti (2019), who used high-frequency data and trading volumes. Findings suggest a significant nexus between volatility and volume that varies with time.

TRY and its volatility have received considerable attention in the recent past. This emphasis could be due to the extreme variability it experienced. In fact, Taskinsoy (2019) argues that the volatility of TRY is in line with those of crypto-currencies and that a channel exists that highlights the influence of the US dollar on the movements of TRY and bitcoin. Our objective is to analyze the volatility from the lira's account. Interest is in the questions like what constitutes a volatility measure? What can traditional and dynamic volatility measures tell us when explained through various variance proxies? How different are various volatility estimates? While the literature is quite clear on the effects and influences of exchange rate volatility, very few studies have addressed the issue of TRY's volatility from a holistic point of view. Our contribution to the current literature lies in an empirical account of these issues. As per our observation, this is the only study that models TRY's volatility through an array of traditional and novel statistical approaches. Also, to encounter the fat-tail issue, we use a wide range of statistical distributions and model specifications. Furthermore, we inject our results into a supervised machine learning (ML) algorithm which gives us further insights into the volatility behavior of estimates and proxies. This approach allows us to compare and draw novel inferences.

Exposure of the Turkish economy to capital movements was relatively higher than some of the other emerging economies. While this exposure made its currency vulnerable, it also is an interesting case study for volatility analysis. Since we aim to investigate the volatility proxies, and their relative effectiveness, our choice of models is within the realm of the conventional and novel empirical literature. To model TRY's volatility, we first applied statistical techniques of GARCH, generalized autoregressive score (GAS), SV, heterogeneous autoregressive (HAR), Multi-Components GARCH, Conditional AutoRegressive Range (CARR) classes. We incorporated various distributions and specifications into our models to capture different features that may be present. Our models cater not just to daily prices but also to intraday and range-based price information. This application allowed us to have a range of estimates we examined under a supervised ML environment.

Specifically, we applied support vector regression (SVR) using different kernel functions to check for the best specifications.

The essay is organized as follows: subsection 2.2 enlists the mathematical specifications of techniques used in this chapter, subsection 2.3 provides data and estimation results of the models, and subsection 2.4 presents the discussion and conclusion of the results obtained through analyses.

2.2 METHODOLOGY

2.2.1 GARCH Models

Let y_t be returns of a financial time series at time t such that $y_t = \mu + \sum_{i=1}^{n} \tau y_{t-1} + \varepsilon_t$ where ε_t is the error term. From the works of Engle (1982) and Bollerslev (1986), GARCH models emerged to estimate conditional volatility as a function of its lags and past error terms:

$$\varepsilon_t = \sqrt{h_t \zeta_t} \qquad \zeta_t(0,1) \tag{2.1}$$

$$h_t = \omega + \sum_{j=1}^{p} \alpha_j \varepsilon_{t-j}^2 + \sum_{j=1}^{q} \beta_j h_{t-j} \tag{2.2}$$

Since its inception, several scholars have supplemented this model through different specifications of Eq. (2.2). This essay uses a few variants of these models for which mathematical representation can be conveniently done through Hentschel's (1995) all nested GARCH (ALLGARCH) model in Eq (2.3): [3]

$$\begin{aligned} \sigma_t^{\lambda} = (\omega + \sum_{j=1}^{m} \gamma_j \nu_{jt}) + \sum_{j=1}^{q} \alpha_j \sigma_{t-j}^{\lambda} (|z_{t-j} - \eta_{2j}| \\ - \eta_{1j}(z_{t-j} - \eta_{2j}))^{\delta} + \sum_{j=1}^{p} \beta_j \sigma_{t-j}^{\lambda} \end{aligned} \tag{2.3}$$

Eq. (2.3) is a Box-Cox transformation of volatility shaped by the parameter λ. It can be used to represent:

- Bollerslev's (1986) GARCH model when $\lambda = \delta = 2$ and $\eta_{1j} = \eta_{2j} = 0$.

[3] Even though it is possible to add higher-order lags, which is evident in Eq. (2.2), we use standard GARCH (1,1) to be the order selection of our model. We do this to keep it parsimonious as financial literature generally suggests that higher-order GARCH models do not significantly outperform lower-order models, especially when the costs of adding complexity to the model are considered.

- Taylor's (1982) and Schwert's (1990) absolute value GARCH (AVGARCH) model when $\lambda = \delta = 1$ and $|\eta_{1j}| \leq 1$.
- Nelson's (1991) exponential GARCH (EGARCH) model when $\delta = 1, \lambda = 0$ and $\eta_{2j} = 0$.
- Higgins and Bera's (1992) nonlinear GARCH (NGARCH) model when $\delta = \lambda$ and $\eta_{1j} = \eta_{2j} = 0$.
- Engle and Ng's (1993) nonlinear asymmetric GARCH (NAGARCH) model when $\delta = \lambda = 2$ and
  $eta_{1j} = 0$.
- Ding, Granger, and Engle's (1993) asymmetric power ARCH (APARCH) model when $\delta = \lambda, \eta_{2j} = 0$ and $|\eta_{1j}| \leq 1$.
- Glosten et al.'s (1993) GARCH (GJRGARCH) model when $\lambda = \delta = 2$ and $\eta_{2j} = 0$.
- Zakoian's (1994) threshold GARCH (TGARCH) model when $\lambda = \delta = 1, \eta_{2j} = 0$ and $|\eta_{1j}| \leq 1$.
- Hentschel's (1995) ALLGARCH when $\lambda = \delta$.

Since all these models exist in closed form, parameters can be estimated by maximizing a log-likelihood (LLH) function which depends on the assumed distribution for errors. For each model used, we use five distributions, the normal distribution (*norm*), the skewed normal distribution (*snorm*), the student-t distribution (*std*), the skewed student-t distribution (*sstd*), and Johnson's SU distribution (*jsu*) to pick the most appropriate error assumption based on LLH and information criteria.[4]

2.2.2 GAS Models

Recently developed GAS models by Harvey (2013) and Creal, Koopman, and Lucas (2013),[5] make use of a mechanism that updates parameter space over time using LLH function. This model is observation driven since instead of only using information from moments, it considers the entire conditional

[4]LLH functions for all distributions are given in Appendix B.1.

[5]Referred to as dynamic conditional score (DCS) by Harvey (2013).

density distribution of the time series. The following equations can specify the GAS model:

$$y_t|\mathscr{Q}_{t-1} \sim p(y_t;\theta_t) \tag{2.4}$$

where $\mathscr{Q}_{t-1}$ and $\theta_t \in \Theta \subseteq \Re^n$ are vectors containing y_t upto $t-1$ and time varying parameters respectively. θ_t satisfies $p(\cdot)$ and depends on $\mathscr{Q}_{t-1}$. It can be defined as:

$$\theta_t = K + As_t + B\theta_{t-1} \tag{2.5}$$

where K, A and B are coefficient matrices. S_t is defined as:

$$s_t = S_t(\theta_t)\nabla_t(y_t,\theta_t) \tag{2.6}$$

where S_t is a positive definite $n \times n$ scaling matrix,[6] and $\nabla_t(y_t,\theta_t)$ is the score of density function in Eq. (2.4).[7] Estimation of $\sum = (K,A,B)$ is done through likelihood maximization. As in GARCH, for each model, we use seven distributions, *norm*, *snorm*, *std*, *sstd*, asymmetric student-t with two tail decay parameters (*ast*), asymmetric student-t with one tail decay parameter (*ast*1), and asymmetric laplace distribution (*ald*) to pick the most appropriate error assumption based on LLH and information criteria.

2.2.3 SV Models

For a vector of mean zero returns $y = (y_1, y_2, ..., y_n)^T$, the hierarchical form of the SV model in its centered parameterization can be given as:

$$y_t|h_t \sim \mathscr{T}(0, exp\, h_t) \tag{2.7}$$

$$h_t|h_{t-1},\mu,\phi,\sigma_n \sim \mathscr{T}(\mu + \phi(h_{t-1}-\mu), \sigma_n^2) \tag{2.8}$$

$$h_0|\mu,\phi,\sigma_n \sim \mathscr{T}(\mu, \sigma_n^2/(1-\phi^2)) \tag{2.9}$$

where μ, ϕ, and σ_n are the level, persistence, and volatility of log-variance respectively, and can be referred to as a vector of parameters to be estimated $\theta = (\mu,\phi,\sigma_n)^T$. The main difference between GARCH and SV models is the nature of h_t. In GARCH models, h_t follows a time-varying deterministic process, whereas SV models presume a stochastic evolution (Kastner, 2019). The standard SV model introduced by Taylor (1982) has evolved, and over

[6] See Harvey (2013) for a detailed account of how to set the scaling matrix.

[7] $\nabla_t(y_t,\theta_t) \equiv \frac{\partial log p(y_t;\theta_t)}{\partial \theta_t}$.

time, numerous extensions have been proposed by econometricians in the literature. In this essay, we incorporate some of these extensions. To be specific, we estimate the SV model with leverage (SVL),[8] SV with student-t errors (SVT), and SV with student-t errors and leverage (SVTL) in addition to generic SV model.[9]

Unlike GARCH models, estimation of SV models through maximization of the likelihood function is difficult since the model lacks a closed form (Poon & Granger, 2003). Here, this issue is navigated by using a Markov chain Monte Carlo (MCMC) algorithm. Demeaned log returns are fed into an MCMC sampler along with prior distributions vector θ. Normal prior $\mu \sim \mathscr{T}(b_\mu, \mathscr{B}_\mu)$, where b_μ=0 and $\mathscr{B}_\mu$=100 is chosen for level parameter $\mu \in \mathbb{R}$. For $\theta \in (-1,1), (\theta+1)/2 \sim \mathscr{B}(a_0, b_0)$ is chosen:

$$p(\phi) = \frac{1}{2\mathscr{B}(a_0,b_0)}(\frac{1+\phi}{2})^{a_0-1}(\frac{1-\phi}{2})^{b_0-1} \tag{2.10}$$

where $\mathscr{B}(x,y) = \int_0^1 t^{x-1}(1-t)^{y-1}\,dt$ is beta function with a_0=5 and b_0=1.5. Log variance $\sigma_n \in \mathbb{R}^+$ is estimated with $\sigma_n^2 \sim B\sigma_n \times \chi_1^2 = \mathscr{L}(1/2, 1/2B\sigma_n)$. For all models, $B\sigma_n$=1 is taken; however, this choice has a minor impact.[10]

2.2.4 HAR Models

The HAR model of Corsi (2009) use *RV* estimates to accommodate different time horizons. Motivation for these models can be found in Müller et al.'s (1993) Heterogeneous Market Hypothesis which states that financial markets consist of participants who are non-homogeneous in nature. Consider r_t be the sum of intraday returns, then RV_t at time t can be given as:

$$RV_t = \sum_{m=1}^{M} r_{t,m}^2 \tag{2.11}$$

where m is the intraday interval. If ε_t is defined as error at time t, then HAR model can be represented as:

$$RV_t = \beta_0 + \beta_1 RV_{t-1} + \beta_2 RV_{t-1}^w + \beta_3 RV_{t-1}^M + \varepsilon_t \tag{2.12}$$

[8] Also known as asymmetric stochastic volatility model.

[9] For a detailed account of the extensions used in this essay, readers are referred to Kim, Shephard, and Chib (1998), J. Yu (2005), Omori, Chib, Shephard, and Nakajima (2007), Nakajima and Omori (2009), Wang, Chan, and Choy (2011), Kastner and Frühwirth-Schnatter (2014), and Hosszejni and Kastner (2018).

[10] For more information on hyperparameters and samplers, please see sections 2 and 3 of Kastner (2016).

where $RV_{t-1}^{W} = \frac{RV_{t-1}+RV_{t-2}+...+RV_{t-5}}{5}$ and $RV_{t-1}^{M} = \frac{RV_{t-1}+RV_{t-2}+...+RV_{t-22}}{22}$. Corsi (2009) also estimated the log HAR (LHAR) model which can be simply obtained by taking natural logarithm on both sides of Eq. (2.12). Additional extensions that we will use in our analysis are: Andersen, Bollerslev, and Diebold's (2007) HAR with jump (HARJ) and continuous HAR (CHAR) models, Bollerslev, Patton, and Quaedvlieg's (2016) HAR quarticity (HARQ), HAR quarticity with jump (HARQJ) and CHAR quarticity (CHARQ) models. These are given in Eqs. (2.13)-(2.17):

$$HARJ : RV_t = \beta_0 + \beta_1 RV_{t-1} + \beta_2 RV_{t-1}^{w} + \beta_3 RV_{t-1}^{M} \beta_4 J_{t-1} + \varepsilon_t \tag{2.13}$$

$$HARQ : RV_t = \beta_0 + (\beta_1 + \beta_{4Q} RQ_{t-1}^{1/2}) RV_{t-1} + \beta_2 RV_{t-1}^{w} + \beta_3 RV_{t-1}^{M} + \varepsilon_t \tag{2.14}$$

$$HARQJ : RV_t = \beta_0 + (\beta_1 + \beta_{4Q} RQ_{t-1}^{1/2}) RV_{t-1} + \beta_2 RV_{t-1}^{w} + \beta_3 RV_{t-1}^{M} \beta_5 J_{t-1} + \varepsilon_t \tag{2.15}$$

$$CHAR : RV_t = \beta_0 + \beta_1 BPV_{t-1} + \beta_2 BPV_{t-1}^{w} + \beta_3 BPV_{t-1}^{M} + \varepsilon_t \tag{2.16}$$

$$CHARQ : RV_t = \beta_0 + (\beta_1 + \beta_{4Q} TPQ_{t-1}^{1/2}) BPV_{t-1} + \beta_2 BPV_{t-1}^{w} + \beta_3 BPV_{t-1}^{M} + \varepsilon_t \tag{2.17}$$

where BPV is bipower variation of Barndorff-Nielsen and Shephard (2004), TPQ is tripower quarticity of Barndorff-Nielsen and Shephard (2006), and RQ is realized quarticity of Bollerslev et al. (2016).

2.2.5 Multi-Components GARCH

Component GARCH (CGARCH) model presented by Lee and Engle (1993) breaks up conditional volatility in Eq. (2.2) into time-varying permanent and transitory components:

$$h_t - q_t = \alpha(\varepsilon_{t-1}^2 - q_{t-1}) + \beta(h_{t-1} - q_{t-1}) \tag{2.18}$$

$$q_t = \omega + \rho q_{t-1} + \varphi(\varepsilon_{t-1}^2 - h_{t-1}) \tag{2.19}$$

Eqs. (2.18) and (2.19) represent transitory (short-run) and permanent (long-run) volatility components, respectively. The reduced form for these equations can be given as:

$$\begin{aligned} h_t = {} & (1-\alpha-\beta)\omega + (\alpha+\varphi)\varepsilon_{t-1}^2 + [-\varphi(\alpha+\beta) - \alpha\rho]\varepsilon_{t-2}^2 \\ & + (\rho+\beta-\varphi)h_{t-1} + [\varphi(\alpha+\beta) - \beta\rho]h_{t-2} \end{aligned} \tag{2.20}$$

this setting makes it an NGARCH (2,2) model with restrictions. Short-run temporary component reverts to long-run volatility following a distur-

bance.[11]

Another mixed data sampling (MIDAS) technique within the GARCH universe that allows the analysis of long and short-term volatility components separately, is GARCH-MIDAS model. This method enables us to incorporate macroeconomic information (usually sampled at a lower frequency) into a long-term component that remains fixed during a period (a month in our case). Consider conditional mean of returns $r_{i,t} = \mu + \varepsilon_{i,t}$ where $i = 1,...,N_t$ and $t = 1,...,T$ are days within month t and monthly frequency respectively. Engle, Ghysels, and Sohn (2013) showed that $\varepsilon_{i,t}$ can be represented as:

$$\varepsilon_{i,t} = \sqrt{h_{i,t}\tau_t} Z_{i,t} \tag{2.21}$$

where $Z_{i,t} \sim i.i.d.(0,1)$ whereas $h_{i,t}$ and τ_t denote short and long term conditional volatility respectively. $h_{i,t}$ is modeled as a GARCH(1,1) process:

$$h_{i,t} = (1 - \alpha - \beta) + \alpha \frac{\varepsilon^2_{i-1,t}}{\tau_t} + \beta h_{i-1,t} \tag{2.22}$$

where standard GARCH restrictions apply on α and β parameters. τ_t is given as:

$$\tau_t = m + \sum_{k=1}^{K} \varphi k(w1, w2) X_{t-k} \tag{2.23}$$

where X_t denotes the explanatory variable. We use the Turkish Economic and Financial Uncertainty Index (TEFUI) recently developed by Bilgin, Demir, Gozgor, Karabulut, and Kaya (2019) to model the long-term volatility component of the TRY.[12] For $\varphi_k(w1, w2)$, a weighting scheme is defined as:

$$\varphi_k(w1, w2) = \frac{(k/(K+1))^{w_1 - 1} \cdot (1 - k/(K+1))^{w_2 - 1}}{\sum_{j=1}^{K} (j/(K+1))^{w_1 - 1} \cdot (1 - j/(K+1))^{w_2 - 1}} \tag{2.24}$$

where weights $\varphi_k(w1, w2) \geq 0, k = 1,...,K$ sum to one. We use $K = 12$, which implies one year lag for the monthly explanatory variable.

[11] For statistical properties and stationarity conditions of the model, readers are referred to section 3 of Engle and Lee (1999).

[12] This index is based on real-time Google Trends data and is updated regularly on a monthly basis. According to Conrad, Custovic, and Ghysels (2018), economic variables' forecasts can be obtained through Google search data.

2.2.6 CARR Models

Based on the premise of modeling range-based volatility, Chou (2005) proposed CARR model, which is similar to Bollerslev's (1986) GARCH and Engle and Russell's (1998) Autoregressive Conditional Duration (ACD) models. Consider the following:

$$RR_t = \frac{High(P_\kappa) - Low(P_\kappa)}{\sqrt{4ln2}}, \quad \kappa\varepsilon(t-1,t) \tag{2.25}$$

where P_t and RR_t are logarithmic price and scaled price range, respectively, observed at time t. RR_t is an unbiased volatility estimator of a financial asset return (Parkinson, 1980). Based on Eq. (2.25) CARR is given by:

$$RR_t = h_t\varepsilon_t \tag{2.26}$$

$$h_t = \omega + \alpha RR_{t-1} + \beta h_{t-1} \tag{2.27}$$

$$\varepsilon|\rho_{t-1} \sim i.i.d.\ \ f(\cdot) \tag{2.28}$$

Volatility clustering is captured in the structure of h_t where $h_t = \mathbb{E}[RR_t|\rho_{t-1}]$. In Eq. (2.27), ω captures the range uncertainty, whereas α and β determine short and long-term shock effects to the range, respectively. All coefficients are restricted to be greater than 0 to ascertain the positiveness of the conditional mean of the price range. To ensure stationarity of h_t, a constraint is imposed which requires: $\alpha+\beta < 1$. The sum of α and β signifies the persistence of shocks to the range. Wu and Hou (2020) put forward an extension, component CARR (CCARR), to decompose the volatility into permanent and transitory components in pursuit of incorporating additional information to the price range of stock market indices. The model is similar to what was proposed by Engle and Lee (1999) in which they used a two-component volatility model which estimates a long and short-run component of mean-based returns. If we consider the price range estimator in Eq. (2.26) to be unbiased, then to capture the long memory more efficiently h_t at time t could be redefined as follows:

$$h_t = q_t + \alpha(RR_{t-1} - q_{t-1}) + \beta(h_{t-1} - q_{t-1}) \tag{2.29}$$

$$q_t = \omega + \varphi RR_{t-1} + \rho q_{t-1} \tag{2.30}$$

$$\varepsilon|\rho_{t-1} \sim i.i.d.\ \ f(\cdot) \tag{2.31}$$

h_t in Eq. (2.29) corresponds to volatility clustering and includes a permanent memory shock. In Eq. (2.30), q_t represents a permanent component of volatility with an expected value of $\frac{\omega}{1-\varphi-\rho}$, whereas $h_t - q_t$ is the transitory part with an expected value of 0. Eqs. (2.29) and (2.30) could be rewritten as:

$$\begin{aligned} h_t = \omega(1-\alpha-\beta) + (\alpha+\varphi)RR_{t-1} - (\alpha\rho+\varphi\beta+\alpha\varphi)RR_{t-2} \\ + (\beta+\rho)h_{t-1} - \beta\rho h_{t-2} \end{aligned} \tag{2.32}$$

From Eq. (2.32), it can be seen that CCARR is CARR(2,2). If $\alpha = \beta = 0, \varphi = \alpha$ and $\rho = \beta$, then Eq. (2.32) will be reduced to CARR. It should be noted that CCARR has the following constraints in its structure:

$$\alpha + \beta < 1 \tag{2.33}$$

$$\varphi + \rho < 1 \tag{2.34}$$

Constraints in Eqs. (2.33) and (2.34) are necessary for the process to be stationary and signify the persistence of transitory and permanent components, respectively. The model defined above is computationally less complex as estimates could be retrieved through a simple maximum likelihood estimation. The LLH function that needs to be maximized to estimate the parameters is as follows:

$$LLH(\alpha,\beta,\omega,\varphi,\rho) = -\sum_{t=1}^{T}[ln(\frac{R_t}{\tau_t}) + ln(h_t)] \tag{2.35}$$

2.2.7 SVR Model

SVR is a modified form of the support vector machine (SVM) algorithm based on the works of Boser, Guyon, and Vapnik (1992) and Vapnik (1998). Volatility modeling through SVR was first done by Pérez-Cruz, Afonso-Rodriguez, and Giner (2003), who estimated GARCH (1,1) and showed the superior capabilities of combined techniques. Following Eqs. present SVR

as a constrained optimization problem:

$$\begin{aligned} \min_{w,b,\xi_i,\xi_i^*} \quad & \{\frac{1}{2}||w||^2 C \sum_{i=1}^{n}(\xi_i + \xi_i^*)\} \\ \text{s.t.} \quad & y_i - w^T \theta(x_i) - b \leq \varepsilon + \xi_i \\ & w^T \theta(x_i) + b - y_i \leq \varepsilon + \xi_i^* \\ & \xi_i, x_i^* \geq 0 \end{aligned} \tag{2.36}$$

where $\theta(\cdot)$ is nonlinear transformation to a higher dimensional space,[13] $x_i \in \mathscr{R}^d$ is input vector and $y_i \in \mathscr{R}$ is the output vector. ξ_i, ξ_i^* and C deal with prediction errors when they are greater than ε.[14] Schölkopf, Smola, Williamson, and Bartlett (2000) proposed an alternate formulation where ε is replaced by ν leading to the same solution.

We use three different proxies for volatility as output vectors: RV_t and RR_t as defined in Eqs. (2.11) and (2.25), respectively, along with another estimate $\hat{\sigma}_t^2$ $(MASR)$ which is the moving average of lagged square returns y_t^2 computed as:

$$\hat{\sigma}_t^2 = \frac{1}{5}\sum_{k=0}^{4} y_{t-k}^2 \tag{2.37}$$

The input vector contains all volatility estimates obtained from the results of estimation techniques defined previously. We estimate SVR using three kernels: linear, polynomial, and radial basis function (RBF). Half of the complete sample is used for training the data, whereas the other half is kept for testing. For the value of ν, finding a priori is challenging; therefore, the models will be first trained using different values between 0 and 1. Then the model that provides the highest R^2 will be picked on which estimation is going to be done using 8-fold cross-validation.

[13] Except when $\theta(x_i) = x_i$ in case of linear kernel.

[14] We follow same convention as is done in Pérez-Cruz et al. (2003) with respect to parameters, and kernel choices. For details concerning how Eq. (2.36) is a maximization problem in connection with Lagrange multipliers, and Karush-Kunh-Tucker (KKT) conditions, please see section 2 of their paper as a reference.

2.3 ESTIMATION

2.3.1 Data

Daily, intraday, and range-based Turkish lira's price data used in our analyses span from January 3, 2011, to December 30, 2021. For models of GARCH, GAS, and SV classes, we used daily continuously compounded log returns. The sample shows signs of non-normality along with ARCH effects, thus warranting the use of AutoRegressive Conditional Heteroskedastic (ARCH) class models. The plot of daily returns is given in Figure B.3.2. For HAR models, RV_t is computed through Eq. (2.11) from intraday prices sampled at 15 min intervals. For CARR models, the daily price range RR was calculated using Eq. (2.25) and is found to have excess kurtosis and positive skewness, which is quite typical of a financial time series. Figure B.3.3 and Figure B.3.4 plots RV and RR, respectively. From these figures, a similar peak and trough pattern is evident. Descriptive statistics of log and range returns are given in Appendix B.2. Weekends and public holidays were excluded from the data.[15]

2.3.2 Results

In this subsection, estimation results are given. We first present our analyses from the volatility models applied to TRY. These include all classes of models described in subsection 2.2. We then proceed to report results from SVR applied to volatility estimates. All result tables are provided in Appendix B.2.

2.3.2.1 Volatility Results

In this subsection, we present the estimation results for each volatility model used in the study. For GARCH models discussed in subsection 2.2.1, based on LLH and information criteria,[16] TRY is modeled best when the error distribution is assumed to be *sstd* across all specifications of GARCH. From the estimates and diagnostics, it is clear that distributions other than normal, provide a decent fit.[17] As mentioned in subsection 2.2.2, GAS estimation is done as a maximization problem. Models with *ast* distributions provide the

[15] Some dates that were missing, in either daily or intraday samples, were removed to match both sets.
[16] AIC, Bayesian information criterion (BIC), and Hannan–Quinn information criterion (HQIC).
[17] To save space, coefficient values are not reported; however, they can be shared upon request.

best estimates based on LLH, AIC, and BIC. Like in GARCH models, distributions other than normal provide better goodness of fit measures for GAS models too. We provide results of SV models' posterior draws along with priors used for estimation. In Figures B.3.5-B.3.8 we plot posterior quantiles of volatility estimates obtained through SV models.[18] For HAR models, we used different estimation schemes stated in subsection 2.2.4. One interesting finding that can be observed in the results is that adding jumps and TPQ does not significantly improve naive HAR models' estimation measured through R^2. The highest value achieved is 55.8% for the logarithmic HAR model. CGARCH model presents some interesting findings as well. Firstly, all parameters are significant at the 1% level. Since α is greater than φ, the implication is that the impact of the shock is greater on transitory volatility than permanent component. $\alpha + \beta < \rho$ ($0.81 < 0.995$) shows that mean reverting is less for the short-run volatility than long-run volatility. Transitory half-life is 3.28 days, whereas permanent half-life corresponds to almost 147 days. To further investigate long-term volatility, we estimated GARCH-MIDAS. Coefficient estimates of GARCH-MIDAS are also reported. The model is covariance stationary since $\alpha + \beta < 1$. θ is found to be positive and highly significant. This implies that when uncertainty increases, long-term volatility also increases. This result makes sense since economic uncertainty is generally linked to higher volatility. Overall, the decomposition of volatility seems to provide additional information that may come in handy for further analyzing the issue. For models estimated using RR_t, the decomposition of volatility done through CCARR produced better estimates than CARR based on LLH and information criteria. The persistence of long-run volatility $\rho + \varphi$ is higher than that of short-run component $\alpha + \beta$ in the CCARR model. The reason for such results may have some explanation in the findings presented in the following text.

2.3.2.2 SVR Results

We take volatility estimates obtained through models defined in previous subsections and analyze them using the SVR algorithm. Figure B.3.13 plots proxies for volatility, used as a dependent variable for all models. Each model is estimated using linear, RBF, and polynomial kernels. For choosing the value of ν, we estimate models with different values between 0 and 1. Results are reported in Figures B.3.14 (a)-B.3.16 (c). ν value that pro-

[18] Trace and density plots for all parameters of each SV model are given, through Figures B.3.9-B.3.12.

duced the highest R^2 was used to estimate models using all three kernels. Polynomial kernel produced a better in-sample fit when dependent variables were *RV* and *RR*, whereas the RBF kernel gave the best R^2 for *MASR*. For all proxies, the best out-of-sample R^2 was given by the RBF kernel. We also checked for feature importance, and the results are reported in Figures B.3.17 (a)-B.3.17 (c).[19] One interesting finding is that variable importance changes according to the proxy used for volatility. For example, as expected, when range based *RR* is used as a volatility measure, estimates for CCARR and CARR models are significantly higher than other volatility models. Another important observation is that no single class of volatility models can produce consistently high estimates across all specifications. Contributions of GARCH, GAS, HAR, SV, and CARR are similar in magnitude depending on the volatility proxy being used.

2.4 DISCUSSION & CONCLUSION

Our study can have numerous policy implications for the volatility of TRY. Firstly, we provide an empirical account of variance, which is of great concern to all stakeholders. Our analyses reveal that while modeling TRY's volatility, even though the choice of the statistical method matters, almost all models provide a better fit when non-normal distributions are allowed for model estimation. This fact confirms that for modeling financial time series, heavy tail distributions are more relevant (Junior, Tiwari, Tweneboah, & Asafo-Adjei, 2022). Secondly, since volatility is a latent feature, the choice of proxy may also matter. The success of an estimate varies depending on the volatility model applied. Therefore choosing between alternative volatility measures may not always be straightforward. Another important finding is that though it may not always be possible, decomposing volatility may reveal additional information. TRY, for example, was shown to have more persistent long-run volatility than the short-run component. The structure of shocks may also provide a good account of risk features. Our MIDAS analysis revealed that economic uncertainty drives long-run volatility and may therefore be able to predict the future course of the currency. All these results may prove critical not only for policy design and contingency planning; but also for trading and general risk management purposes. We also analyzed

[19]This result is obtained only for the linear kernel as it would not make sense to use other kernels for interpretability since RBF and polynomial kernels map vectors into high dimensions, and meaningful interpretation will not be possible.

our volatility estimates under the SVR framework. Results revealed that for all models, kernels other than linear provide better results. Polynomial kernel provided a better in-sample fit. RBF proved superior for generating high out-of-sample R^2 values.

In this study, we attempted to analyze the volatility structure of TRY, which may provide a new perspective on its behavior. One limitation of our study is that almost all specifications do not consider macroeconomic information since our purpose was to analyze TRY from its account. Future studies could incorporate other financial variables that may provide additional insights into volatility behavior. Another option for further investigation could be the allowance of more complex models. Generally, each class of models can have numerous extensions, so we leave the choice of statistical augmentation for subsequent studies. We understand the criticism regarding commonly used metrics such as standard deviations under the mean-variance modeling framework.[20] Another avenue for volatility modeling could be information inclusion, which could reflect behavioral patterns, especially related to volatility in connected capital markets.

[20] see Nwogugu (2006).

CHAPTER 3

A TWO-STAGE ANALYSIS OF INTERACTION BETWEEN STOCK AND EXCHANGE RATE MARKETS: EVIDENCE FROM TURKEY

3.1 INTRODUCTION

Understanding the depths of interaction among financial markets is imperative. After scrutinizing modern literature, we can observe that researchers place the utmost value on the links between FX markets and stock markets. One of the reasons for putting this much importance on analyzing this phenomenon could be due to the critical economic consequences of the relationship (Reboredo, Rivera-Castro, & Ugolini, 2016). For instance, to offset the risk associated with hedging portfolios, investors must understand the braided dynamics of both these markets. If an increase in currency value denotes loss, a positive correlation between both markets may neutralize risk, whereas a negative correlation might amplify the risk associated with both variables (Živkov, Njegić, & Pavlović, 2016). The implications of the nexus are multi-fold. It provides insights not only to investors and portfolio managers but also helps policymakers understand the financial perspective (Aloui, 2007).

Numerous empirical studies have provided evidence for a clear linkage between these two assets and axiomatically in their respective returns. However, since most studies analyze asset returns with their nominal values, is there a difference in correlation that can be linked to separate frequencies as in short-term and long-term fluctuations? How much do we know about the connectivity in the tails of returns? Many papers explored the direction and strength of causality and correlation, but rarely a piece of evidence has been provided that which frequency helps more in explaining the directional

predictability. Furthermore, how this relation evolves when these markets experience both, that is, calm and crisis periods? Any insights we can obtain from answering these questions can be of great significance, especially towards hedging tail risk, which is often the most challenging part of portfolio management.

Two theoretical approaches can explain the connection between FX and stock markets: flow-oriented and stock-oriented. The first approach presents the idea that exchange rate fluctuations will impact export competitiveness and the balance of trade. Due to this, profits and income will get affected, thereby shifting stock prices (Dornbusch & Fischer, 1980). Also, Gavin (1989) proposed that because of the exchange rate, stock market innovations affect aggregate demand through liquidity and wealth effects, hence inducing money demand and exchange rates. Another way of understanding it is by explaining the effect of exchange rates on both, that is, the international and the domestic operations of a company. Regarding overseas operations, exchange rates influence exports, imports, and assessments of assets and liabilities, whereas domestic operations are affected by competition and input/output prices. It affects the cash flows and profitability of a company, thereby influencing investors' assessment of stocks and inducing a change in the prices of stocks.[1] The stock-oriented approach suggests an effect flowing from stock prices toward exchange rates. In literature, this approach has two explanations, monetary models and portfolio balance models. Under a monetary-based model, financial asset prices absorb exchange rate effects. Asset prices obtained through discounting expected future cash flows and common macroeconomic factors may affect stock prices and exchange rate dynamics (Rahman & Uddin, 2009; Zhao, 2010). Portfolio balance models suggest a negative relation between stock prices and exchange rates.[2] The inverse relationship can be viewed through direct and indirect channels (Walid, Chaker, Masood, & Fry, 2011). To account for direct channels, consider an increase in domestic stock prices. Hence, it will encourage foreign investors to sell foreign assets in their portfolios and buy more domestic assets with domestic currency. Increased demand will appreciate the local currency. Indirect channel considers that a rise in the stock market will attract foreign investment, increasing net worth and domestic wealth. As demand for domestic goods increases, interest rates will have to be synced. Subsequently,

[1] For details, readers are referred to Ball and Brown (1968) and Yücel and Kurt (2003).

[2] For details, readers are referred to Frenkel (1976), Branson (1981), Branson and Henderson (1985), and Macdonald and Taylor (1992).

an increase in interest rates will lead to higher demand for local currency and therefore, the currency will appreciate (Branson, 1981).

Franck and Young (1972) conducted one of the early empirical studies on the linkage between FX and stock markets. Results suggested that there was no significant interaction between these two markets. Agarwal (1981) propounded a positive correlation between stock and exchange rate markets; however, the relation was coincidental rather than predictive. Since then, numerous scholars have evaluated this relationship through different perspectives, but results vary due to the employed statistical approach, data, and its respective time frame. Considering this issue from within the Turkish context, we observe several studies that provide valuable insights into the interaction between these two markets. Yücel and Kurt (2003) applied OLS regression on the monthly data comprising export volume and stock returns of listed firms, along with exchange rate. Their findings suggest that exposure to foreign risk varies across firms, and currency depreciation leads to an increase in firm value. Kasman (2003) used Granger causality tests on daily closing values of aggregate sector indices, and exchange rates. They found that a long-run relationship exists, but significant Granger causality only runs from the exchange rate toward the industrial sector index. Aydemir and Demirhan (2009) analyzed the relation between TL and individual indices (technology, industry, financial, services, and national index) and proposed a significant presence of a bi-directional effect between the two markets. Altin (2014) applied the Johansen Cointegration Test on daily closing prices of exchange rates and stock index for the period 2001-2013 and found that while the effect runs from forex to stock index providing evidence of a clear long-term relationship between the two markets; however, it varies depending on the denominations of TL. Another option is to check for the embedding volatility between the two markets. Sensoy and Sobaci (2014) applied a dynamic hybrid model & penalized contrast functions on TL, interest rates, and Borsa Istanbul (BIST) 100 values to conclude that short-term volatility shocks generated in stocks, bonds, and FX markets possess an effect on dynamic correlations; however, this effect does not hold for an extended period. Aydin and Cavdar (2015) took exchange rate, gold prices, and stock index data for the period 2000-2014 for applying VAR & artificial neural network (ANN). Econometric forecasting obtained with ANN produced better results in comparison to VAR for predicting fluctuations in variables for the period 2015-2017. Demir (2019) used autoregressive dis-

tributive lag (ARDL) Bounds Test and error correction model on quarterly data of stock index, interest rate, portfolio investment flows, FDI flows, GDP, and oil price & GDP, exchange rate, portfolio inflows for the period 2003-2017. Their conclusion tells us that FDI had a positive impact on the stock market, whereas oil and interest rates affect it negatively. Tiryaki, Ceylan, and Erdoğan (2019) showed through nonlinear ARDL (NARDL) analysis that an appreciation in the real rate of TL causes a decrease in stock index returns, which is in line with the theory. He, Gokmenoglu, Kirikkaleli, and Rizvi (2021) studied the causality between exchange rates and stock index using the wavelet coherence approach. Both time and frequency domain results suggest that the direction and strength of causality vary over time and frequency domains. Additionally, they note that even though the relationship between exchange rates and stock markets possesses a theoretical foundation, the evidence lacks adequate econometric methods employed.

In this essay, we attempt to fill the gap in the literature by introducing a unique two-step approach. In the first stage, we decompose the nominal returns into separate intrinsic mode functions (IMFs) and a residual using a novel decomposition technique, complete ensemble empirical mode decomposition with adaptive noise (CEEMDAN). We used a fine-to-coarse algorithm to construct high and low-frequency components for the original time series. In the next step, we applied the cross-quantilogram (CQ) method, testing for possible dependence in conditional quantiles of returns' series. Tekin and Hatipoğlu (2017) used quantile regression on the Turkish stock market to test the effect of exchange rate and oil prices. The main difference between quantile regression and CQ is that in a regression framework, only the quantile of the dependent variable gets checked for predictability through independent variable(s). On the other hand, CQ measures predictability in the quantiles of both, that is, dependent and independent variables (Lyócsa, Vašaničová, & Litavcová, 2020). Our contribution holds in the difference of approach that we apply here, thereby supplementing the present literature. Our method to analyze the relationship relies on a two-stage process presented in the next section. Ordering of the essay is as follows: Section 2 sets forth the methodology used in the analysis. Section 3 describes data and estimation results. Section 4 presents the discussion, policy implications, and summary of the results.

3.2 METHODOLOGY

3.2.1 CEEMDAN Method

3.2.1.1 EMD

Based on the spirit of the Fourier transform, the empirical mode decomposition (EMD) method introduced by Huang et al. (1998) is a nucleus of the Hilbert-Huang transform (HHT). It plainly is a signal processing technique that decomposes a complex signal into finite functions known as IMFs. These are signals at different time scales. Consider $X(t)$ to be a signal with the following representation:

$$X(t) = \sum_{i=1}^{n} IMF_i(t) + \varepsilon_n(t) \tag{3.1}$$

where $\varepsilon_n(t)$ is extracted residual of the signal. EMD can be defined in the following steps:

1. Considering the signal $X(t)$ and its local extrema, lower and upper envelopes are found by fitting a cubic spline function.
2. Let $fm(t)$ be the local mean of the lower and upper envelopes, the curve of this local mean and the difference between the original signal and local mean is the first residue (ε_1) and IMF_1, respectively.
3. The above steps are repeated until the residue $\varepsilon(t)$ becomes a constant or monotonic function.

3.2.1.2 EEMD

To counter mode mixing, Huang et al. (1998) used ensemble empirical mode decomposition (EEMD), which is adding Gaussian white noise to the original series and then performing EMD.[3] Steps are given below:

1. Add noise component $n_j(t)$ to the signal $X(t)$.
2. Perform EMD to get IMF component $K_{i,j}(t)$, which is j^{th} component at the i^{th} time.
3. Repeat the above steps for N times, adding different noises each time.

[3]It refers to the situation where an IMF contains the signals of another IMF.

4. After decomposing IMFs N times, the resulting mean value is considered to be the final IMF:

$$K_j(t) = \frac{1}{N}\sum_{i=1}^{N} K_{i,j}(i = 1,2,...,N_j = 1,2,...,K) \tag{3.2}$$

3.2.1.3 CEEMDAN

Torres, Colominas, Schlotthauer, and Flandrin (2011) proposed that EEMD could not eliminate the white noise error after computation and therefore put forward another method CEEMDAN. It follows the following steps:

1. First IMF and residue are obtained as in EMD, then the second IMF and the corresponding residue are given by:

$$\begin{aligned} \overline{IMF_2}(t) &= \frac{1}{N}\sum_{i=1}^{N} E_1(\varepsilon_t(t) + \tau_1 E_1(w_i(t))) \\ \varepsilon_2(t) &= \varepsilon_1(t) - \overline{IMF_2}(t) \end{aligned} \tag{3.3}$$

where E_1 is IMF1 and τ_1 is signal-to-noise ratio.

2. Similarly k^{th} IMF and ε_n can be taken as:

$$\begin{aligned} \overline{IMF_k}(t) &= \frac{1}{N}\sum_{i=1}^{N} E_1(\varepsilon_{n-1}(t) + \tau_{k-1} E_{k-1}(w_i(t))) \\ \varepsilon_k(t) &= \varepsilon_{k-1}(t) - \overline{IMF_k}(t) \end{aligned} \tag{3.4}$$

3. Above process carries on until the ending criterion is met by residual ε_n. Finally, the original signal can be obtained as:

$$X(t) = \sum_{i=1}^{M} \overline{IMF_i}(t) + \varepsilon(t) \tag{3.5}$$

where $\varepsilon(t)$ is the residual signal.

Cao, Li, and Li (2019) combined the estimation power of CEEMDAN with neural networks to generate one-step-ahead forecasts for major global indices.

3.2.2 Fine-to-Coarse Algorithm

We follow Yang, Sun, and Wang (2020) to construct high and low-frequency components from IMFs.[4] Following steps summarize our process:

1. Keep adding $IMF_1(t)$ to $IMF_i(t)$ for each component except residual.
2. Perform the Jarque-Bera (JB) test on each step.
3. Perform the Wilcoxon rank sum (WRS) test and check for which i the median departs significantly from 0.
4. Set i identified in step 3 as a breakpoint.
5. All IMFs until point i are considered high-frequency components, whereas the rest of the IMFs are taken as a low-frequency element of the original signal.

3.2.3 CQ Method

Han, Linton, Oka, and Whang (2016) developed a method that measures the cross-quantile dependence of the two time series. Let $\{y_{i,t}, t \in z, i = 1,2$ be a bidimensional time series.[5] We define $y_{1,t}$ and $y_{2,t}$ as TL and BIST returns, respectively. Denoting $F_i(\cdot)$ as the distribution function of $y_{i,t}$ having density function $f_i(\cdot)$, corresponding conditional quantile function can be represented as $q_i(B_i) = inf\{v : F_i(v) \geq \beta_i\}$ for $\beta_i \in (0,1)$. The range of quantiles we require is denoted by $\tilde{\beta}$, assuming $\tilde{\beta}$ is a Cartesian product of closed intervals (0,1) such that $\tilde{\beta} \equiv \tilde{\beta}_1 \times \tilde{\beta}_2$, where $\tilde{\beta}_i = [\beta_i, \bar{\beta}_i]$ for some $0 \leq \beta_i \leq \bar{\beta}_i \leq 1$.

For an arbitrary pair of quantiles, we consider a measure of serial dependence between two events $\{y_{1,t} \leq q_{1,t}(\beta_1)\}$ & $\{y_{2,t-k} \leq q_{2,t-k}(\beta_2)\}$. According to Han et al. (2016), $\{1[y_{i,t} \leq q_{i,t}[\cdot]]\}$ is called the quantile exceedance process or quantile-hit for $i = 1,2$. CQ is simply the cross-correlation of such processes and can be defined as:

$$\rho_\beta(k) = \frac{E[\Phi_{\beta_1}(y_{1,t} - q_{1,t}(\beta_1))\Phi_{\beta_2}(y_{2,t-k} - q_{2,t-k}(\beta_2))]}{\sqrt{E[\Phi^2_{\beta_1}(y_{1,t} - q_{1,t}(\beta_1))]}\sqrt{E[\Phi^2_{\beta_2}(y_{2,t-k} - q_{2,t-k}(\beta_2))]}} \tag{3.6}$$

[4] To construct separate components, we preferred the WRS test over the t-test used by X. Zhang, Lai, and Wang (2008) to overcome misspecifying normal distribution assumption of IMF sums.

[5] The process requires both time series to be strictly stationary.

for $k = 0, \pm 1, \pm 2, \ldots$, where $\Phi_\beta(\mu) \equiv 1[\mu \leq 0] - a$.[6] Unconditional quantile functions are estimated by minimizing two separate problems: $\hat{q}_1(\beta_1) = \arg\min_{v_1 \in R} \sum_{t=1}^{T} \pi_{\beta_1}(y_1 - v_1)$ and $\hat{q}_2(\beta_2) = \arg\min_{v_2 \in R} \sum_{t=1}^{T} \pi_{\beta_2}(y_2 - v_2)$ where $\pi_\beta(\mu) \equiv \mu(\alpha - 1[\mu \leq 0])$. Sample cross quantilogram is given as:

$$\hat{\rho}_\beta(k) = \frac{\sum_{t=k+1}^{T} \Phi_{\beta_1}(y_{1,t} - \hat{q}_{1,t}(\beta_1)) \Phi_{\beta_2}(y_{2,t-k} - \hat{q}_{2,t-k}(\beta_2))}{\sqrt{\sum_{t=k+1}^{T} \Phi^2_{\beta_1}(y_{1,t} - \hat{q}_{1,t}(\beta_1))} \sqrt{\Phi^2_{\beta_2}(y_{2,t-k} - \hat{q}_{2,t-k}(\beta_2))}} \tag{3.7}$$

for $k = 0, \pm 1, \pm 2, \ldots, \hat{\Phi}_\beta(k) \in [-1, 1]$. Here we are interested in testing null hypothesis: $\hat{\Phi}_\beta(k) = 0$ (indicates no directional predictability) against alternative $\hat{\Phi}_\beta(k) \neq 0$ (corresponding to the presence of directional predictability). Han et al. (2016) proposed a stationary bootstrap procedure to construct confidence interval bands around estimated values. In this essay, we opt for a Box-Ljung portmanteau test $\hat{Q}^p_\beta = T(T+2)\sum_{k=1}^{p} \hat{\Phi}^2_\beta(k)/(T-k)$.[7]

3.3 ESTIMATION

3.3.1 Data

Our data sample comprises closing prices of the USD/TRY exchange rate and the BIST 100 index taken over the period January 2005 and October 2022.[8] We use daily log differences of closing prices as returns R_t.[9] We report summary statistics and unit root tests for both returns in Table C.1.1. While both series are not normally distributed, ADF and PP tests suggest the absence of unit roots within both financial returns at levels. The correlation between the two asset returns is given in Figure C.2.1. The top right panel shows the Pearson correlation coefficient along with test significance. Both asset returns move in an opposite direction with a moderate correlation.

[6] CQ is defined for a bivariate process. For the analysis of a single series, the process is simply a quantilogram of Linton and Whang (2007).

[7] In practice, the Box-Ljung version is preferred due to its superior performance for a small sample and a large p (Cho & Han, 2021).

[8] For creating a matching sample for the two series, we remove missing dates so that both returns are synced.

[9] $R_t = 100 * log(P_t/P_{t-1})$, where P_t is the price at time t.

3.3.2 Results

3.3.2.1 CEEMDAN

We decompose both asset returns using the CEEMDAN algorithm. With an ensemble size of 100, each member estimated contained additional white noise with a standard deviation of 0.3.[10] In Figures C.2.2 and C.2.3, we plot IMFs extracted through signal processing. Frequencies with sharp fluctuations are apparent in initial functions but gradually smoothed into low amplitudes. The last frequency carries residue, which we consider as the long-term trend for financial returns. Statistics for IMFs of TL and BIST returns are given in Tables C.1.2 and C.1.3, respectively. We report the correlation between the original series and obtained IMFs with: Pearson's and Kendall's coefficients. Let us first consider FX returns. A highly significant correlation exists between IMFs and returns, with decreasing magnitude as we move towards higher IMFs. Variance as a sum of IMFs & residual reported in the last column is suggestive that the first three IMFs account for over 81% of the total variance. It highlights the importance of short-term fluctuations. If we observe stock returns, a similar pattern is clear. Correlation is gradually declining, from IMF 1 to IMF 11 though almost all values are significant. Like FX returns, the sum of the variance of the first 3 IMFs explains around 80% of the total variance. Hence, short-term fluctuations are crucial for stock returns as well. The shortest mean period for both assets is around 2.7 days.

3.3.2.2 Fine-to-Coarse

Following Yang et al. (2020) and as detailed in subsection 3.2.2, we use the fine-to-coarse algorithm to reconstruct high-frequency and low-frequency components from IMFs obtained previously. Table C.1.4 reports estimation results. JB test results find significant non-normality in IMFs of both asset returns. Then we use the WRS test to identify the median departing significantly from zero. Test statistics for FX returns started to be statistically significant at acceptable levels from IMF 5 and onwards, whereas, in the case of stock returns, IMF 7 is the index i. Therefore as high-frequency components, we use the sum of IMFs 1-4 for the exchange rate; and the sum of IMFs 1-6 for stock index returns. The sum of all remaining IMFs is used as

[10] In their original paper, Huang et al. (1998) defined two conditions that an IMF must satisfy, our obtained functions fulfill both the conditions. For details, readers are referred to section 4 of their paper.

a low-frequency component, whereas, the residual is the long-term trend for both series. To show the phenomenon visually, we plot only last year's values containing the original series and estimated components in Figures C.2.4 and C.2.5.

3.3.2.3 CQ Analysis

For comprehension, we present our results through CQ plots and heat maps. We subdivide this section into two parts. First, we present predictability directed from TL returns toward BIST returns for all components. In the second part, we provide the possible linkage moving in the opposite direction, i.e., from BIST to TL returns. We provide sample CQ $\hat{\rho}_{\beta}(k)$ and portmanteau test $\hat{Q}_{\beta}^{p}$ for possible dependence in tails of both returns so that we'll be able to infer how extreme events impact returns in the other market. Precisely, we consider $\beta_1 = 0.1, 0.9$ and $\beta_2 = 0.1, 0.9$ for the quantiles. We also checked for an effect on the median quantile, i.e., when $\beta = 0.5$ but, for brevity, results are not reported.[11] To summarize the effect in median returns, significant directional predictability in both directions exists only in the first few lags of the low-frequency component.

Exchange rate to stock index: In Figures C.2.6(a)-C.2.6(c), we plot predictability from the exchange rate to the stock index. We also show 95% confidence interval bootstrap values based on 1000 replicates testing the null hypothesis of no directional predictability. Consider the case when β_2 and $\beta_1 = 0.1$, CQ is not significant for many lags given through the portmanteau test for 60 lags. It means that high loss in TL failed to predict greater negative returns in BIST. When $\beta_1 = 0.9$, CQ is negative but mostly insignificant. This result suggests that high losses in TL returns do not facilitate significant prediction in tail returns of BIST. Fig. C.2.6(b) presents CQ when $\beta_2 = 0.9$. It shows significance but only in the initial lags. The implication is that when TL is higher than its 0.9 quantiles, there is a likelihood of a large loss in BIST returns within the first few days. For $\beta_1 = 0.9$, CQ is positive and significant for the initial lags implying that there is a chance of a high positive return in BIST when TL is in a high quantile. However, the magnitude of the correlation is not too strong. Fig. C.2.6(c) plots the CQ heatmap of directional predictability with one day lag for all quantiles. A star in the box means the significance of the portmanteau test. As noted before, even though there

[11] Results can be shared upon request.

is some correlation, it may not be considered evidence of strong directional predictability.

In Figures C.2.7(a)-C.2.7(c), we plot the high-frequency component of the returns. The outcomes are very close to the results of the original series. There exists some dependence, but only in the first few lags and when TL is in a high quantile. It shows weak evidence of directional predictability. It is expected since the results obtained in the previous section showed that initial IMFs explain most of the variance present in the original series. When TL is lower than its 0.1 quantiles, the CQ is insignificant for the low-frequency component plotted in Figures C.2.8(a)-C.2.8(c). In addition to that, most of the lags are not significant when TL is in its quantile 0.9. It suggests that the tail returns of TL's low-frequency component do not help in predicting the tail returns of BIST's low-frequency component.

Stock index to exchange rate: In Figures C.2.9 (a)-C.2.9 (c), we show estimation results of directional predictability of returns from BIST to TL. Figure C.2.9 (a) presents $q_1(\beta_1) = 0.1$, which is when BIST returns are in low quantile. When β_2=0.1, the CQ plot is positive and significant for most lags, implying that when BIST returns are negative, it is likely to have a high negative return in the TL market. Similarly, when $\beta_2 = 0.9$, CQ is negative and significant in most lags suggesting a large gain in TL returns. The portmanteau test confirms this relation. Figure C.2.9 (b) presents a scenario when $q_1(\beta_1) = 0.9$, which is when BIST returns are within a high quantile. Considering $\beta_2 = 0.1$, sample CQ is mainly negative and significant for some lags, providing evidence that there is a chance of having a high loss in TL returns. Likewise, when $\beta_2 = 0.9$, CQ bars are positive but mostly insignificant for almost all lags, suggesting a low likelihood of having a high positive gain. Heatmap given in Fig. C.2.9 (c) shows strong directional predictability in the returns from BIST to TL in almost all quantiles with one day lag. Another observation to note here is that, compared to the effect from TL to BIST, the correlation is relatively higher in most quantiles. Like the case with high-frequency dependability from TL to BIST, here we notice a similar pattern plotted in Figures C.2.10 (a)-C.2.10 (c). High-frequency component results are akin to the return series results. It implies that BIST tail returns in high frequency provide significant predictability for the tail returns of TL. However, the effect is not significantly strong for all lags. As far as low-frequency dependence is concerned, it does not provide significant connectivity from

BIST to TL plotted in Figures C.2.11 (a)-C.2.11 (c).

3.3.2.4 Rolling Window Analysis

Based on the results that we obtained in the previous sections, it is quite evident that directional predictability is stronger from BIST to TL returns, and within components, the high-frequency component reveals more information compared to the low-frequency component. We decided to explore how this relationship has evolved over the period under analysis. For this purpose, we used a one-year rolling window analysis to check if any irregular movements may provide us with some further insights. Here we plot dependence in tails that is $\beta_1 = \beta_2 = 0.1, 0.9$ and $k = 1$ for the years $2005, ..., 2022$. Considering returns in the lower tail, Figure C.2.12 shows that dependence was significantly high until around 2009, after which it mostly stayed constant throughout the whole sample under analysis. Moving towards the opposite direction, i.e., on the other side of the tail, we see that it has remained rather calm with no significant peaks and troughs; however, post-2020, it slightly increased but reverted towards its mean trajectory. This behavior can be accredited to the extreme jump in TL's nominal rate gesturing to a weakening of the currency. A similar pattern is obvious for the high-frequency component of the returns plotted in Fig. C.2.13.

3.4 DISCUSSION & CONCLUSION

In this essay, we analyzed the returns of TL and BIST-100 through a two-stage process. In the first part of the process, we use the CEEMDAN algorithm to decompose individual nominal returns into separate IMFs and a residual. Then we applied a fine-to-coarse algorithm aided by the WRS test to obtain high and low-frequency components of returns. Both these components could be interpreted as short-term and long-term fluctuations, respectively. As suggested by Yang et al. (2020), the short-term component's attribution may be due to investor sentiments, and the long-term movements could be due to fundamentals such as supply and demand, interest rates, inflation, economic growth, and current account, among others. In the second stage, we used CQ analysis to check for tail dependency in conditional quantiles of original returns and components constructed in the previous phase.

These results could be of great importance not only to policymakers but also to other market participants. For instance, our inference based on tail

dependence present between two return series could be used as further insight into hedging behavior especially, when any of the markets is in its bearish or bullish state. Another implication from observing individual components is that market sentiment is of greater importance in determining the market prices than long-term fundamentals since it explains most of the variance out of the total variance observed. Even though low-frequency fluctuations moved in opposite directions confirming the theoretical relation, it was not found to be highly significant in the explanation of tail dependence. Finally, as far as directional predictability is concerned, BIST returns have relatively more influence on TL returns than the other way around.

Future work could incorporate additional causality methods to provide further evidence of dependence. In addition, since the technique employed in this essay only allows for a bi-directional relationship, which constrains the use of other variables, econometricians could extend this method into higher domains, hence allowing the inclusion of additional information into the analysis.

References

Agarwal, R. (1981). Exchange rate and stock prices: A study of us capital markets under floating exchange rate. *Akron Business and Economics Review*, *12*(2), 7–12.

Akar, C., & Çiçek, S. (2016). "new" monetary policy instruments and exchange rate volatility. *Empirica*, *43*(1), 141–165.

Akgül, I., & Sayyan, H. (2008). Modelling and forecasting long memory in exchange rate volatility vs. stable and integrated garch models. *Applied Financial Economics*, *18*(6), 463–483.

Aloui, C. (2007). Price and volatility spillovers between exchange rates and stock indexes for the pre-and post-euro period. *Quantitative finance*, *7*(6), 669–685.

Altin, H. (2014). Stock price and exchange rate: the case of bist 100. *European Scientific Journal*, *10*(16).

Andersen, T. G., Bollerslev, T., & Diebold, F. X. (2007). Roughing it up: Including jump components in the measurement, modeling, and forecasting of return volatility. *The review of economics and statistics*, *89*(4), 701–720.

Asimakopoulos, I., Ayling, D., & Mahmood, W. M. (2000). Non-linear granger causality in the currency futures returns. *Economics Letters*, *68*(1), 25–30.

AuYong, H. H., Gan, C., & Treepongkaruna, S. (2004). Cointegration and causality in the asian and emerging foreign exchange markets: Evidence from the 1990s financial crises. *International Review of Financial Analysis*, *13*(4), 479–515.

Aydemir, O., & Demirhan, E. (2009). The relationship between stock prices and exchange rates: Evidence from turkey. *International research journal of finance and economics*, *23*(2), 207–215.

Aydin, A. D., & Cavdar, S. C. (2015). Comparison of prediction performances of artificial neural network (ann) and vector autoregressive (var) models by using the macroeconomic variables of gold prices, borsa istanbul (bist) 100 index and us dollar-turkish lira (usd/try) exchange rates. *Procedia Economics and Finance*, *30*, 3–14.

Bahmani-Oskooee, M., & Durmaz, N. (2016). Exchange rate volatility and turkish commodity trade with the rest of the world. *Economic Change and Restructuring*, *49*, 1–21.

Bahmani-Oskooee, M., & Durmaz, N. (2021). Exchange rate volatility and turkey–eu

commodity trade: An asymmetry analysis. *Empirica*, *48*(2), 429–482.

Bajo-Rubio, O., Berke, B., & McMillan, D. (2017). The behaviour of asset return and volatility spillovers in turkey: A tale of two crises. *Research in International Business and Finance*, *41*, 577–589.

Ball, R., & Brown, P. (1968). An empirical evaluation of accounting income numbers. *Journal of accounting research*, 159–178.

Barndorff-Nielsen, O. E., & Shephard, N. (2004). Power and bipower variation with stochastic volatility and jumps. *Journal of financial econometrics*, *2*(1), 1–37.

Barndorff-Nielsen, O. E., & Shephard, N. (2006). Econometrics of testing for jumps in financial economics using bipower variation. *Journal of financial Econometrics*, *4*(1), 1–30.

Barunik, J., Kocenda, E., & Vacha, L. (2017). Asymmetric volatility connectedness on the forex market. *Journal of International Money and Finance*, *77*, 39–56.

Baruník, J., & Křehlík, T. (2018). Measuring the frequency dynamics of financial connectedness and systemic risk. *Journal of Financial Econometrics*, *16*(2), 271–296.

Berument, H., Coskun, M. N., & Sahin, A. (2007). Day of the week effect on foreign exchange market volatility: Evidence from turkey. *Research in International Business and Finance*, *21*(1), 87–97.

Bilgin, M. H., Demir, E., Gozgor, G., Karabulut, G., & Kaya, H. (2019). A novel index of macroeconomic uncertainty for turkey based on google-trends. *Economics Letters*, *184*, 108601.

Bollerslev, T. (1986). Generalized autoregressive conditional heteroskedasticity. *Journal of econometrics*, *31*(3), 307–327.

Bollerslev, T., Patton, A. J., & Quaedvlieg, R. (2016). Exploiting the errors: A simple approach for improved volatility forecasting. *Journal of Econometrics*, *192*(1), 1–18.

Boser, B. E., Guyon, I. M., & Vapnik, V. N. (1992). A training algorithm for optimal margin classifiers. In *Proceedings of the fifth annual workshop on computational learning theory* (pp. 144–152).

Branson, W. H. (1981, November). *Macroeconomic determinants of real exchange rates* (Working Paper No. 801). National Bureau of Economic Research. Retrieved from `http://www.nber.org/papers/w0801` doi: 10.3386/w0801

Branson, W. H., & Henderson, D. W. (1985). The specification and influence of asset markets. *Handbook of international economics*, *2*, 749–805.

Cao, J., Li, Z., & Li, J. (2019). Financial time series forecasting model based on ceemdan and lstm. *Physica A: Statistical mechanics and its applications*, *519*, 127–139.

Cho, D., & Han, H. (2021). The tail behavior of safe haven currencies: A cross-

quantilogram analysis. *Journal of International Financial Markets, Institutions and Money*, *70*, 101257.

Chou, R. Y. (2005). Forecasting financial volatilities with extreme values: the conditional autoregressive range (carr) model. *Journal of Money, Credit and Banking*, 561–582.

Ciner, C. (2011). Information transmission across currency futures markets: Evidence from frequency domain tests. *International Review of Financial Analysis*, *20*(3), 134–139.

Conrad, C., Custovic, A., & Ghysels, E. (2018). Long-and short-term cryptocurrency volatility components: A garch-midas analysis. *Journal of Risk and Financial Management*, *11*(2), 23.

Corsi, F. (2009). A simple approximate long-memory model of realized volatility. *Journal of Financial Econometrics*, *7*(2), 174–196.

Creal, D., Koopman, S. J., & Lucas, A. (2013). Generalized autoregressive score models with applications. *Journal of Applied Econometrics*, *28*(5), 777–795.

Dedi, L., & Yavas, B. F. (2016). Return and volatility spillovers in equity markets: An investigation using various garch methodologies. *Cogent Economics & Finance*, *4*(1), 1266788.

Demir, C. (2019). Macroeconomic determinants of stock market fluctuations: The case of bist-100. *Economies*, *7*(1), 8.

Diebold, F. X., & Yilmaz, K. (2009). Measuring financial asset return and volatility spillovers, with application to global equity markets. *The Economic Journal*, *119*(534), 158–171.

Diebold, F. X., & Yilmaz, K. (2012). Better to give than to receive: Predictive directional measurement of volatility spillovers. *International Journal of forecasting*, *28*(1), 57–66.

Ding, Z., Granger, C. W., & Engle, R. F. (1993). A long memory property of stock market returns and a new model. *Journal of empirical finance*, *1*(1), 83–106.

Dornbusch, R., & Fischer, S. (1980). Exchange rates and the current account. *The American economic review*, *70*(5), 960–971.

Engle, R. F. (1982). Autoregressive conditional heteroscedasticity with estimates of the variance of united kingdom inflation. *Econometrica: Journal of the econometric society*, 987–1007.

Engle, R. F., Ghysels, E., & Sohn, B. (2013). Stock market volatility and macroeconomic fundamentals. *Review of Economics and Statistics*, *95*(3), 776–797.

Engle, R. F., & Lee, G. (1999). A long-run and short-run component model of stock return volatility. *Cointegration, causality, and forecasting: A Festschrift in honour*

of Clive WJ Granger, 475–497.

Engle, R. F., & Ng, V. K. (1993). Measuring and testing the impact of news on volatility. *The journal of finance*, *48*(5), 1749–1778.

Engle, R. F., & Russell, J. R. (1998). Autoregressive conditional duration: a new model for irregularly spaced transaction data. *Econometrica*, 1127–1162.

Engle III, R. F., Ito, T., & Lin, W.-L. (1988). *Meteor showers or heat waves? heteroskedastic intra-daily volatility in the foreign exchange market.* National Bureau of Economic Research Cambridge, Mass., USA.

Erdem, C., Arslan, C. K., & Sema Erdem, M. (2005). Effects of macroeconomic variables on istanbul stock exchange indexes. *Applied Financial Economics*, *15*(14), 987–994.

Fedorova, E., & Saleem, K. (2009). Volatility spillovers between stock and currency markets: Evidence from emerging eastern europe. In *22nd australasian finance and banking conference.*

Franck, P., & Young, A. (1972). Stock price reaction of multinational firms to exchange realignments. *Financial Management*, 66–73.

Frenkel, J. A. (1976). A monetary approach to the exchange rate: Doctrinal aspects and empirical evidence. *The Scandinavian Journal of Economics*, 200–224.

Fung, H.-G., & Patterson, G. A. (1999). Volatility linkage among currency futures markets during us trading and non-trading periods. *Journal of Multinational Financial Management*, *9*(2), 129–153.

Glosten, L. R., Jagannathan, R., & Runkle, D. E. (1993). On the relation between the expected value and the volatility of the nominal excess return on stocks. *The journal of finance*, *48*(5), 1779–1801.

Gökbulut, R. İ., & Pekkaya, M. (2014). Estimating and forecasting volatility of financial markets using asymmetric garch models: An application on turkish financial markets. *International Journal of Economics and Finance*, *6*(4), 23–35.

Greenwood-Nimmo, M., Nguyen, V. H., & Rafferty, B. (2016). Risk and return spillovers among the g10 currencies. *Journal of Financial Markets*, *31*, 43–62.

Han, H., Linton, O., Oka, T., & Whang, Y.-J. (2016). The cross-quantilogram: Measuring quantile dependence and testing directional predictability between time series. *Journal of Econometrics*, *193*(1), 251–270.

Harvey, A. C. (2013). *Dynamic models for volatility and heavy tails: with applications to financial and economic time series* (Vol. 52). Cambridge University Press.

He, X., Gokmenoglu, K. K., Kirikkaleli, D., & Rizvi, S. K. A. (2021). Co-movement of foreign exchange rate returns and stock market returns in an emerging market: Evidence from the wavelet coherence approach. *International Journal of Finance*

& Economics.

Hentschel, L. (1995). All in the family nesting symmetric and asymmetric garch models. *Journal of financial economics*, *39*(1), 71–104.

Higgins, M. L., & Bera, A. K. (1992). A class of nonlinear arch models. *International Economic Review*, 137–158.

Hoesli, M., & Reka, K. (2013). Volatility spillovers, comovements and contagion in securitized real estate markets. *The Journal of Real Estate Finance and Economics*, *47*(1), 1–35.

Hosszejni, D., & Kastner, G. (2018). Approaches toward the bayesian estimation of the stochastic volatility model with leverage. In *International conference on bayesian statistics in action* (pp. 75–83).

Huang, N. E., Shen, Z., Long, S. R., Wu, M. C., Shih, H. H., Zheng, Q., ... Liu, H. H. (1998). The empirical mode decomposition and the hilbert spectrum for nonlinear and non-stationary time series analysis. *Proceedings of the Royal Society of London. Series A: mathematical, physical and engineering sciences*, *454*(1971), 903–995.

Ji, Q., Liu, B.-Y., & Fan, Y. (2019). Risk dependence of covar and structural change between oil prices and exchange rates: A time-varying copula model. *Energy Economics*, *77*, 80–92.

Junior, P. O., Tiwari, A. K., Tweneboah, G., & Asafo-Adjei, E. (2022). Gas and garch based value-at-risk modeling of precious metals. *Resources Policy*, *75*, 102456.

Kasman, S. (2003). The relationship between exchange rates and stock prices: A causality analysis. *Dokuz Eylül Üniversitesi Sosyal Bilimler Enstitüsü Dergisi*, *5*(2), 70–79.

Kasman, S., Vardar, G., & Tunç, G. (2011). The impact of interest rate and exchange rate volatility on banks' stock returns and volatility: Evidence from turkey. *Economic Modelling*, *28*(3), 1328–1334.

Kastner, G. (2016). Dealing with stochastic volatility in time series using the r package stochvol. *Journal of Statistical Software*, *69*(5), 1–30. Retrieved from `https://www.jstatsoft.org/index.php/jss/article/view/v069i05` doi: 10.18637/jss.v069.i05

Kastner, G. (2019). Dealing with stochastic volatility in time series using the r package stochvol. *arXiv preprint arXiv:1906.12134*.

Kastner, G., & Frühwirth-Schnatter, S. (2014). Ancillarity-sufficiency interweaving strategy (asis) for boosting mcmc estimation of stochastic volatility models. *Computational Statistics & Data Analysis*, *76*, 408–423.

Kim, S., Shephard, N., & Chib, S. (1998). Stochastic volatility: likelihood inference and comparison with arch models. *The review of economic studies*, *65*(3), 361–393.

Koop, G., Pesaran, M. H., & Potter, S. M. (1996). Impulse response analysis in nonlinear multivariate models. *Journal of econometrics*, *74*(1), 119–147.

Kumar, A. S., & Anandarao, S. (2019). Volatility spillover in crypto-currency markets: Some evidences from garch and wavelet analysis. *Physica A: Statistical Mechanics and its Applications*, *524*, 448–458.

Kumar, S. (2016). Evidence of information transmission across currency futures markets using frequency domain tests. *The North American Journal of Economics and Finance*, *37*, 319–327.

Laurini, M. P., & Mauad, R. B. (2015). A common jump factor stochastic volatility model. *Finance Research Letters*, *12*, 2–10.

Lee, G. G., & Engle, R. F. (1993). A permanent and transitory component model of stock return volatility. *Available at SSRN 5848*.

Lin, A. J., Chang, H. Y., & Hsiao, J. L. (2019). Does the baltic dry index drive volatility spillovers in the commodities, currency, or stock markets? *Transportation Research Part E: Logistics and Transportation Review*, *127*, 265–283.

Linton, O., & Whang, Y.-J. (2007). The quantilogram: With an application to evaluating directional predictability. *Journal of Econometrics*, *141*(1), 250–282.

Lyócsa, Š., Vašaničová, P., & Litavcová, E. (2020). Quantile dependence of tourism activity between southern european countries. *Applied Economics Letters*, *27*(3), 206–212.

MacDonald, R., & Marsh, I. W. (2004). Currency spillovers and tri-polarity: a simultaneous model of the us dollar, german mark and japanese yen. *Journal of International Money and Finance*, *23*(1), 99–111.

Macdonald, R., & Taylor, M. P. (1992). Exchange rate economics: A survey. *Staff Papers (International Monetary Fund)*, *39*(1), 1–57. Retrieved 2023-04-15, from `http://www.jstor.org/stable/3867200`

MATLAB version 9.6.0.1150989 (R2019a) Update 4. (2019). Natick, Massachusetts.

McMillan, D. G., & Speight, A. E. (2010). Return and volatility spillovers in three euro exchange rates. *Journal of Economics and Business*, *62*(2), 79–93.

Mechri, N., Ben Hamad, S., de PERETTI, C., & Charfi, S. (2018). The impact of the exchange rate volatilities on stock markets dynamics: Evidence from tunisia and turkey. *Christian and Charfi, Sahar, The Impact of the Exchange Rate Volatilities on Stock Markets Dynamics: Evidence from Tunisia and Turkey (September 19, 2018)*.

Mensi, W., Hammoudeh, S., Shahzad, S. J. H., Al-Yahyaee, K. H., & Shahbaz, M. (2017). Oil and foreign exchange market tail dependence and risk spillovers for mena, emerging and developed countries: Vmd decomposition based copulas. *Energy*

economics, *67*, 476–495.

Mozumder, N., De Vita, G., Kyaw, S., & Larkin, C. (2015). Volatility spillover between stock prices and exchange rates: New evidence across the recent financial crisis period. *Economic Issues*, *20*(1), 43–64.

Müller, U. A., Dacorogna, M. M., Davé, R. D., Pictet, O. V., Olsen, R. B., & Ward, J. R. (1993). Fractals and intrinsic time: A challenge to econometricians. *Unpublished manuscript, Olsen & Associates, Zürich*, *130*.

Nakajima, J., & Omori, Y. (2009). Leverage, heavy-tails and correlated jumps in stochastic volatility models. *Computational Statistics & Data Analysis*, *53*(6), 2335–2353.

Nazlioglu, S. (2013). Exchange rate volatility and turkish industry-level export: Panel cointegration analysis. *The Journal of International Trade & Economic Development*, *22*(7), 1088–1107.

Nelson, D. B. (1991). Conditional heteroskedasticity in asset returns: A new approach. *Econometrica: Journal of the econometric society*, 347–370.

Nwogugu, M. (2006). Further critique of garch/arma/var/evt stochastic-volatility models and related approaches. *Applied mathematics and computation*, *182*(2), 1735–1748.

Omori, Y., Chib, S., Shephard, N., & Nakajima, J. (2007). Stochastic volatility with leverage: Fast and efficient likelihood inference. *Journal of Econometrics*, *140*(2), 425–449.

Parkinson, M. (1980). The extreme value method for estimating the variance of the rate of return. *Journal of business*, 61–65.

Pérez-Cruz, F., Afonso-Rodriguez, J. A., & Giner, J. (2003). Estimating garch models using support vector machines. *Quantitative Finance*, *3*(3), 163.

Pesaran, H. H., & Shin, Y. (1998). Generalized impulse response analysis in linear multivariate models. *Economics letters*, *58*(1), 17–29.

Poon, S.-H., & Granger, C. W. (2003). Forecasting volatility in financial markets: A review. *Journal of economic literature*, *41*(2), 478–539.

R Core Team. (2021). R: A language and environment for statistical computing [Computer software manual]. Vienna, Austria. Retrieved from `https://www.R-project.org/`

Rahman, M. L., & Uddin, J. (2009). Dynamic relationship between stock prices and exchange rates: Evidence from three south asian countries. *International Business Research*, *2*(2), 167–174.

Reboredo, J. C., Rivera-Castro, M. A., & Ugolini, A. (2016). Downside and upside risk spillovers between exchange rates and stock prices. *Journal of Banking & Finance*, *62*, 76–96.

Sabri, R., Abdul Rahman, A. A., Meero, A., Abro, L. A., & AsadUllah, M. (2022). Forecasting turkish lira against the us dollars via forecasting approaches. *Cogent Economics & Finance*, *10*(1), 2049478.

Schölkopf, B., Smola, A. J., Williamson, R. C., & Bartlett, P. L. (2000). New support vector algorithms. *Neural computation*, *12*(5), 1207–1245.

Schwert, G. W. (1990). Stock volatility and the crash of'87. *The review of financial studies*, *3*(1), 77–102.

Sehgal, S., Ahmad, W., & Deisting, F. (2015). An investigation of price discovery and volatility spillovers in india's foreign exchange market. *Journal of Economic Studies*.

Sensoy, A., & Serdengeçti, S. (2019). Intraday volume-volatility nexus in the fx markets: Evidence from an emerging market. *International Review of Financial Analysis*, *64*, 1–12.

Sensoy, A., & Sobaci, C. (2014). Effects of volatility shocks on the dynamic linkages between exchange rate, interest rate and the stock market: The case of turkey. *Economic Modelling*, *43*, 448–457.

Taskinsoy, J. (2019). Turkish lira–a fiat currency that resembles the volatility of cryptocurrencies: the effects of exchange rate volatility on turkish economy. *Available at SSRN 3335545*.

Taylor, S. J. (1982). Financial returns modelled by the product of two stochastic processes-a study of the daily sugar prices 1961-75. *Time series analysis: theory and practice*, *1*, 203–226.

Tekin, B., & Hatipoğlu, M. (2017). The effects of vix index, exchange rate & oil prices on the bist 100 index: A quantile regression approach. *Tekin, B, Hatipoğlu, M.(2017). The Effects of VIX Index, Exchange Rate & Oil Prices on the BIST*, *100*, 627–634.

Tiryaki, A., Ceylan, R., & Erdoğan, L. (2019). Asymmetric effects of industrial production, money supply and exchange rate changes on stock returns in turkey. *Applied Economics*, *51*(20), 2143–2154.

Torres, M. E., Colominas, M. A., Schlotthauer, G., & Flandrin, P. (2011). A complete ensemble empirical mode decomposition with adaptive noise. In *2011 ieee international conference on acoustics, speech and signal processing (icassp)* (pp. 4144–4147).

Türkyılmaz, S., & Balıbey, M. (2013). The relationships among interest rate, exchange rate and stock price: A bekk-mgarch approach. *International Journal of Economics, Finance and Management Sciences*, *1*(3), 166–74.

Van Rossum, G., & Drake Jr, F. L. (1995). *Python reference manual*. Centrum voor Wiskunde en Informatica Amsterdam.

Vapnik, V. (1998). Statistical learning theory new york. *NY: Wiley*, *1*(2), 3.

Vardar, G., & Aydogan, B. (2019). Return and volatility spillovers between bitcoin and other asset classes in turkey: Evidence from var-bekk-garch approach. *EuroMed Journal of Business*.

Vergil, H. (2002). Exchange rate volatility in turkey and its effect on trade flows. *Journal of Economic & Social Research*, *4*(1).

Walid, C., Chaker, A., Masood, O., & Fry, J. (2011). Stock market volatility and exchange rates in emerging countries: A markov-state switching approach. *Emerging Markets Review*, *12*(3), 272–292.

Wang, J. J., Chan, J. S., & Choy, S. B. (2011). Stochastic volatility models with leverage and heavy-tailed distributions: A bayesian approach using scale mixtures. *Computational Statistics & Data Analysis*, *55*(1), 852–862.

Wen, D., Wang, Y., Ma, C., & Zhang, Y. (2020). Information transmission between gold and financial assets: Mean, volatility, or risk spillovers? *Resources Policy*, *69*, 101871.

Wu, X., & Hou, X. (2020). Forecasting volatility with component conditional autoregressive range model. *The North American Journal of Economics and Finance*, *51*, 101078.

Yang, B., Sun, Y., & Wang, S. (2020). A novel two-stage approach for cryptocurrency analysis. *International Review of Financial Analysis*, *72*, 101567.

Yu, J. (2005). On leverage in a stochastic volatility model. *Journal of Econometrics*, *127*(2), 165–178.

Yu, L., Zha, R., Stafylas, D., He, K., & Liu, J. (2020). Dependences and volatility spillovers between the oil and stock markets: New evidence from the copula and var-bekk-garch models. *International Review of Financial Analysis*, *68*, 101280.

Yücel, T., & Kurt, G. (2003). Foreign exchange rate sensitivity and stock price: estimating economic exposure of turkish companies. *European Trade Study Group, Madrid: www. etsg. org*.

Zakoian, J. (1994). Threshold heteroskedastic models. *Journal of Economic Dynamics and Control*, *18*(5), 931–955.

Zhang, D., & Broadstock, D. C. (2020). Global financial crisis and rising connectedness in the international commodity markets. *International Review of Financial Analysis*, *68*, 101239.

Zhang, X., Lai, K. K., & Wang, S.-Y. (2008). A new approach for crude oil price analysis based on empirical mode decomposition. *Energy economics*, *30*(3), 905–918.

Zhao, H. (2010). Dynamic relationship between exchange rate and stock price: Evidence from china. *Research in International Business and Finance*, *24*(2), 103–112.

Živkov, D., Njegić, J., & Pavlović, J. (2016). Dynamic correlation between stock returns and exchange rate and its dependence on the conditional volatilities–the case of several eastern european countries. *Bulletin of Economic Research*, *68*(S1), 28–41.

APPENDIX A

CHAPTER 1

A.1 TABLES

Table A.1.1
Summary statistics of currency futures
This table presents summary statistics of six currency futures for the period January 2001 to September 2021, including mean (Mean), median (Med), minimum (Min), maximum (Max), standard deviation (Sd), skewness (Skew), and kurtosis (Kurt). Numbers in the last two rows of each panel are *p-values* of Augmented Dickey-Fuller (ADF) and Phillips–Perron (PP) tests.

	EUR	JPY	GBP	AUD	CAD	CHF
Panel A: Volatility Series						
Mean	7.12E-04	0.04	7.18E-04	1.31E-03	6.55E-04	9.39E-04
Med	5.77E-04	9.82E-04	5.16E-04	8.14E-04	4.38E-04	6.20E-04
Min	8.22E-05	1.28E-04	6.14E-05	1.71E-04	8.82E-05	9.94E-05
Max	3.92E-03	10.49	9.44E-03	0.03	8.49E-03	0.03
Sd	5.64E-04	0.66	8.64E-04	2.42E-03	7.63E-04	1.94E-03
Skew	2.37	15.59	6.07	10.35	5.65	11.17
Kurt	7.86	242.02	47.95	132.26	47.33	145.56
ADF	0.01***	0.01***	0.01***	0.01***	0.07**	0.01***
PP	0.01***	0.01***	0.01***	0.01***	0.01***	0.01***
Panel B: Skewness Series						
Mean	-0.01	-0.05	-0.04	-0.1	0.01	0.05
Med	-0.01	2.31E-15	-0.03	-0.17	0.02	0.1
Min	-2.43	-4.69	-2.9	-1.86	-1.92	-3.52
Max	2.02	2.19	2.45	2.11	2.42	3.71
Sd	0.83	0.89	0.86	0.84	0.88	0.92
Skew	-0.04	-1	0.04	0.26	-0.02	-0.21
Kurt	-0.33	3.37	-4.86E-04	-0.61	-0.71	0.89
ADF	0.01***	0.01***	0.01***	0.01***	0.01***	0.01***
PP	0.01***	0.01***	0.01***	0.01***	0.01***	0.01***
Panel C: Kurtosis Series						
Mean	2.99	3.73	3.14	3.01	3.09	3.19
Med	2.79	3.17	2.95	2.77	2.91	2.85
Min	1.61	1.43	1.48	1.65	1.64	1.64
Max	7.78	22	11.14	6.94	9.16	15.76
Sd	0.98	2	1.14	0.96	0.95	1.5
Skew	1.95	3.91	2.6	1.6	1.97	4.61
Kurt	5.66	27.99	11.71	3	7.67	32.02
ADF	0.01***	0.01***	0.01***	0.01***	0.01***	0.01***
PP	0.01***	0.01***	0.01***	0.01***	0.01***	0.01***

***, ** Significant at 1% and 10% levels, respectively.

Table A.1.2
Spillover results of DY
This table presents *RV*, *RS*, and *RK* spillovers among six currency futures. DY estimates are given for the period January 2001 to September 2021. Forecast error variance, from market j to market i, is represented by each ij^{th} entry in the tables. The last row 'To' shows directional spillovers from each asset towards other assets, whereas the last column 'From' gives spillover from all other assets collectively towards each asset.

	EUR	JPY	GBP	AUD	CAD	CHF	From
Panel A: Volatility Series							
EUR	48.83	0.09	7.83	18.54	20.14	4.58	8.53
JPY	0.39	99.24	0.03	0.08	0.18	0.08	0.13
GBP	17.22	0.02	48.49	16.42	17.07	0.78	8.59
AUD	19.25	0	8.95	39.64	30.98	1.17	10.06
CAD	18.68	0.02	8.44	31.78	38.77	2.3	10.2
CHF	10.15	0.05	0.61	1.94	3.08	84.17	2.64
To	10.95	0.03	4.31	11.46	11.91	1.48	**40.14**
Panel B: Skewness Series							
EUR	47.22	2.74	11.4	9.13	6.19	23.33	8.8
JPY	5.26	81.25	0.37	3.16	1.73	8.22	3.12
GBP	15.44	2.19	61.74	6.87	3.93	9.82	6.38
AUD	12.13	2.24	6.21	61.42	11.8	6.2	6.43
CAD	8.84	1.68	5.21	12.61	68.74	2.92	5.21
CHF	25.93	5.32	8.53	5.11	2.57	52.54	7.91
To	11.26	2.36	5.29	6.15	4.37	8.41	**37.85**
Panel C: Kurtosis Series							
EUR	80.33	0.85	4.41	0.99	1.36	12.05	3.28
JPY	0.81	97.4	0.48	0.19	0.35	0.77	0.43
GBP	4.92	0.04	92.03	0.22	1.33	1.46	1.33
AUD	0.51	0.21	0.02	95.08	2.77	1.42	0.82
CAD	0.06	0.32	0.08	2.92	95.25	1.37	0.79
CHF	12.43	0.23	1.65	1.26	1.29	83.15	2.81
To	3.12	0.27	1.11	0.93	1.18	2.84	**9.46**

Note: Bold values given in each panel are total spillovers.

Table A.1.3
Spillover results of BK - Volatility series
This table presents *RV* spillovers among six currency futures. BK estimates are given for the period January 2001 to September 2021. Forecast error variance, from market j to market i, is represented by each ij^{th} entry in the tables. First, second, and third panels present short, medium, and long-term frequencies, respectively.

	EUR	JPY	GBP	AUD	CAD	CHF	From-ABS	From-WTH
1-6 months								
EUR	17.57	0.06	3.23	5.01	5.54	1.54	2.56	4.67
JPY	0.36	82.66	0.01	0.03	0.05	0.07	0.08	0.15
GBP	5.77	0.01	31.8	6.09	6.42	0.15	3.08	5.61
AUD	6.05	0	4.3	22.39	16.76	0.29	4.57	8.32
CAD	5.05	0.01	3.44	13.45	17.44	0.65	3.77	6.87
CHF	4.98	0.05	0.26	0.58	1.17	65.94	1.17	2.14
To-ABS	3.7	0.02	1.87	4.19	4.99	0.45	15.23	-
To-WTH	6.74	0.04	3.41	7.65	9.09	0.82	-	27.76
6-12 months								
EUR	9.6	0.01	1.42	4.01	4.34	0.92	1.78	11.63
JPY	0.03	7.8	0.01	0.02	0.04	0	0.02	0.11
GBP	3.44	0	6.6	3.36	3.45	0.17	1.74	11.34
AUD	4.05	0	1.63	5.93	4.72	0.25	1.77	11.57
CAD	4	0.01	1.69	6.1	7.19	0.51	2.05	13.36
CHF	1.68	0	0.09	0.38	0.57	7.97	0.45	2.97
To-ABS	2.2	0	0.81	2.31	2.19	0.31	7.82	-
To-WTH	14.34	0.02	5.26	15.08	14.27	2.01	-	50.97
12-∞ months								
EUR	21.65	0.02	3.19	9.51	10.25	2.12	4.18	14.03
JPY	0.01	8.78	0.02	0.03	0.09	0	0.03	0.09
GBP	8.02	0	10.08	6.96	7.19	0.46	3.77	12.66
AUD	9.16	0	3.02	11.31	9.51	0.63	3.72	12.48
CAD	9.64	0	3.31	12.23	14.14	1.15	4.39	14.72
CHF	3.5	0	0.25	0.97	1.35	10.25	1.01	3.39
To-ABS	5.05	0	1.63	4.95	4.73	0.73	17.1	-
To-WTH	16.96	0.02	5.47	16.61	15.88	2.44	-	57.37

Table A.1.4
Spillover results of BK - Skewness series
This table presents *RS* spillovers among six currency futures. BK estimates are given for the period January 2001 to September 2021. Forecast error variance, from market j to market i, is represented by each ij^{th} entry in the tables. First, second, and third panels present short, medium, and long-term frequencies, respectively.

	EUR	JPY	GBP	AUD	CAD	CHF	From-ABS	From-WTH
1-6 months								
EUR	37.63	2.22	9.6	7.29	5.48	18.56	7.19	8.61
JPY	3.81	68.44	0.34	2.3	1.42	6.42	2.38	2.85
GBP	11.86	1.66	51.93	4.95	3.1	7.46	4.84	5.79
AUD	9.46	1.72	5.56	51.89	10.69	4.74	5.36	6.42
CAD	7.24	1.34	4.98	11.05	59.23	2.36	4.5	5.38
CHF	22.28	4.26	7.71	4.46	2.41	45.27	6.85	8.21
To-ABS	9.11	1.87	4.7	5.01	3.85	6.59	31.13	-
To-WTH	10.91	2.23	5.63	6	4.61	7.89	-	37.27
6-12 months								
EUR	4.47	0.25	0.84	0.86	0.35	2.22	0.75	9.71
JPY	0.67	6.06	0.01	0.4	0.15	0.84	0.35	4.46
GBP	1.65	0.25	4.63	0.89	0.39	1.09	0.71	9.2
AUD	1.24	0.24	0.31	4.5	0.54	0.68	0.5	6.47
CAD	0.75	0.16	0.12	0.74	4.51	0.26	0.34	4.37
CHF	1.72	0.5	0.39	0.31	0.08	3.44	0.5	6.45
To-ABS	1.01	0.23	0.28	0.53	0.25	0.85	3.15	-
To-WTH	12.97	3.02	3.6	6.88	3.23	10.96	-	40.67
12-∞ months								
EUR	5.11	0.28	0.95	0.98	0.37	2.54	0.85	9.79
JPY	0.78	6.75	0.02	0.46	0.16	0.96	0.4	4.55
GBP	1.92	0.29	5.18	1.03	0.44	1.27	0.82	9.44
AUD	1.42	0.27	0.34	5.04	0.57	0.78	0.57	6.48
CAD	0.85	0.18	0.12	0.81	5	0.29	0.37	4.28
CHF	1.92	0.56	0.43	0.34	0.08	3.83	0.56	6.38
To-ABS	1.15	0.26	0.31	0.6	0.27	0.97	3.57	-
To-WTH	13.17	3.01	3.54	6.92	3.11	11.18	-	40.92

Table A.1.5
Spillover results of BK - Kurtosis series
This table presents *RK* spillovers among six currency futures. BK estimates are given for the period January 2001 to September 2021. Forecast error variance, from market j to market i, is represented by each ij^{th} entry in the tables. First, second, and third panels present short, medium, and long-term frequencies, respectively.

	EUR	JPY	GBP	AUD	CAD	CHF	From-ABS	From-WTH
1-6 months								
EUR	67.47	0.6	3.34	0.99	1.02	10.31	2.71	3.32
JPY	0.74	77.9	0.33	0.17	0.34	0.52	0.35	0.43
GBP	4.35	0.03	75.21	0.19	0.98	1.24	1.13	1.39
AUD	0.46	0.2	0.01	76.54	2	1.2	0.64	0.79
CAD	0.04	0.31	0.06	2.76	77.81	1.3	0.75	0.92
CHF	10.14	0.16	1.12	1.01	0.87	67.72	2.22	2.72
To-ABS	2.62	0.22	0.81	0.85	0.87	2.43	7.8	-
To-WTH	3.21	0.26	0.99	1.04	1.06	2.98	-	9.56
6-12 months								
EUR	6.07	0.11	0.5	0.01	0.16	0.83	0.27	3.1
JPY	0.04	9.09	0.07	0.01	0.01	0.11	0.04	0.46
GBP	0.27	0	7.89	0.02	0.16	0.11	0.09	1.08
AUD	0.02	0.01	0	8.67	0.35	0.1	0.08	0.95
CAD	0.01	0.01	0.01	0.08	8.18	0.04	0.02	0.27
CHF	1.08	0.03	0.24	0.12	0.19	7.23	0.28	3.2
To-ABS	0.24	0.03	0.14	0.04	0.14	0.2	0.78	-
To-WTH	2.73	0.31	1.59	0.45	1.67	2.29	-	9.05
12-∞ months								
EUR	6.79	0.13	0.58	0	0.18	0.91	0.3	3.07
JPY	0.04	10.41	0.09	0.01	0	0.14	0.05	0.46
GBP	0.3	0	8.93	0.02	0.18	0.12	0.1	1.06
AUD	0.03	0	0	9.88	0.42	0.11	0.09	0.96
CAD	0.01	0	0.01	0.08	9.26	0.03	0.02	0.21
CHF	1.21	0.04	0.28	0.13	0.23	8.2	0.32	3.22
To-ABS	0.26	0.03	0.16	0.04	0.17	0.22	0.88	-
To-WTH	2.7	0.31	1.63	0.41	1.72	2.22	-	8.99

A.2 PLOTS

Figure A.2.1
Time series plots for *RV*
This figure plots the *RV* of six currency futures for the period January 2001 to September 2021.

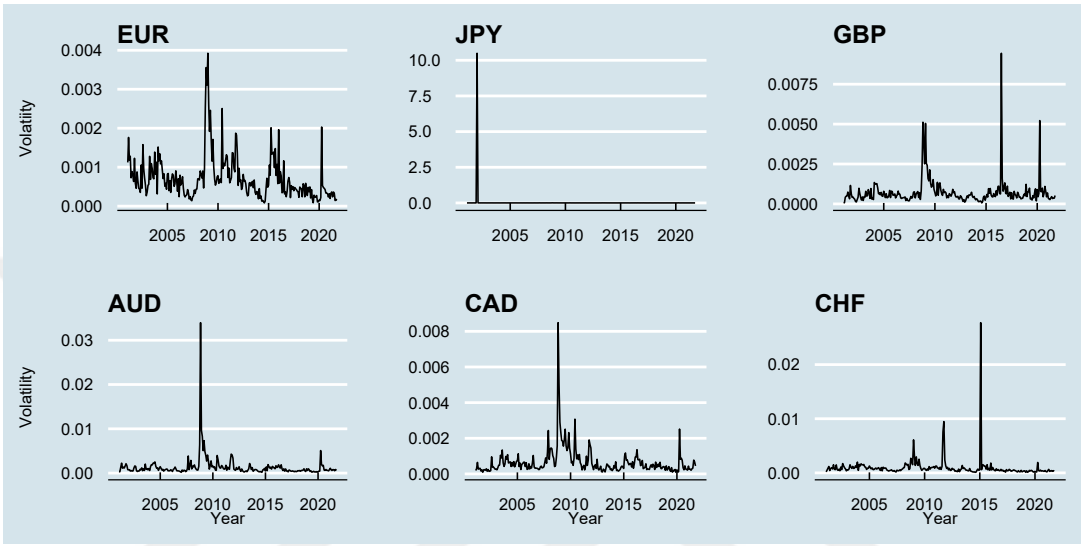

Figure A.2.2
Time series plots for *RS*
This figure plots the *RS* of six currency futures for the period January 2001 to September 2021.

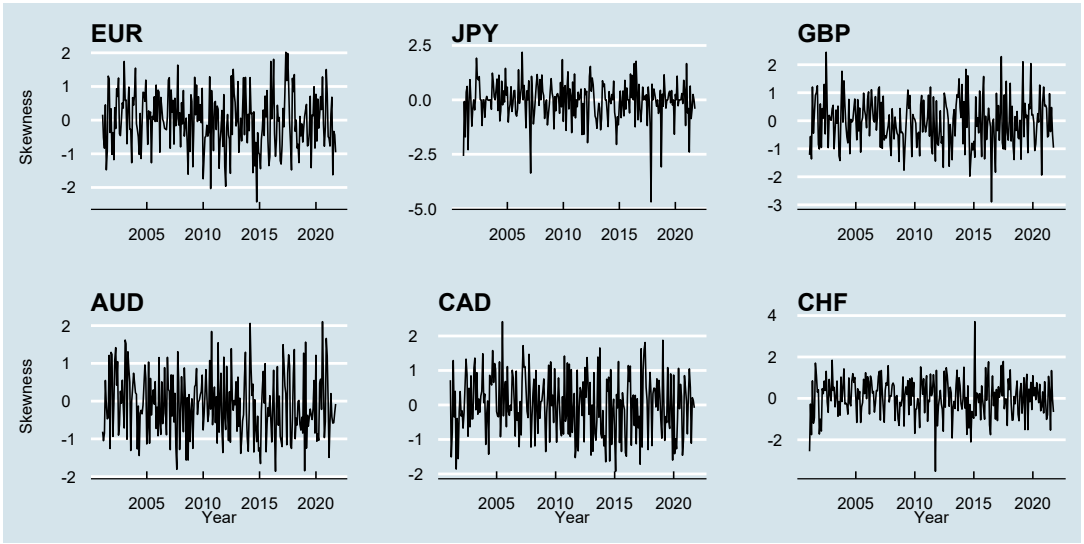

Figure A.2.3
Time series plots for *RK*
This figure plots the *RK* of six currency futures for the period January 2001 to September 2021.

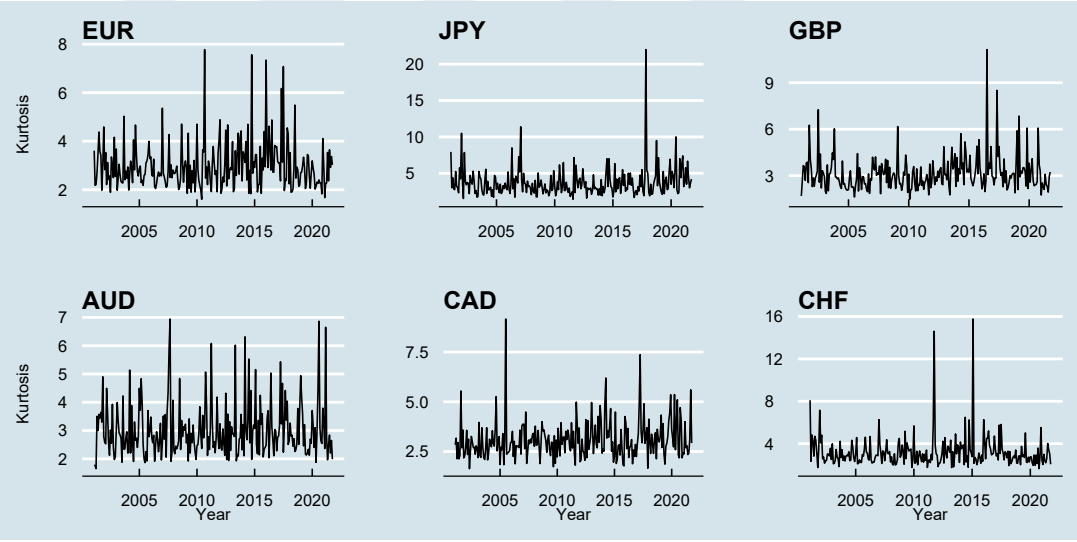

Figure A.2.4 (a)
Pairwise connectivity for *RV* (DY)
This subfigure plots the DY pairwise *RV* of six currency futures for the period January 2001 to September 2021. The strength of the connection between pairs is represented through shades moving from lighter (weak) to darker (strong) lines.

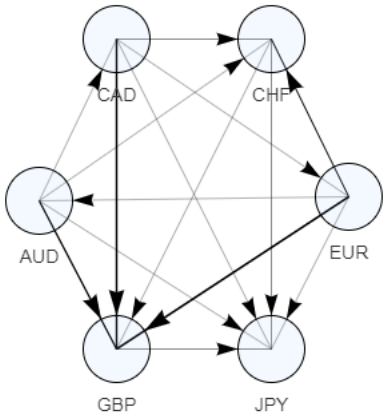

Figure A.2.4 (b)
Pairwise connectivity for *RV* (BK-short)
This subfigure plots the BK-short frequency pairwise *RV* of six currency futures for the period January 2001 to September 2021. The strength of the connection between pairs is represented through shades moving from lighter (weak) to darker (strong) lines.

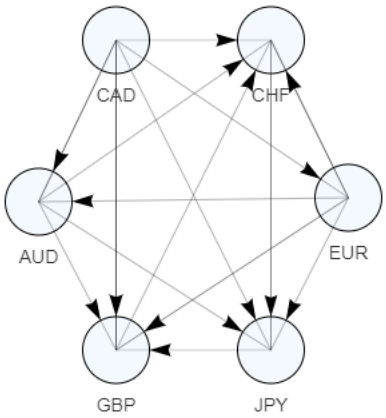

Figure A.2.4 (c)
Pairwise connectivity for *RV* (BK-mid)
This subfigure plots the BK-mid frequency pairwise *RV* of six currency futures for the period January 2001 to September 2021. The strength of the connection between pairs is represented through shades moving from lighter (weak) to darker (strong) lines.

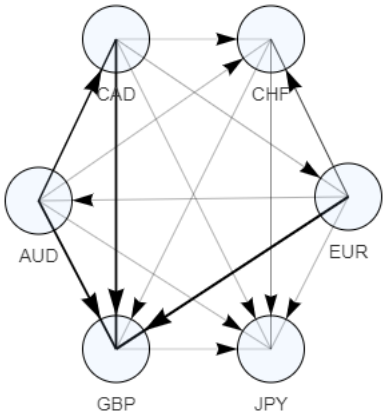

Figure A.2.4 (d)
Pairwise connectivity for *RV* (BK-long)
This subfigure plots the BK-long frequency pairwise *RV* of six currency futures for the period January 2001 to September 2021. The strength of the connection between pairs is represented through shades moving from lighter (weak) to darker (strong) lines.

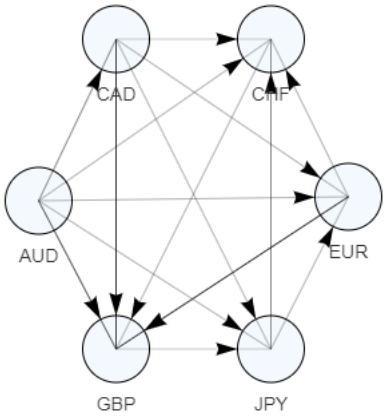

Figure A.2.5 (a)
Pairwise connectivity for *RS* (DY)
This subfigure plots the DY pairwise *RS* of six currency futures for the period January 2001 to September 2021. The strength of the connection between pairs is represented through shades moving from lighter (weak) to darker (strong) lines.

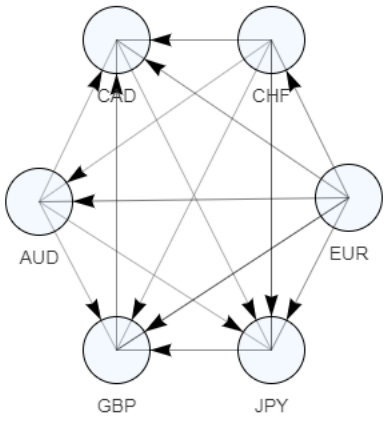

Figure A.2.5 (b)
Pairwise connectivity for *RS* (BK-short)
This subfigure plots the BK-short frequency pairwise *RS* of six currency futures for the period January 2001 to September 2021. The strength of the connection between pairs is represented through shades moving from lighter (weak) to darker (strong) lines.

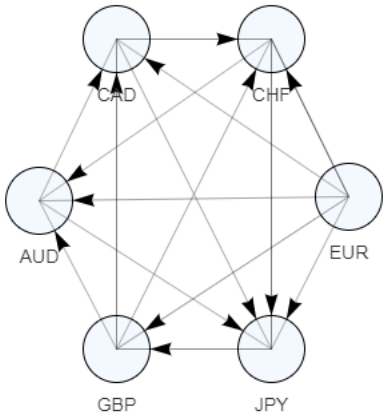

Figure A.2.5 (c)
Pairwise connectivity for *RS* (BK-mid)
This subfigure plots the BK-mid frequency pairwise *RS* of six currency futures for the period January 2001 to September 2021. The strength of the connection between pairs is represented through shades moving from lighter (weak) to darker (strong) lines.

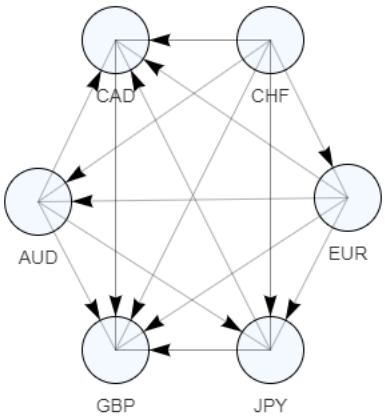

Figure A.2.5 (d)
Pairwise connectivity for *RS* (BK-long)
This subfigure plots the BK-long frequency pairwise *RS* of six currency futures for the period January 2001 to September 2021. The strength of the connection between pairs is represented through shades moving from lighter (weak) to darker (strong) lines.

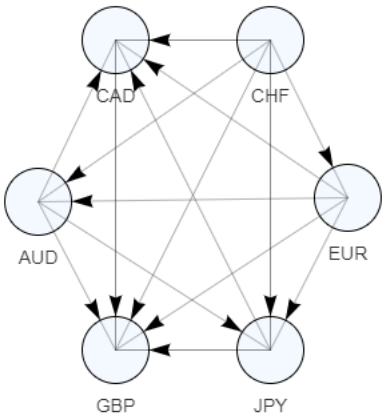

Figure A.2.6 (a)
Pairwise connectivity for *RK* (DY)
This subfigure plots the DY pairwise *RK* of six currency futures for the period January 2001 to September 2021. The strength of the connection between pairs is represented through shades moving from lighter (weak) to darker (strong) lines.

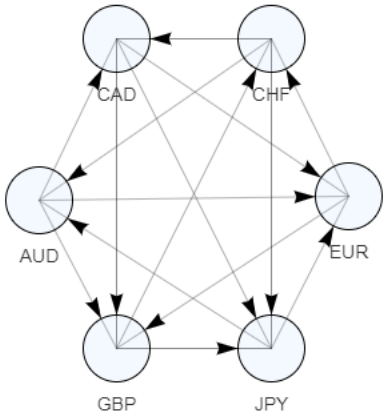

Figure A.2.6 (b)
Pairwise connectivity for *RK* (BK-short)
This subfigure plots the BK-short frequency pairwise *RK* of six currency futures for the period January 2001 to September 2021. The strength of the connection between pairs is represented through shades moving from lighter (weak) to darker (strong) lines.

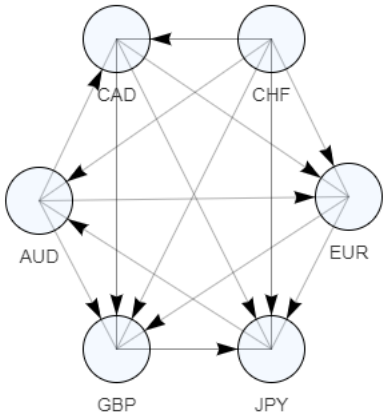

Figure A.2.6 (c)
Pairwise connectivity for *RK* (BK-mid)
This subfigure plots the BK-mid frequency pairwise *RK* of six currency futures for the period January 2001 to September 2021. The strength of the connection between pairs is represented through shades moving from lighter (weak) to darker (strong) lines.

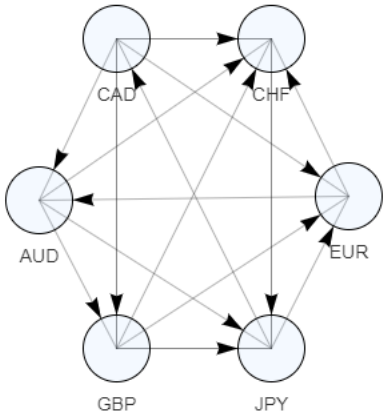

Figure A.2.6 (d)
Pairwise connectivity for *RK* (BK-long)
This subfigure plots the BK-long frequency pairwise *RK* of six currency futures for the period January 2001 to September 2021. The strength of the connection between pairs is represented through shades moving from lighter (weak) to darker (strong) lines.

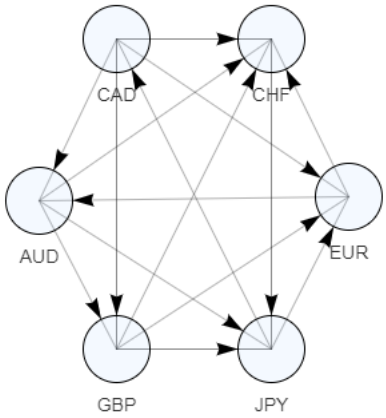

Figure A.2.7 (a)
36 month rolling window for *RV*
This subfigure plots the rolling window *RV* spillover among six currency futures. A 36 month window is rolled for the period January 2001 to September 2021.

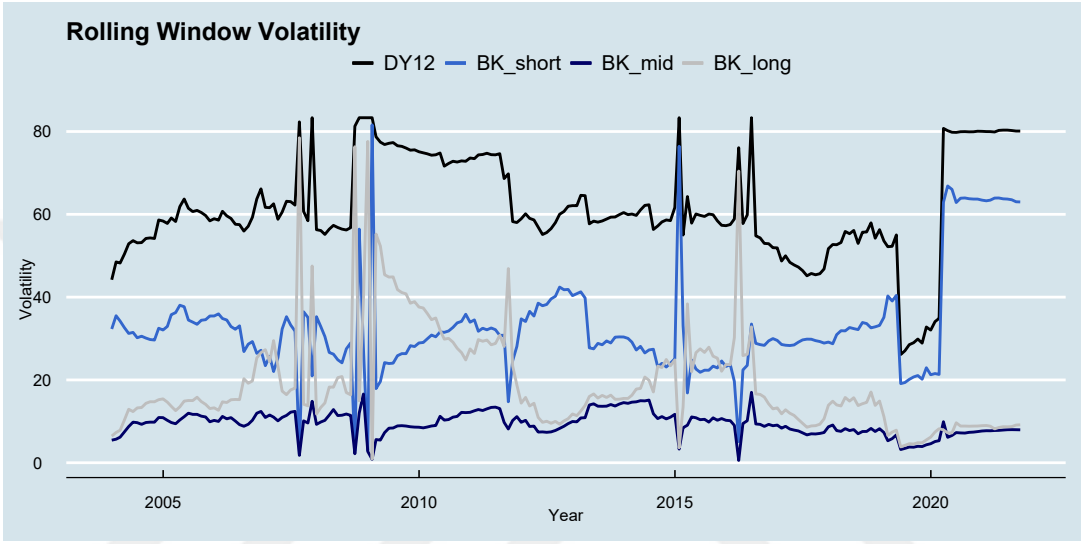

Figure A.2.7 (b)
36 month rolling window for *RS*
This subfigure plots the rolling window *RS* spillover among six currency futures. A 36 month window is rolled for the period January 2001 to September 2021.

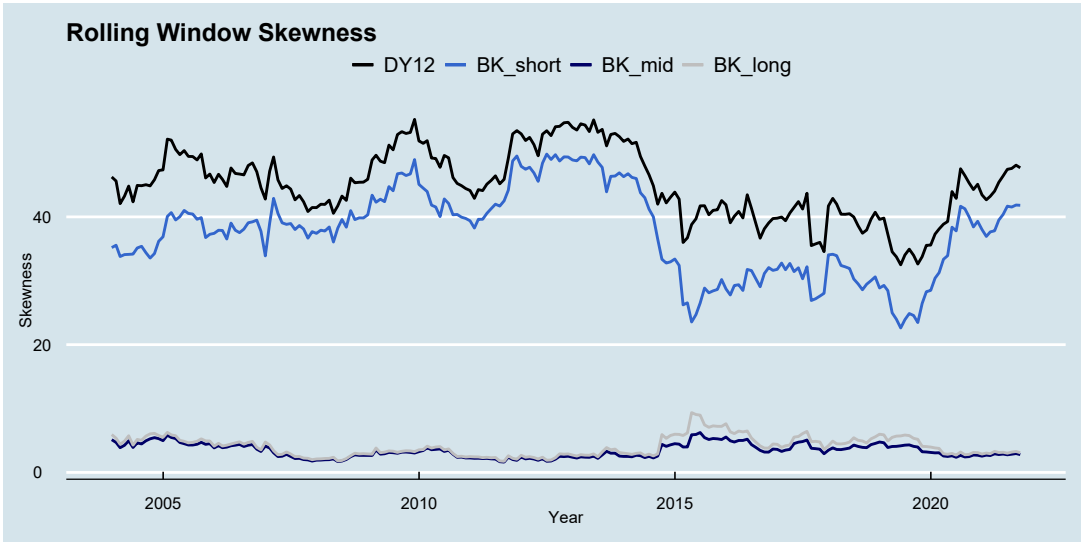

Figure A.2.7 (c)
36 month rolling window for *RK*
This subfigure plots the rolling window *RK* spillover among six currency futures. A 36 month window is rolled for the period January 2001 to September 2021.

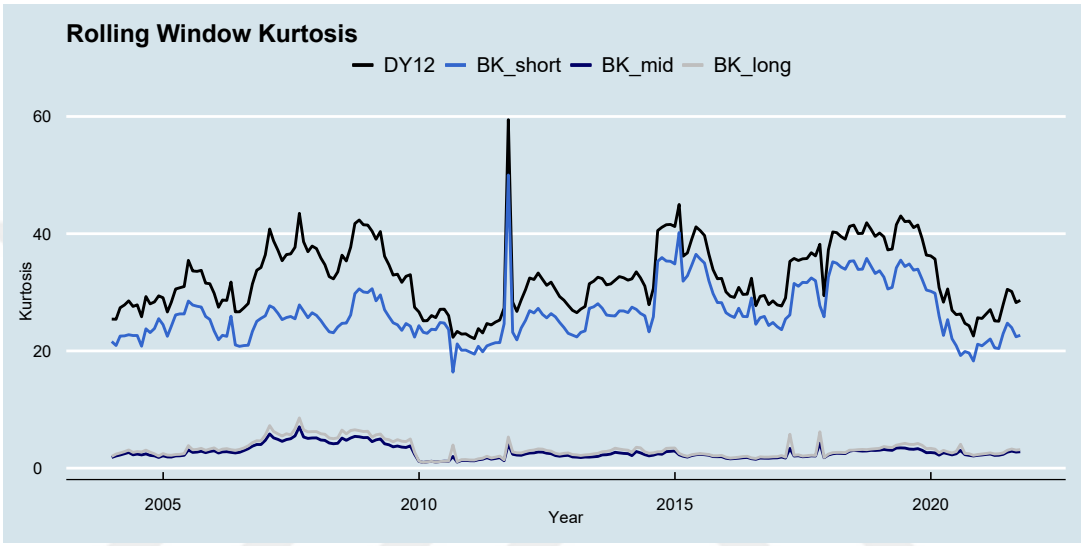

Figure A.2.8 (a)
48 month rolling window for *RV*
This subfigure plots the rolling window *RV* spillover among six currency futures. A 48 month window is rolled for the period January 2001 to September 2021.

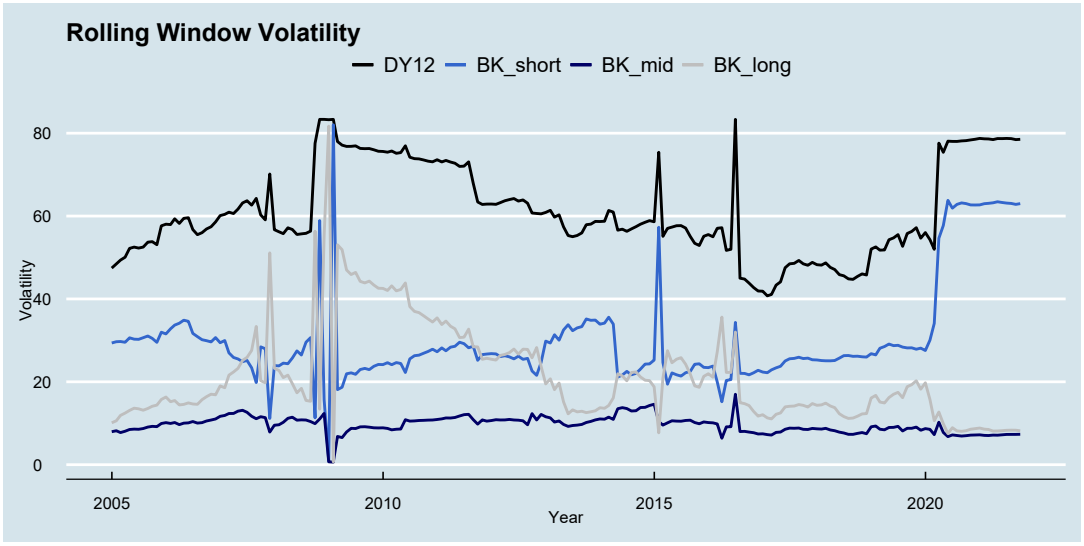

Figure A.2.8 (b)
48 month rolling window for *RS*
This subfigure plots the rolling window *RS* spillover among six currency futures. A 48 month window is rolled for the period January 2001 to September 2021.

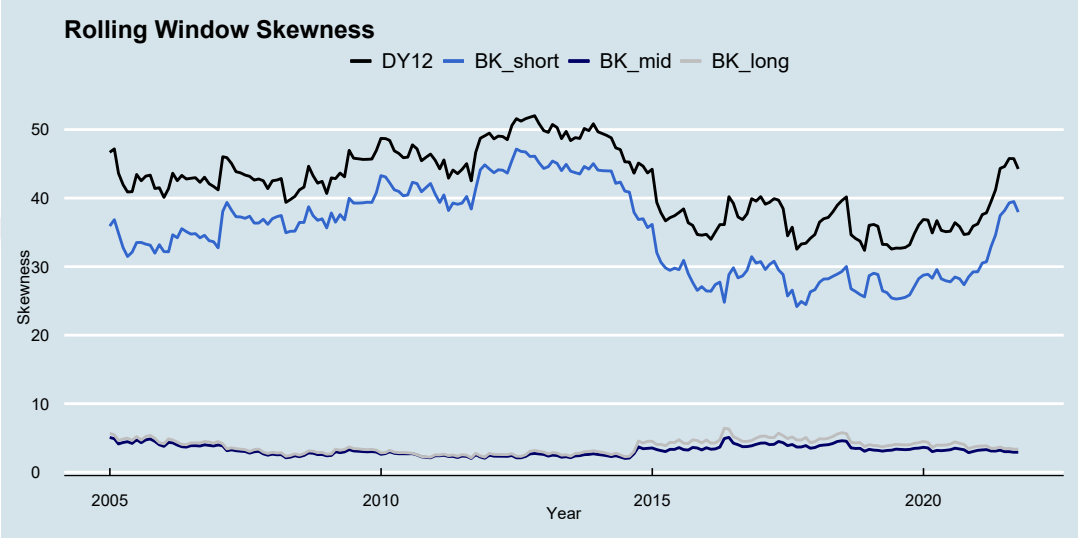

Figure A.2.8 (c)
48 month rolling window for *RK*
This subfigure plots the rolling window *RK* spillover among six currency futures. A 48 month window is rolled for the period January 2001 to September 2021.

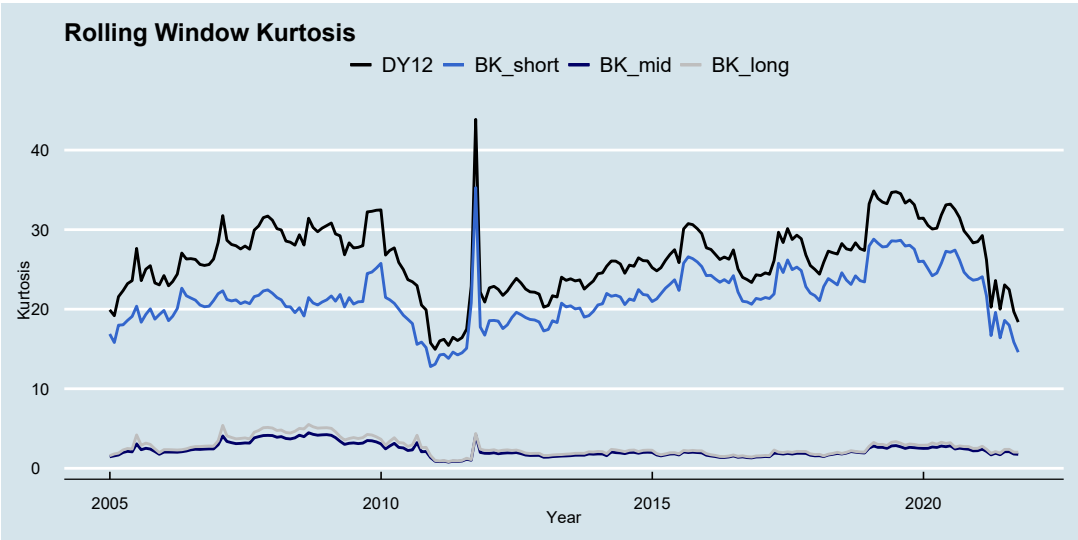

Figure A.2.9 (a)
60 month rolling window for *RV*
This subfigure plots the rolling window *RV* spillover among six currency futures. A 60 month window is rolled for the period January 2001 to September 2021.

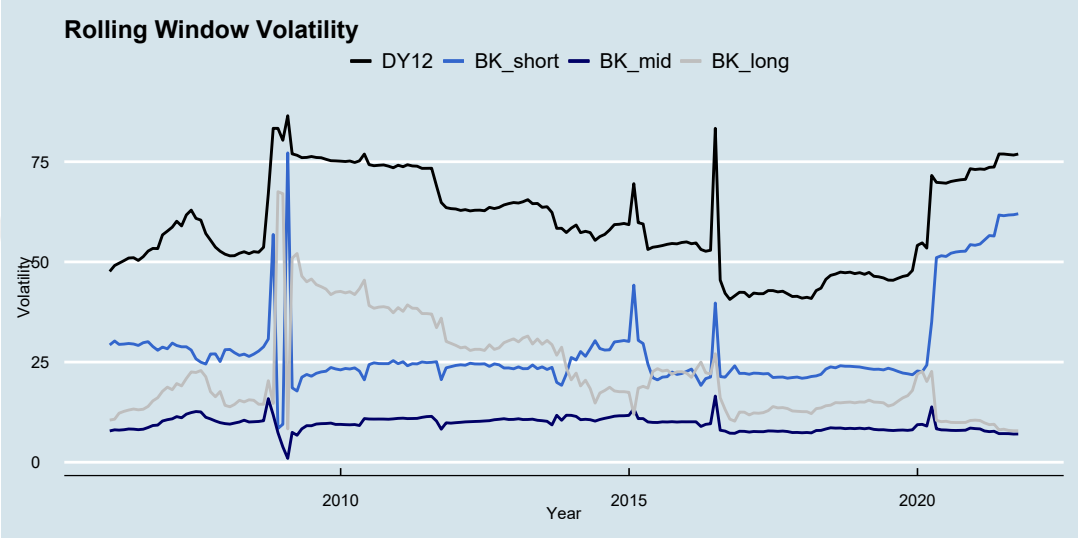

Figure A.2.9 (b)
60 month rolling window for *RS*
This subfigure plots the rolling window *RS* spillover among six currency futures. A 60 month window is rolled for the period January 2001 to September 2021.

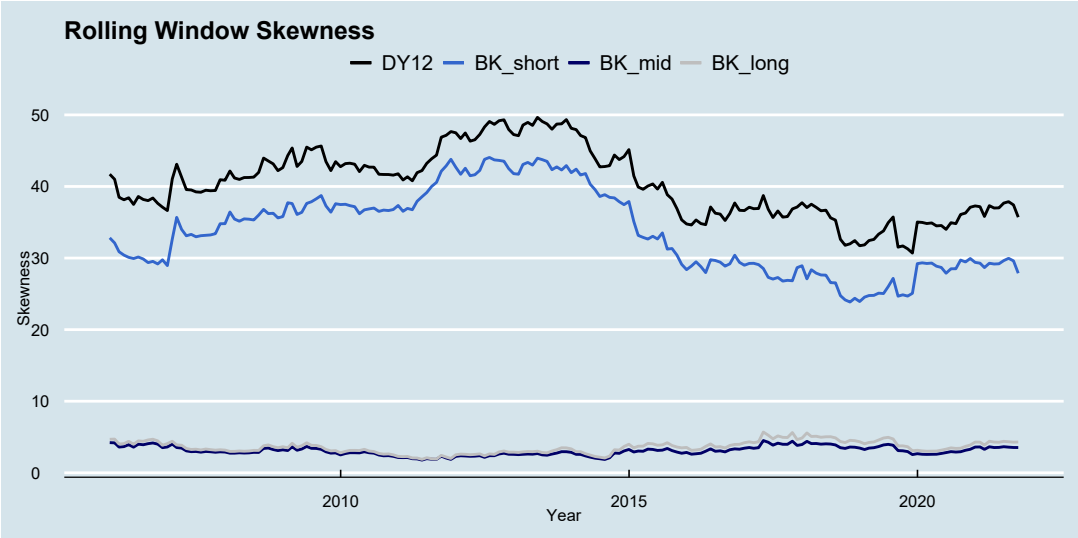

Figure A.2.9 (c)
60 month rolling window for *RK*
This subfigure plots the rolling window *RK* spillover among six currency futures. A 60 month window is rolled for the period January 2001 to September 2021.

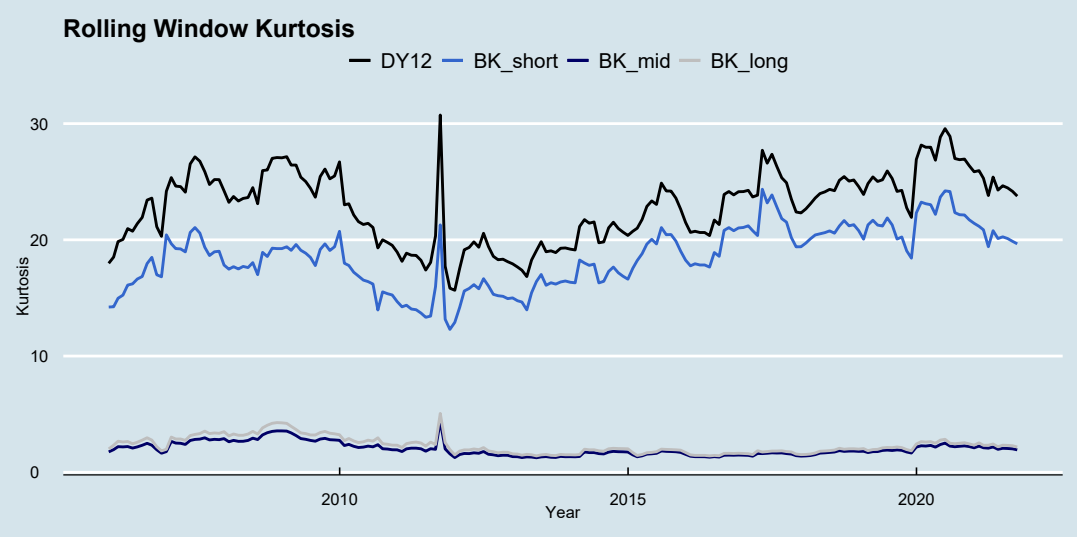

APPENDIX B

CHAPTER 2

B.1 LLH FUNCTIONS

$$LLH(norm) = \sigma^{-n}(2\pi)^{-n/2}exp[-\frac{1}{2\sigma^2}\sum_{i=1}^{n}(x_i-\mu)^2] \tag{B.1.1}$$

$$LLH(snorm) = n\ ln(\frac{2}{\sigma}) - \frac{n}{2}ln(2\pi) - \frac{1}{2}\sum_{i=1}^{n}(\frac{x_i-\mu}{\sigma})^2 + \sum_{i=1}^{n} ln(\phi(\lambda\frac{x_i-\mu}{\sigma})) \tag{B.1.2}$$

$$\begin{aligned} LLH(std) =& T(ln\Gamma(\frac{\nu+1}{2}) - ln\Gamma\frac{\nu}{2} - \frac{1}{2}ln(\pi(\nu-2))) - \frac{1}{2}\sum_{i=1}^{T}[ln(\sigma_t^2) \\ &+ (1+\nu)ln[1+(\frac{z_t^2}{\sigma_t^2(\nu-2)})]] \end{aligned} \tag{B.1.3}$$

$$\begin{aligned} LLH(sstd) = T(ln\Gamma(\frac{\nu+1}{2}) - ln\Gamma\frac{\nu}{2} - \frac{1}{2}ln(\pi(\nu-2)) + ln(\frac{2}{\varepsilon+1/\varepsilon}) + lns) - \\ \frac{1}{2}\sum_{t=1}^{T}[ln(\sigma_t^2) + (1+\nu)ln[1+(\frac{(sz_t+m)^2}{\nu-2})\varepsilon^{-2It}]] \end{aligned} \tag{B.1.4}$$

$$LLH(jsu) = nln\tau - nln\sigma - \frac{n}{2}ln(2\pi) + \sum_{i=1}^{n} g(\frac{x-\mu}{\sigma}) - \frac{1}{2}\sum_{i=1}^{n}(\nu+\tau g(\frac{x-\mu}{\sigma}))^2 \tag{B.1.5}$$

$$\begin{aligned} LLH(ast) =& -Tln\sigma - \frac{\nu_1+1}{2}\sum_{i=1}^{T} ln[1+\frac{1}{\nu_1}(\frac{y_t-\mu}{2\alpha\sigma K(\nu_1)})^2]1(y_t \le \mu) \\ & \frac{-\nu_2+1}{2}\sum_{i=1}^{T} ln[1+\frac{1}{\nu_2}(\frac{y_t-\mu}{2(1-\alpha)\sigma K(\nu_2)})^2]1(y_t > \mu) \end{aligned} \tag{B.1.6}$$

$$LLH(ald) = \frac{2^{n/2}}{\sigma^n}\frac{K^n}{(1+K^2)^n}exp[-\frac{\sqrt{2K}}{\sigma}\sum_{j=1}^{n}(x_j-\theta)^+ - \frac{\sqrt{2}}{K\sigma}\sum_{j=1}^{A}(x_j-\theta)^-] \tag{B.1.7}$$

B.2 TABLES

Table B.2.1
Summary statistics of daily log returns
This table presents summary statistics of daily log returns of TRY for the period January 2011 to December 2021, including mean (Mean), standard deviation (Sd), skewness (Skew), and kurtosis (Kurt). JB is Jarque-Bera statistic, $Q(L)$ and $Q^2(L)$ are Ljung-Box test statistics performed on lag L of returns and squared returns respectively, LM(L) represents ARCH Lagrange Multiplier performed on lag L, and ADF is Augmented Dickey-Fuller unit root test.

Mean	Sd	Skew	Kurt	JB	$Q(20)$	$Q^2(20)$	LM(12)	ADF
0.08	1.13	0.26	91.95	1E+06***	80.47	334.64	156.63	-12.44

***Significant at 1% level.

Table B.2.2
Summary statistics of *RR*
This table presents summary statistics of *RR* of TRY for the period January 2011 to December 2021, including mean (Mean), standard deviation (Sd), skewness (Skew), and kurtosis (Kurt). JB is the Jarque-Bera statistic, and $Q(L)$ is Ljung-Box test statistics performed on lag L of returns.

Mean	Sd	Skew	Kurt	JB	$Q(20)$
0.01	0.01	8.44	114.55	1.59E+06***	7307

***Significant at 1% level.

Table B.2.3
GARCH results

This table presents the estimation results (and diagnostics) of GARCH class models. LLH is log-likelihood, whereas AIC, BIC, and HQIC are selection criteria. $Q(L)$ and $Q^2(L)$ are Ljung-Box statistics for serial correlation upto L lag of standardized residuals ε_t and squared standardized residuals ε_t^2 respectively, $LM(L)$ represents weighted ARCH Lagrange Multiplier test performed on lag L of residuals (5% χ^2 critical value = 31.4).

Model	LLH	AIC	BIC	HQIC	$Q(20)$	$Q^2(20)$	$LM(20)$
GARCH-*norm*	-3382.4347	2.3815	2.3898	2.3845	15.9546	8.2111	7.4367
GARCH-*snorm*	-3351.0941	2.3601	2.3706	2.3639	16.3586	9.0620	7.4126
GARCH-*std*	-3213.4461	2.2633	2.2738	2.2671	15.4430	9.2368	7.1251
GARCH-*sstd*	**-3201.7304**	**2.2558**	**2.2683**	**2.2603**	16.2748	9.7231	7.0259
GARCH-*jsu*	-3203.0984	2.2567	2.2693	2.2613	16.3505	9.6613	7.0817
EGARCH-*norm*	-3362.2282	2.3680	2.3784	2.3717	13.7362	9.8665	5.8267
EGARCH-*snorm*	-3331.6764	2.3472	2.3597	2.3517	14.6949	11.4972	5.2292
EGARCH-*std*	-3200.1726	2.2547	2.2673	2.2592	13.4155	10.8573	4.8882
EGARCH-*sstd*	**-3189.0459**	**2.2476**	**2.2622**	**2.2529**	14.5519	11.7783	4.8062
EGARCH-*jsu*	-3191.1347	2.249	2.2637	2.2543	14.6070	11.7286	4.8257
GJRGARCH-*norm*	-3363.0634	2.3685	2.3790	2.3723	14.8352	9.9510	9.6216
GJRGARCH-*snorm*	-3331.2271	2.3469	2.3594	2.3514	15.4574	10.3126	9.0239
GJRGARCH-*std*	-3209.7807	2.2614	2.2740	2.2660	14.2990	9.5514	8.0126
GJRGARCH-*sstd*	**-3197.6948**	**2.2537**	**2.2683**	**2.2589**	15.2990	10.0503	7.8847
GJRGARCH-*jsu*	-3198.8316	2.2545	2.2691	2.2597	15.3849	10.0527	7.9753
AVGARCH-*norm*	-3350.8929	2.3607	2.3732	2.3652	13.7133	10.8765	5.2639
AVGARCH-*snorm*	-3320.1745	2.3398	2.3544	2.3451	14.1925	12.9740	4.6239
AVGARCH-*std*	-3198.0570	2.2539	2.2686	2.2592	12.8000	11.7517	4.3377
AVGARCH-*sstd*	**-3187.9742**	**2.2475**	**2.2643**	**2.2536**	13.7626	12.8318	4.1603
AVGARCH-*jsu*	-3189.8540	2.2488	2.2656	2.2549	13.7952	12.8090	4.1728
TGARCH-*norm*	-3357.5297	2.3646	2.3751	2.3684	13.2120	11.8824	5.2933
TGARCH-*snorm*	-3327.3645	2.3441	2.3567	2.3487	14.2068	14.0215	4.7559
TGARCH-*std*	-3200.2448	2.2547	2.2673	2.2593	12.8211	12.9943	4.3364
TGARCH-*sstd*	**-3189.8549**	**2.2481**	**2.2628**	**2.2534**	13.8481	14.5022	4.2227
TGARCH-*jsu*	-3191.7941	2.2495	2.2642	2.2548	13.8951	14.4638	4.2518
NGARCH-*norm*	-3380.8933	2.3811	2.3915	2.3849	15.7319	8.5124	7.0775
NGARCH-*snorm*	-3350.2240	2.3602	2.3728	2.3647	16.2295	9.3093	7.0937
NGARCH-*std*	-3208.2731	2.2604	2.2729	2.2649	15.1466	11.2417	5.5585
NGARCH-*sstd*	**-3197.4797**	**2.2535**	**2.2682**	**2.2588**	15.9713	11.6588	5.6611
NGARCH-*jsu*	-3199.3647	2.2548	2.2695	2.2601	16.0538	11.3493	5.7877
NAGARCH-*norm*	-3355.9811	2.3636	2.3740	2.3673	14.6685	9.0238	8.4203
NAGARCH-*snorm*	-3322.9872	2.3411	2.3536	2.3456	15.2449	9.8033	8.0131
NAGARCH-*std*	-3206.6141	2.2592	2.2718	2.2638	13.8363	9.1977	7.6106
NAGARCH-*sstd*	**-3195.0934**	**2.2518**	**2.2665**	**2.2571**	14.9649	9.6631	7.4393
NAGARCH-*jsu*	-3196.1561	2.2526	2.2672	2.2579	15.0584	9.6704	7.5016
APARCH-*norm*	-3353.7488	2.3627	2.3753	2.3672	13.8816	10.7347	7.3515
APARCH-*snorm*	-3322.8223	2.3416	2.3563	2.3469	14.7045	11.8048	6.9656
APARCH-*std*	-3199.7031	2.2551	2.2697	2.2604	13.0774	11.8711	5.02
APARCH-*sstd*	**-3188.7454**	**2.2481**	**2.2648**	**2.2541**	14.2033	12.6807	5.1733
APARCH-*jsu*	-3190.4677	2.2493	2.2660	2.2553	14.2977	12.5235	5.3211
ALLGARCH-*norm*	-3347.7570	2.3592	2.3738	2.3645	14.1689	9.5088	6.8022
ALLGARCH-*snorm*	-3316.1433	2.3377	2.3544	2.3437	14.8065	10.6638	6.3364
ALLGARCH-*std*	-3197.6827	2.2543	2.2711	2.2604	13.0449	10.7568	4.9133
ALLGARCH-*sstd*	**-3187.1755**	**2.2477**	**2.2665**	**2.2545**	14.1034	11.5054	4.9587
ALLGARCH-*jsu*	-3188.8523	2.2488	2.2677	2.2556	14.2003	11.3485	5.0988

Note: Bold values represent best model estimates.

Table B.2.4
GAS results
This table presents the estimation results of GAS class models. LLH is log-likelihood, whereas AIC and BIC are selection criteria. np is the number of parameters for each model.

Model	LL	AIC	BIC	np
GAS-*norm*	-3449.9	6911.8	6947.5	6
GAS-*snorm*	-3430.1	6874.1	6915.8	7
GAS-*std*	-3206.2	6426.5	6468.1	7
GAS-*sstd*	-3202.5	6420.9	6468.5	8
GAS-*ast*	**-3197.6**	6413.3	6466.8	9
GAS-*ast*1	-3197.7	**6411.5**	**6459.1**	8
GAS-*ald*[a]	-3242.1	6494.3	6524.1	5

Notes: Bold values represent best model estimates.
[a]To allow the solver to converge, the location parameter is kept constant while estimating GAS with *ald* distribution.

Table B.2.5
SV results
This table presents the estimation results of the SV model. The model is estimated with the following prior distributions:
$\mu \sim normal\ mean = 0\ S.D. = 100$
$(\phi + 1)/2 \sim \beta\ \alpha_0 = 5\ b_0 = 1.5$
$\sigma^2 \sim \chi^2(df = 1)$
Stored 10000 MCMC draws after a burn-in of 1000.
Posterior draws of SV parameters (thinning = 1).

	Mean	S.D.	5%	50%	95%
μ	-9.936	0.1393	-10.163	-9.936	-9.7086
ϕ	0.953	9.22E-03	0.9374	0.954	0.9677
σ	0.334	0.0271	0.2911	0.334	0.3796
$\exp(\mu/2)$	7.0E-03	4.9E-04	6.2E-03	7.0E-03	7.8E-03
σ^2	0.113	0.0183	0.0847	0.111	0.1441

Table B.2.6
SVL results
This table presents the estimation results of the SVL model. The model is estimated with the following prior distributions:
$\mu \sim normal\ mean = 0\ S.D. = 100$
$(\phi + 1)/2 \sim \beta\ \alpha_0 = 5\ b_0 = 1.5$
$\sigma^2 \sim \gamma(shape = 0.5, rate = 0.5)$
$\nu \sim Infinity$
$\rho \sim \beta(\alpha = 4, \beta = 4)$
Stored 20000 MCMC draws after a burn-in of 2000.
Posterior draws of SV parameters (thinning = 1).

	Mean	S.D.	5%	50%	95%
μ	-9.8909	0.1318	-10.1053	-9.8913	-9.6834
ϕ	0.9512	9.2E-03	0.9358	0.951	0.9663
σ	0.3263	0.0284	0.2805	0.3256	0.3745
ρ	0.2169	0.0547	0.1306	0.2142	0.3088
$\exp(\mu/2)$	7.1E-03	4.7E-04	6.4E-03	7.1E-03	7.9E-03
σ^2	0.1073	0.0186	0.0787	0.106	0.1402

Table B.2.7
SVT results
This table presents the estimation results of the SVT model. The model is estimated with the following prior distributions:
$\mu \sim normal\ mean = 0\ S.D. = 100$
$(\phi + 1)/2 \sim \beta\ \alpha_0 = 5\ b_0 = 1.5$
$\sigma^2 \sim \gamma(shape = 0.5, rate = 0.5)$
$\nu - 2 \sim Exponential(rate = 0.1)$
$\rho \sim Constant(value = 0)$
Stored 10000 MCMC draws after a burn-in of 1000.
Posterior draws of SV parameters (thinning = 1).

	Mean	S.D.	5%	50%	95%
μ	-9.8867	0.1619	-10.1425	-9.8898	-9.6151
ϕ	0.9628	9.15E-03	0.9477	0.9629	0.9779
σ	0.2895	0.0322	0.2308	0.2911	0.3405
ν	20.5162	8.8602	10.6837	17.5734	38.2960
$\exp(\mu/2)$	7.2E-03	5.9E-04	6.3E-03	7.1E-03	8.2E-03
σ^2	0.0849	0.0185	0.0532	0.0847	0.116

Table B.2.8
SVTL results
This table presents the estimation results of the SVTL model. The model is estimated with the following prior distributions:
$\mu \sim normal\ mean = 0\ S.D. = 100$
$(\phi + 1)/2 \sim \beta\ \alpha_0 = 5\ b_0 = 1.5$
$\sigma^2 \sim \gamma(shape = 0.5, rate = 0.5)$
$\nu - 2 \sim Exponential(rate = 0.1)$
$\rho \sim \beta(\alpha = 4, \beta = 4)$
Stored 20000 MCMC draws after a burn-in of 2000.
Posterior draws of SV parameters (thinning = 1).

	Mean	S.D.	5%	50%	95%
μ	-9.8028	0.1495	-10.0420	-9.8062	-9.5607
ϕ	0.9638	9.5E-03	0.9475	0.9644	0.9780
σ	0.2647	0.0344	0.2117	0.2624	0.3232
ν	15.6525	7.6955	8.8943	13.2552	34.5894
ρ	0.2921	0.056	0.1970	0.2951	0.3759
$\exp(\mu/2)$	7.5E-03	5.6E-04	6.6E-03	7.4E-03	8.4E-03
σ^2	0.0713	0.0188	0.0448	0.0688	0.1044

Table B.2.9
HAR results
This table presents the estimation results of HAR class models. Newey-West standard errors are reported in parentheses.

Model	B_0	B_1	B_2	B_3	B_4	B_5	R^2
HAR	1.3E-05***	0.3438***	0.1938***	0.411***	-	-	0.3131
	(0)	(0.0148)	(0.029)	(0.0725)			
LHAR	-1.2615***	0.4375***	0.2593**	0.1876***	-	-	0.5578
	(0.2082)	(0.0984)	(0.1069)	(0.0343)			
HARJ	1.3e-05***	0.4581***	0.1806**	0.3885***	-0.4981***	-	0.326
	(0)	(0.0172)	(0.0209)	(0.0683)	(0.0335)		
HARQ	1e-05***	0.4191***	0.1699***	0.4062***	-2.6352	-	0.3138
	(0)	(0.0599)	(0.0256)	(0.0739)	(58.1768)		
HARQJ	1.6E-05***	0.4023***	0.2***	0.3909***	2.2535	-0.5356	0.3264
	(0)	(0.0508)	(0.0193)	(0.0685)	(21.7831)	(0.0263)	
CHAR	1.2E-05***	0.3876***	0.2096***	0.5426***	-	-	0.3221
	(0)	(0.0247)	(0.0482)	(0.1422)			
CHARQ	2E-05***	0.1682***	0.2705***	0.5511***	8.7878	-	0.3269
	(0)	(0.0724)	(0.0311)	(0.1416)	(36.9165)		

***, **Significant at 1% and 5% levels respectively.

Table B.2.10
CGARCH results
This table presents the estimation results of CGARCH model. Standard errors are reported in parentheses.

	μ	ω	α	β	ρ	φ	ν	ε
CGARCH	0.0543***	8.099E-03***	0.1204***	0.6889***	0.9953***	0.0843***	1.1416***	5.2937***
	(0.014)	(2.126E-03)	(0.0348)	(0.0505)	(2.320E-04)	(0.0186)	(0.0314)	(0.5063)

***Significant at 1% level.

Table B.2.11
GARCH-MIDAS results
This table presents the estimation results of GARCH-MIDAS model. Standard errors are reported in parentheses.

	μ	α	β	m	θ	w_2
GARCH-MIDAS	0.0353***	0.2272***	0.748***	-5.0001***	0.073***	2.1065***
	(0.0137)	(0.0616)	(0.0647)	(1.6444)	(0.0206)	(0.6712)

***Significant at 1% level.

Table B.2.12
CARR results
This table presents the estimation results of CARR class models. LLH is log-likelihood, whereas AIC and BIC are the selection criteria. Standard errors are reported in parentheses.

	ω	α	β	φ	ρ	*LLH*	*AIC*	*BIC*
CARR	3E-04	0.3115***	0.6507***	-	-	11675	-23344	-23339.6
	(1.2E-03)	(0.0659)	(0.1431)					
CCARR	5.1E-03	0.2985***	0.4366***	0.0621***	0.9364***	11680	-23350	-23342.7
	(3.3E-03)	(0.034)	(0.0148)	(0.0164)	(0.017)			

***Significant at 1% level.

Table B.2.13
R^2 for all values of ν
This table presents R^2 estimates for all values of ν of all kernels used in SVR models.

Kernels:	Linear			RBF			POLY		
ν	*MASR*	*RV*	*RR*	*MASR*	*RV*	*RR*	*MASR*	*RV*	*RR*
0.05	0.2787	-1.3866	0.3543	0.2892	-13.3829	-0.2668	-2.6285	-19.6108	-1.4614
0.1	0.5598	-0.2322	**0.4291**	0.5497	-3.22	0.0762	-0.3364	-4.8249	-0.6182
0.15	0.6209	0.0906	0.4216	0.6788	-0.7164	0.0951	0.1001	-1.9651	-0.4236
0.2	0.64	0.0953	0.4075	0.7798	-0.3489	0.2403	0.2414	-1.0286	-0.2418
0.25	0.628	0.0846	0.3941	**0.7963**	0.0154	0.3189	0.3619	-0.7438	-0.1443
0.3	0.6344	0.0681	0.3998	0.7743	0.1565	0.3697	0.4742	-0.4495	-0.0999
0.35	0.6214	0.084	0.4152	0.7756	0.1467	0.3982	0.5479	-0.2613	-0.042
0.4	0.6535	0.0986	0.4038	0.7883	0.2106	0.4196	0.5888	-0.1435	-8.6E-03
0.45	0.6426	0.0639	0.3995	0.7924	0.2046	0.4283	0.6166	-0.069	0.0233
0.5	0.6425	0.0919	0.3996	0.7943	**0.2184**	**0.4289**	0.6366	-9.40E-03	0.0338
0.55	0.6584	0.1045	0.4023	0.7953	0.2133	0.4286	0.645	0.0553	0.0359
0.6	0.6707	0.1171	0.4022	0.7942	0.209	0.4276	0.6548	0.0895	0.0372
0.65	0.6648	0.1192	0.4029	0.7934	0.2099	0.4253	0.6597	0.1051	0.0348
0.7	**0.676**	0.1289	0.4032	0.7939	0.2106	0.4265	0.6615	0.1131	0.0399
0.75	0.6629	0.1369	0.4	0.7898	0.2166	0.4268	0.6652	0.1362	0.0426
0.8	0.6604	0.1419	0.4055	0.7898	0.2098	0.4288	**0.6661**	0.1407	**0.0437**
0.85	0.6427	0.1433	0.4127	0.7857	0.2085	0.4279	0.6647	0.1481	0.0379
0.9	0.6284	**0.146**	0.4053	0.7807	0.2051	0.4257	0.6653	0.1579	0.0379
0.95	0.6264	0.1236	0.4009	0.7802	0.2071	0.4276	0.666	**0.1627**	0.0393

Note: Bold values are highest R^2 estimates.

Table B.2.14
SVR results
This table presents in-sample and out-sample R^2 estimates of all kernels used in SVR models.

In-sample			
	Linear	RBF	Poly
MASR	0.1742	**0.2104**	0.1645
RV	0.2793	0.429	**0.448**
RR	0.2093	0.2707	**0.4042**
Out-sample			
	Linear	RBF	Poly
MASR	0.0121	**0.1234**	0.0037
RV	0.0025	**0.2056**	0.0048
RR	0.0202	**0.1878**	0.0206

Note: Bold values represent best estimates.

B.3 PLOTS

Figure B.3.1
Price series of TRY
This figure graphs the Turkish lira's price against USD for the period January 2011 to December 2021. It also marks global (light blue) and domestic (dark blue) events over the period under analysis.

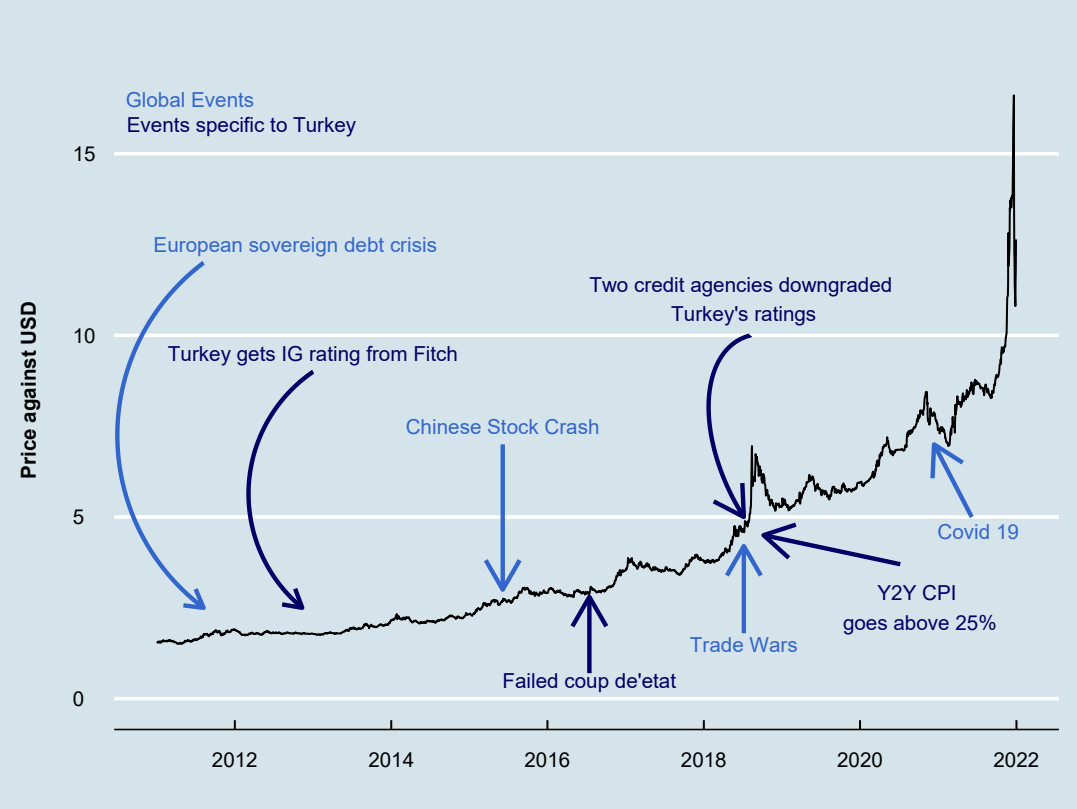

Figure B.3.2
Log returns of TRY
This figure graphs the Turkish lira's daily log returns for the period January 2011 to December 2021.

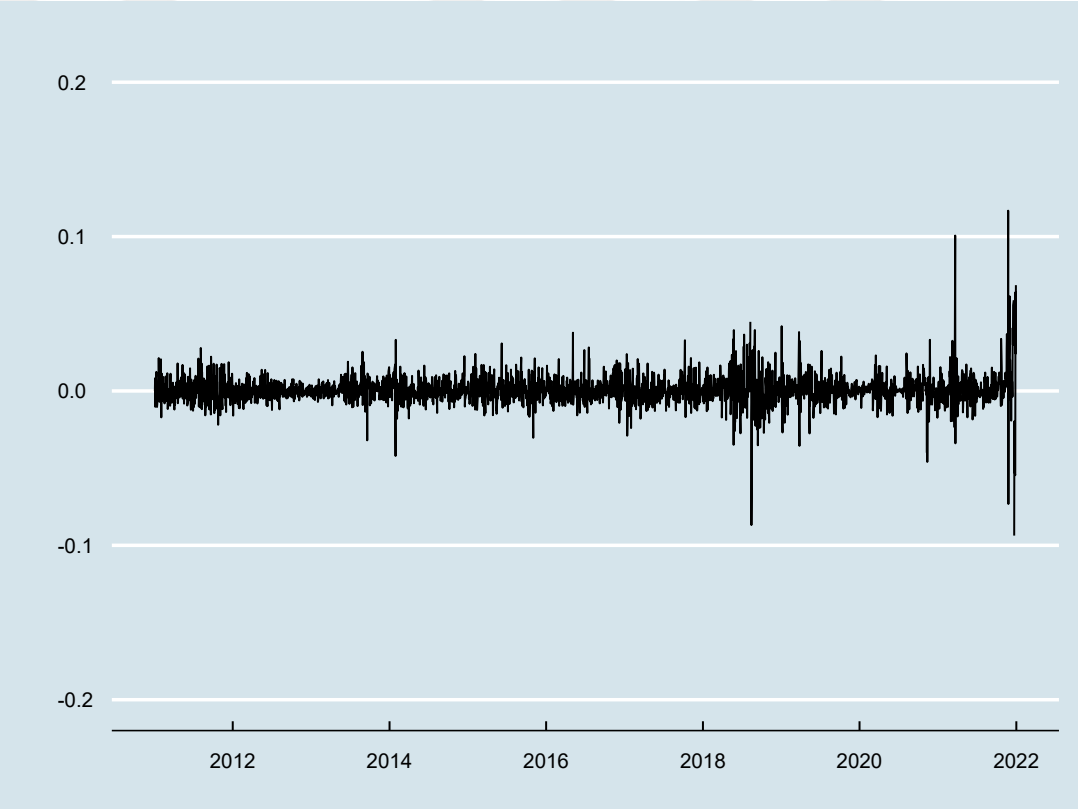

Figure B.3.3
***RV* of TRY**
This figure graphs the Turkish lira's *RV* for the period January 2011 to December 2021. *RV* is computed from intraday prices sampled at 15 min intervals.

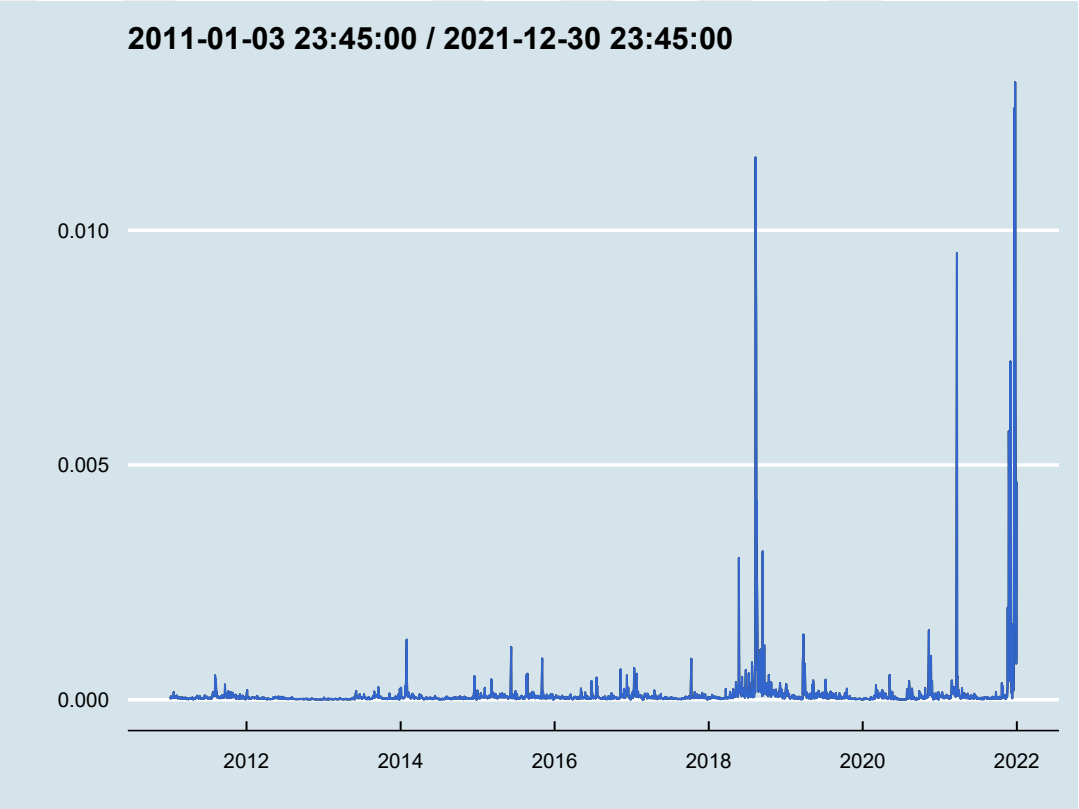

Figure B.3.4
***RR* of TRY**
This figure graphs the Turkish lira's *RR* for the period January 2011 to December 2021. Returns are computed using Parkinson's formula.

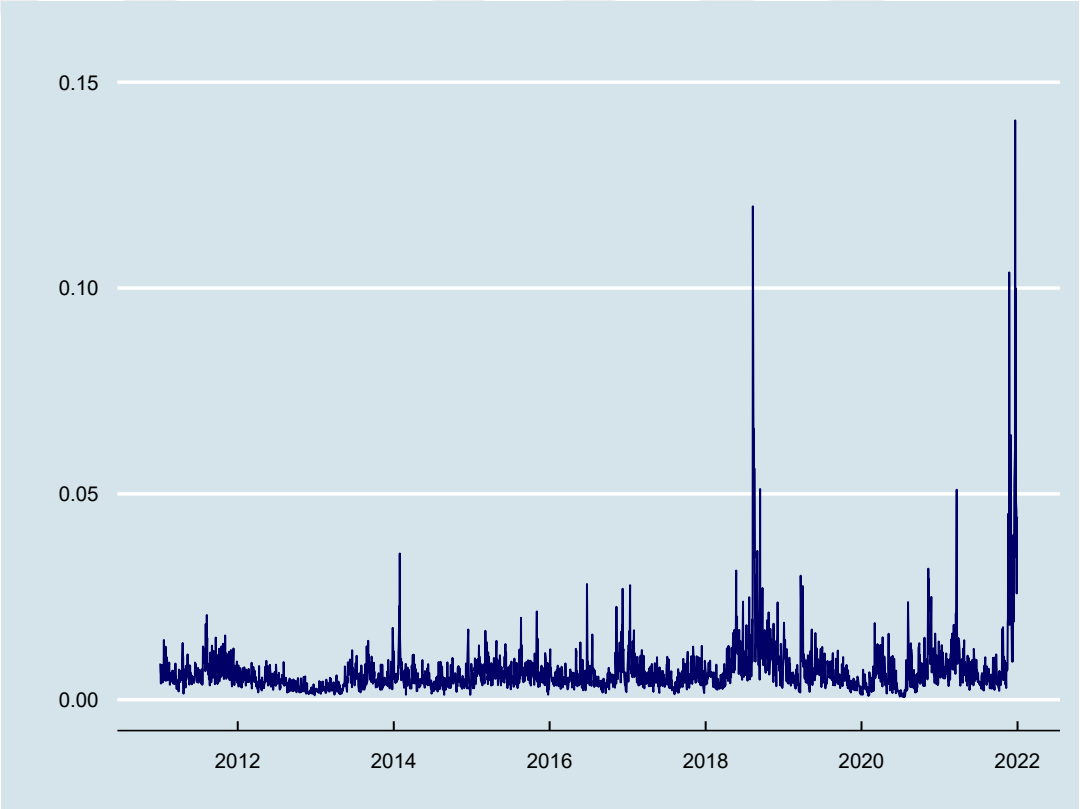

Figure B.3.5
Posterior quantiles of SV
This figure graphs the lira's estimated posterior quantiles of the SV model for the period January 2011 to December 2021.

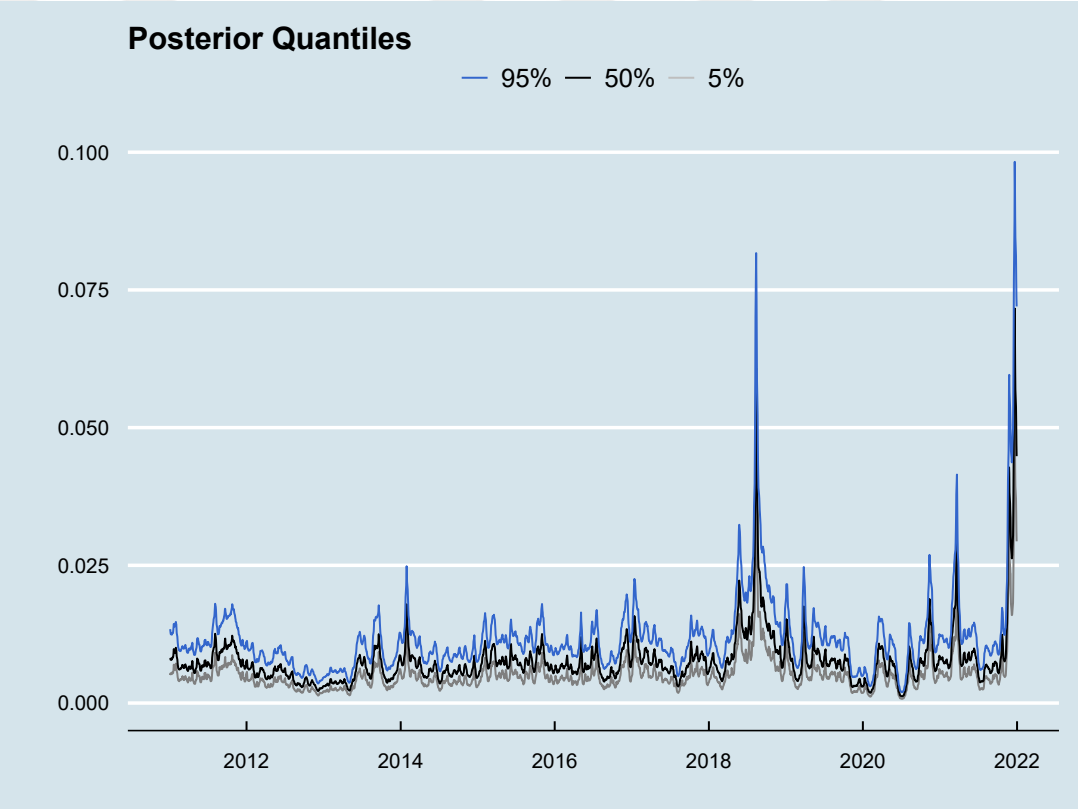

Figure B.3.6
Posterior quantiles of SVL
This figure graphs the lira's estimated posterior quantiles of the SVL model for the period January 2011 to December 2021.

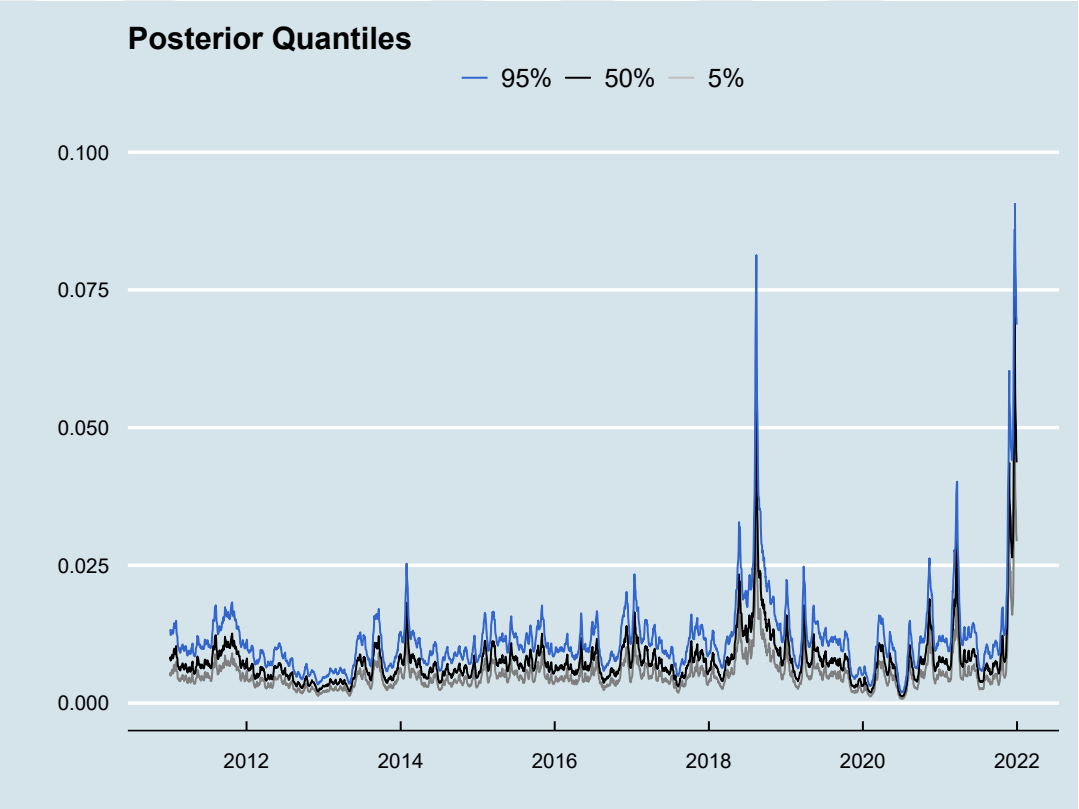

Figure B.3.7
Posterior quantiles of SVT
This figure graphs the lira's estimated posterior quantiles of the SVT model for the period January 2011 to December 2021.

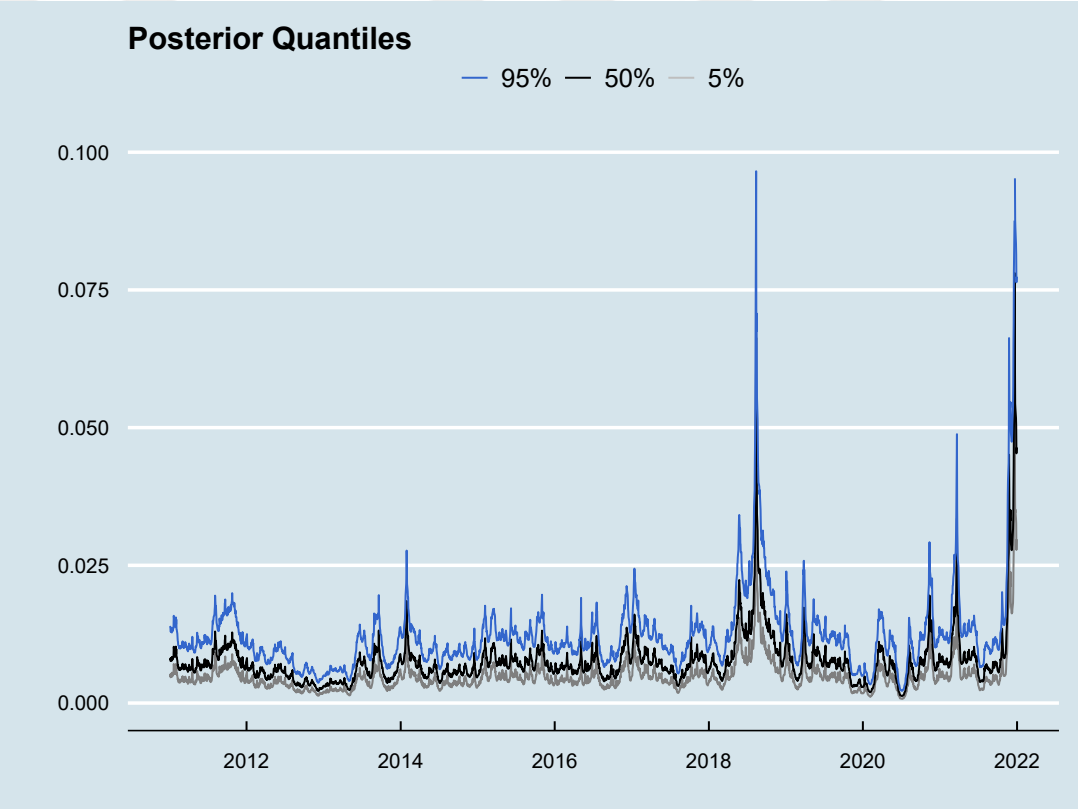

Figure B.3.8
Posterior quantiles of SVTL
This figure graphs the lira's estimated posterior quantiles of the SVTL model for the period January 2011 to December 2021.

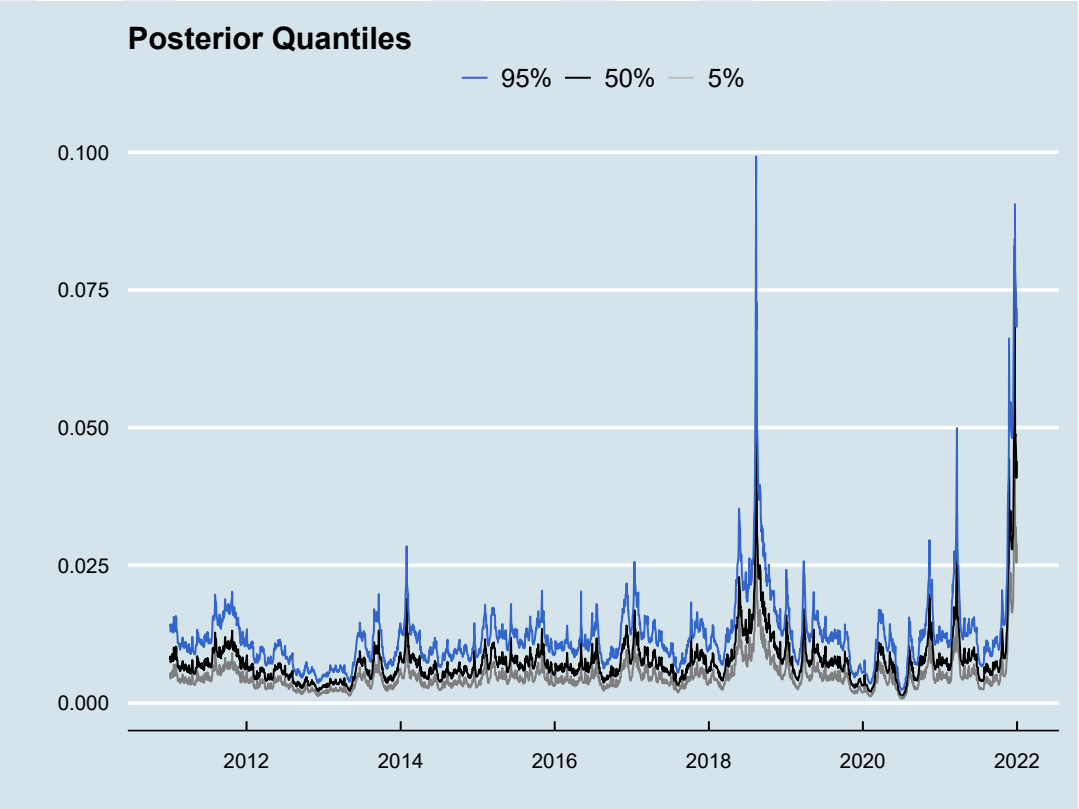

Figure B.3.9
Posterior draws of SV
This figure presents the lira's trace and density plots of posterior draws (SV model) for the period January 2011 to December 2021.

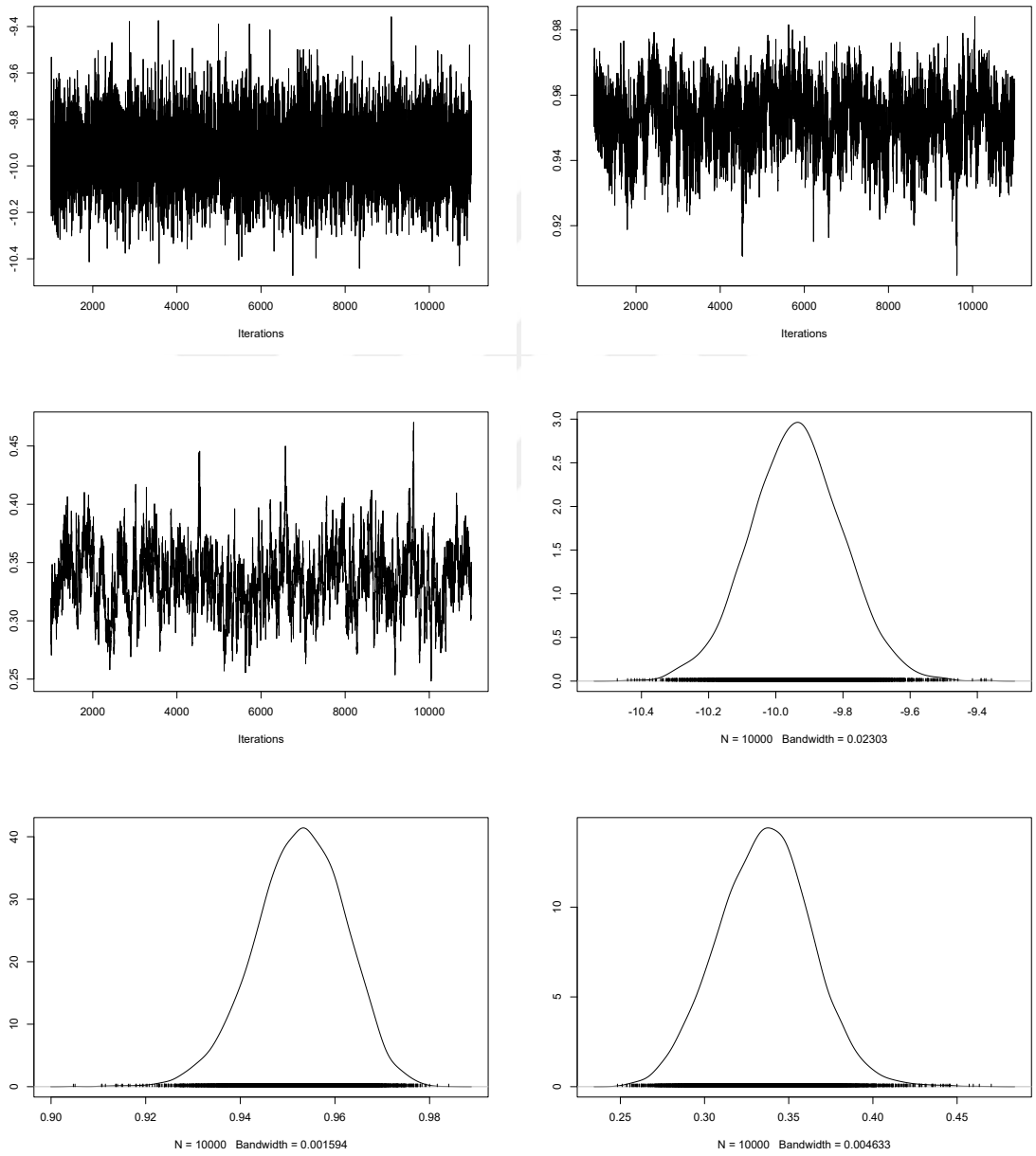

Figure B.3.10
Posterior draws of SVT
This figure presents the lira's trace and density plots of posterior draws (SVT model) for the period January 2011 to December 2021.

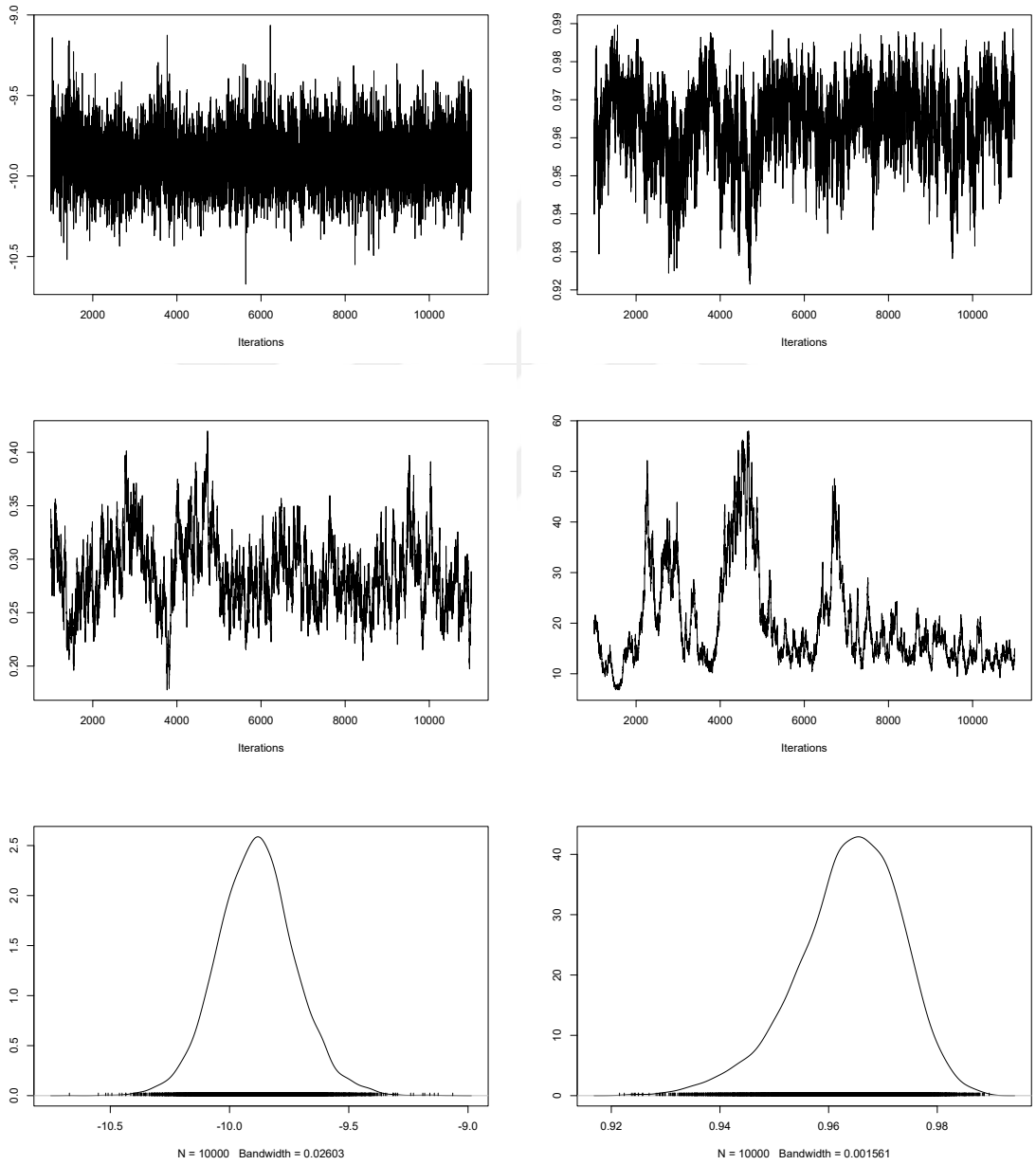

Figure B.3.10
Posterior draws of SVT
This figure presents the lira's trace and density plots of posterior draws (SVT model) for the period January 2011 to December 2021.

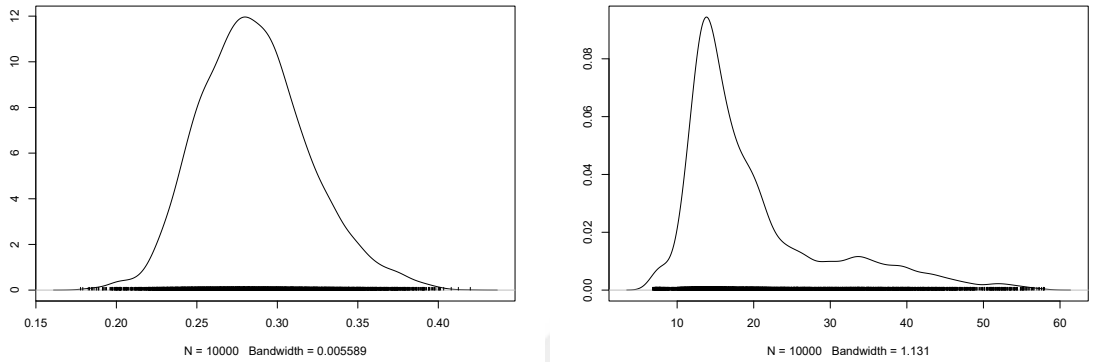

Figure B.3.11
Posterior draws of SVL
This figure presents the lira's trace and density plots of posterior draws (SVL model) for the period January 2011 to December 2021.

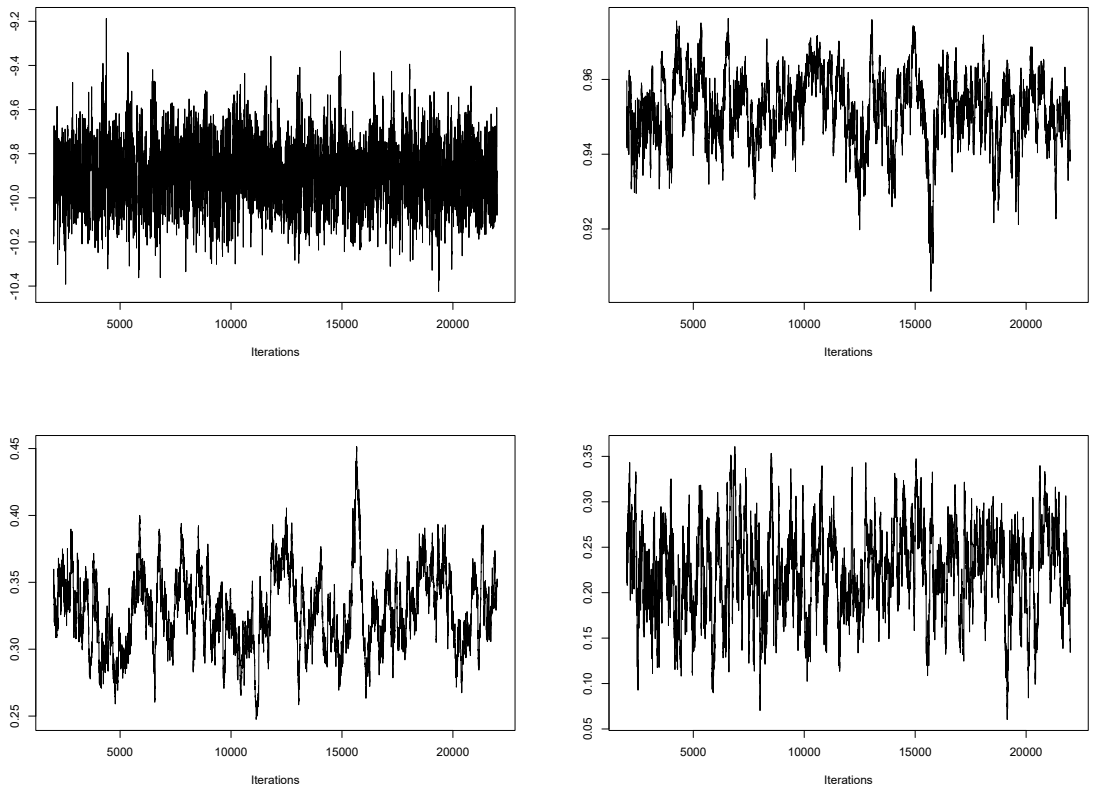

Figure B.3.11
Posterior draws of SVL
This figure presents the lira's trace and density plots of posterior draws (SVL model) for the period January 2011 to December 2021.

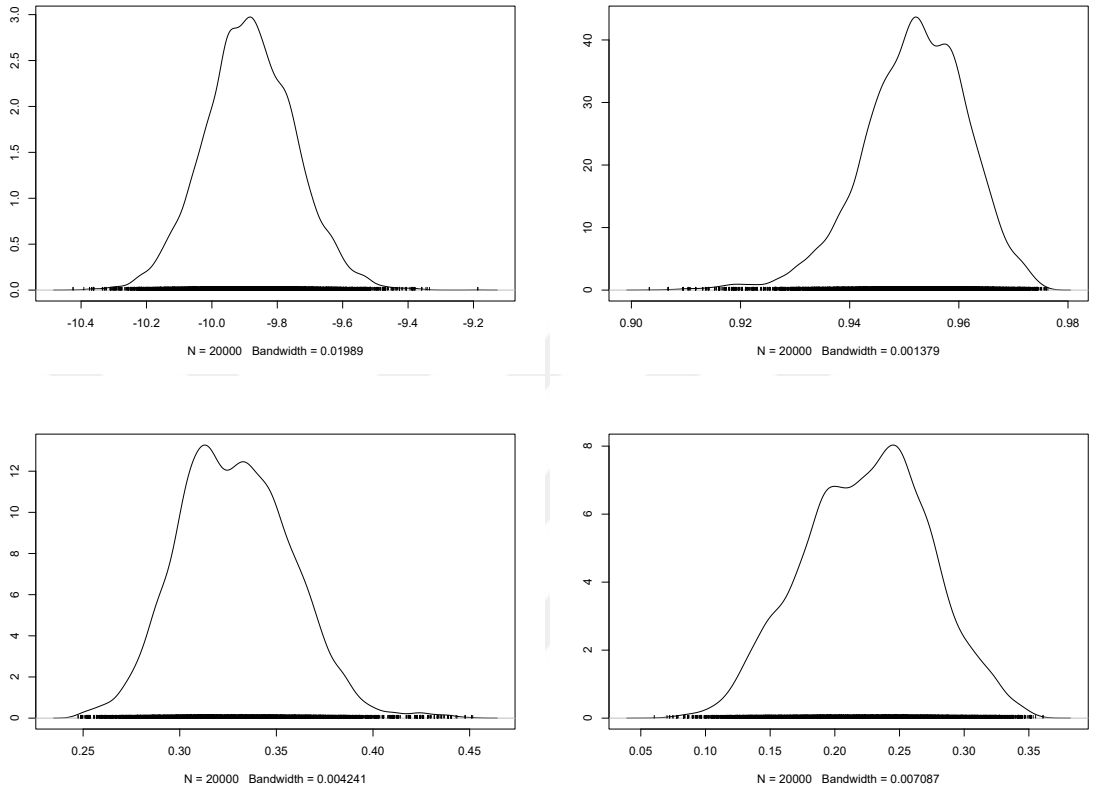

Figure B.3.12
Posterior draws of SVTL
This figure presents the lira's trace and density plots of posterior draws (SVTL model) for the period January 2011 to December 2021.

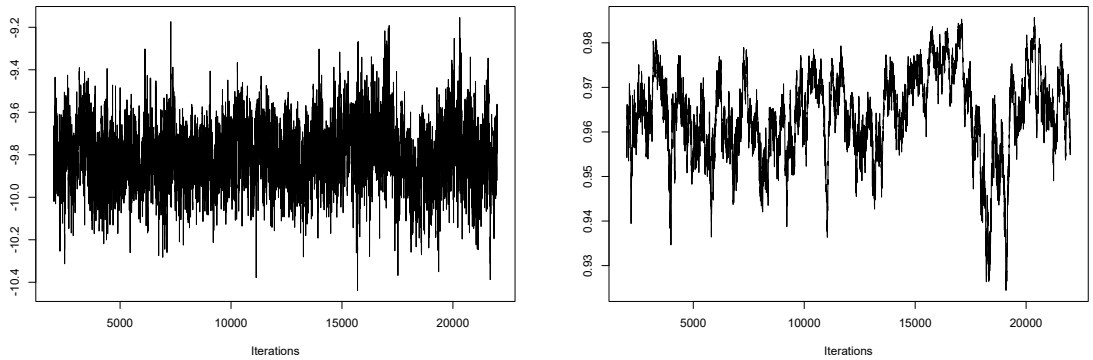

Figure B.3.12
Posterior draws of SVTL
This figure presents the lira's trace and density plots of posterior draws (SVTL model) for the period January 2011 to December 2021.

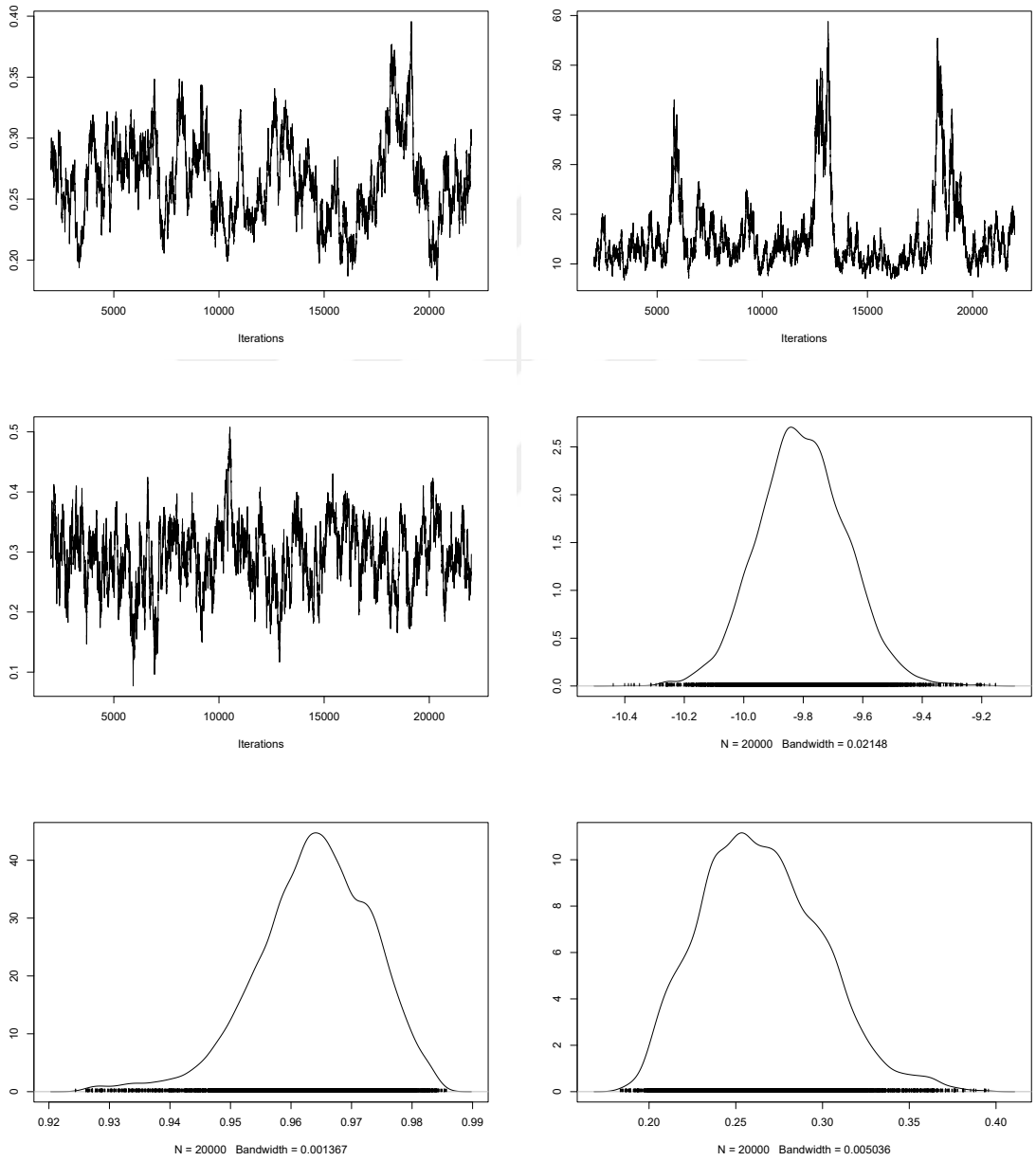

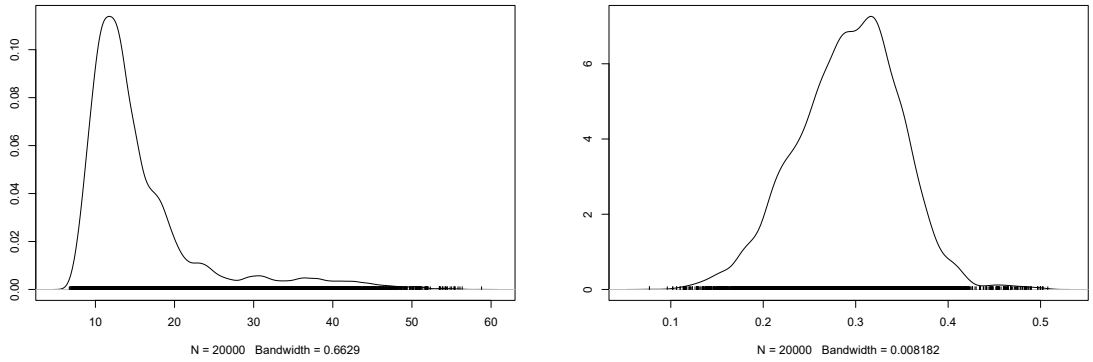

Figure B.3.13
Volatility proxies
This figure graphs the volatility proxies used as separate dependent variables in the estimation of SVR models.

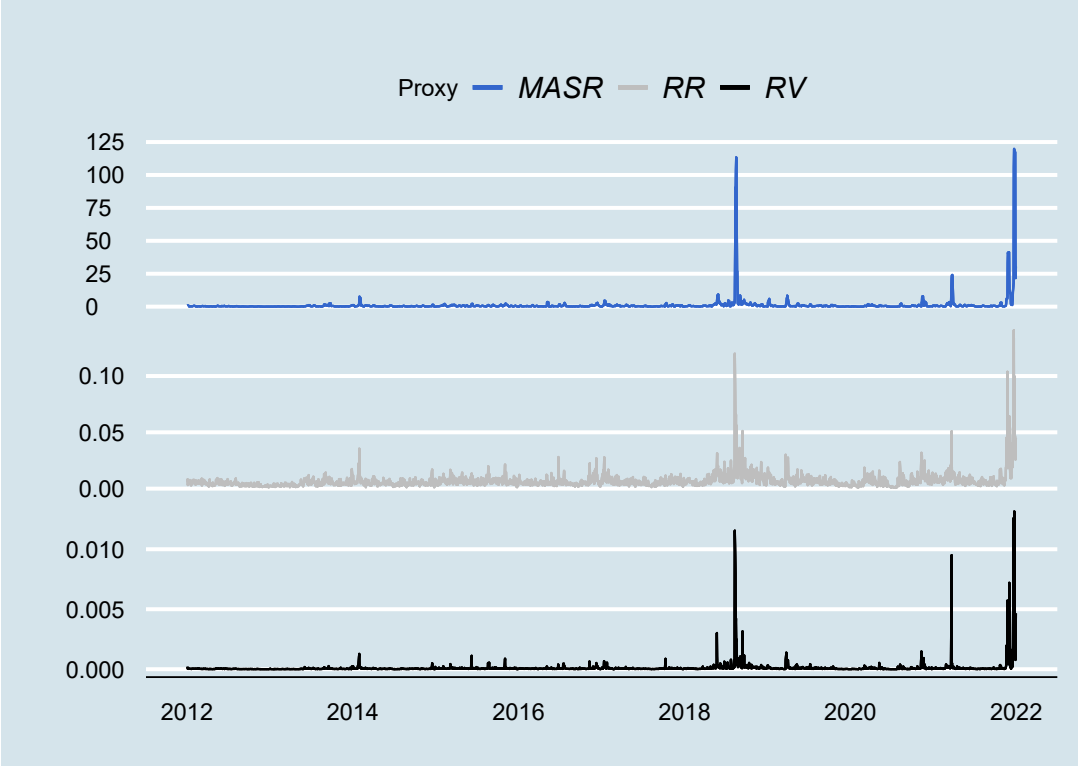

Figure B.3.14 (a)
R^2 for all values of ν (*MASR*-linear kernel)
This subfigure presents the R^2 for all values of ν. Estimates are given for the proxy *MASR* (linear kernel). Lighter shades mean low R^2, whereas darker shades represent relatively higher R^2.

Figure B.3.14 (b)
R^2 for all values of ν (*RV*-linear kernel)
This subfigure presents the R^2 for all values of ν. Estimates are given for the proxy *RV* (linear kernel). Lighter shades mean low R^2, whereas darker shades represent relatively higher R^2.

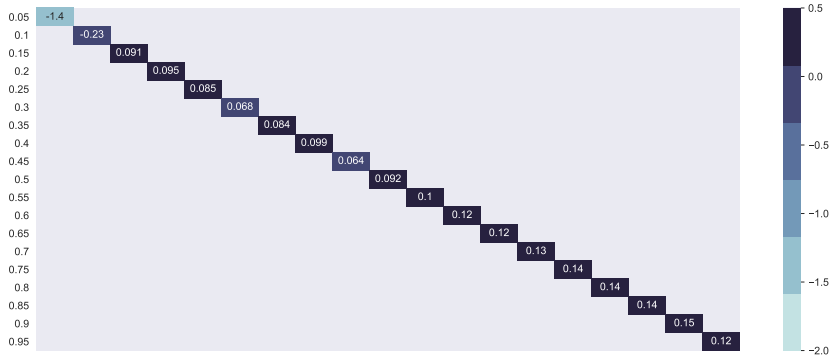

Figure B.3.14 (c)
R^2 for all values of ν (RR-linear kernel)
This subfigure presents the R^2 for all values of ν. Estimates are given for the proxy RR (linear kernel). Lighter shades mean low R^2, whereas darker shades represent relatively higher R^2.

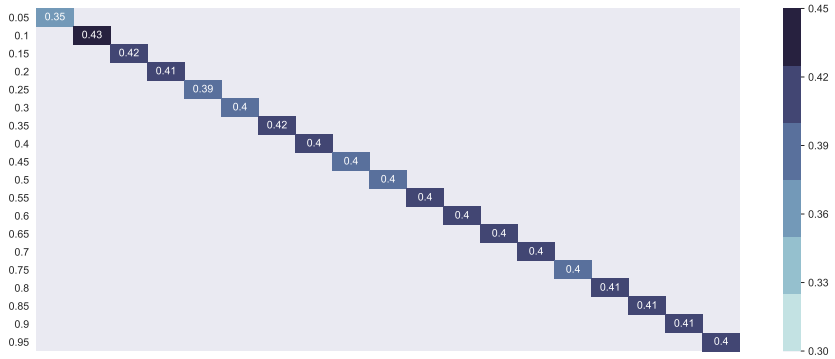

Figure B.3.15 (a)
R^2 for all values of ν ($MASR$-RBF kernel)
This subfigure presents the R^2 for all values of ν. Estimates are given for the proxy $MASR$ (RBF kernel). Lighter shades mean low R^2, whereas darker shades represent relatively higher R^2.

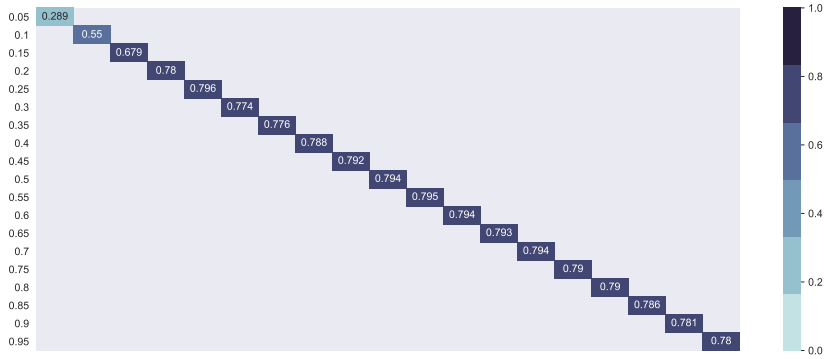

Figure B.3.15 (b)
R^2 for all values of ν (RV-RBF kernel)
This subfigure presents the R^2 for all values of ν. Estimates are given for the proxy RV (RBF kernel). Lighter shades mean low R^2, whereas darker shades represent relatively higher R^2.

Figure B.3.15 (c)
R^2 for all values of ν (RR-RBF kernel)
This subfigure presents the R^2 for all values of ν. Estimates are given for the proxy RR (RBF kernel). Lighter shades mean low R^2, whereas darker shades represent relatively higher R^2.

Figure B.3.16 (a)
R^2 for all values of ν (*MASR*-Polynomial kernel)
This subfigure presents the R^2 for all values of ν. Estimates are given for the proxy *MASR* (Polynomial kernel). Lighter shades mean low R^2, whereas darker shades represent relatively higher R^2.

Figure B.3.16 (b)
R^2 for all values of ν (*RV*-Polynomial kernel)
This subfigure presents the R^2 for all values of ν. Estimates are given for the proxy *RV* (Polynomial kernel). Lighter shades mean low R^2, whereas darker shades represent relatively higher R^2.

Figure B.3.16 (c)
R^2 for all values of ν (*RR*-Polynomial kernel)
This subfigure presents the R^2 for all values of ν. Estimates are given for the proxy *RR* (Polynomial kernel). Lighter shades mean low R^2, whereas darker shades represent relatively higher R^2.

Figure B.3.17 (a)
Feature importance (*MASR*)
This subfigure presents the feature importance of *MASR* proxy for the linear kernel. Model values show the order of importance, with the top being the most important.

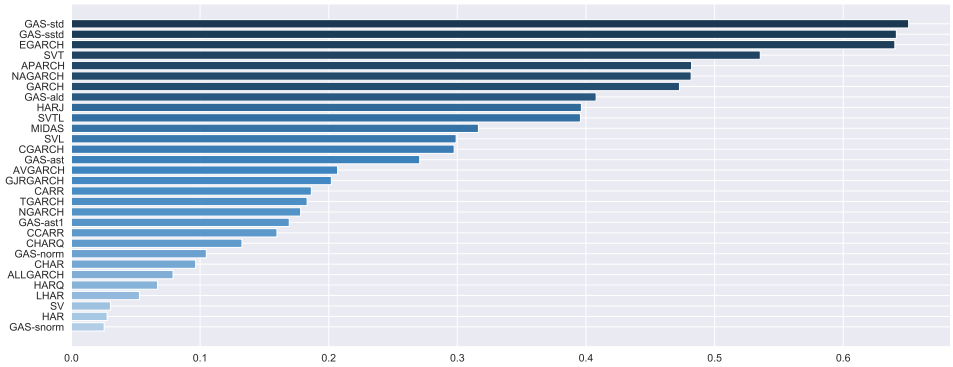

Figure B.3.17 (b)
Feature importance (*RV*)
This subfigure presents the feature importance of *RV* proxy for the linear kernel. Model values show the order of importance, with the top being the most important.

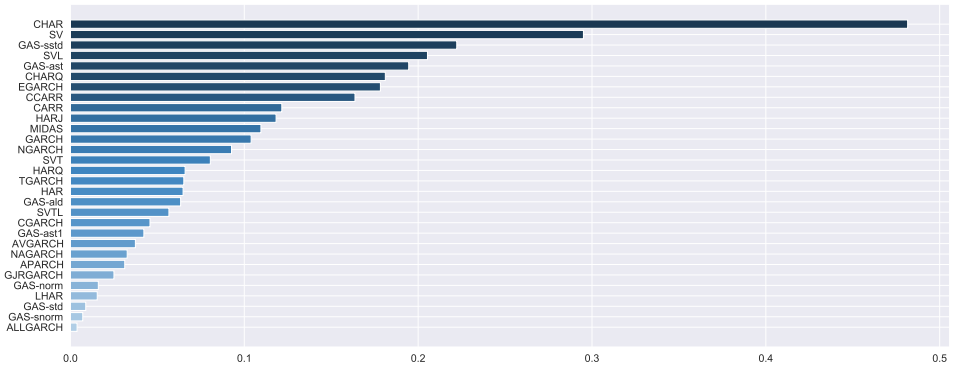

Figure B.3.17 (c)
Feature importance (*RR*)
This subfigure presents the feature importance of *RR* proxy for the linear kernel. Model values show the order of importance, with the top being the most important.

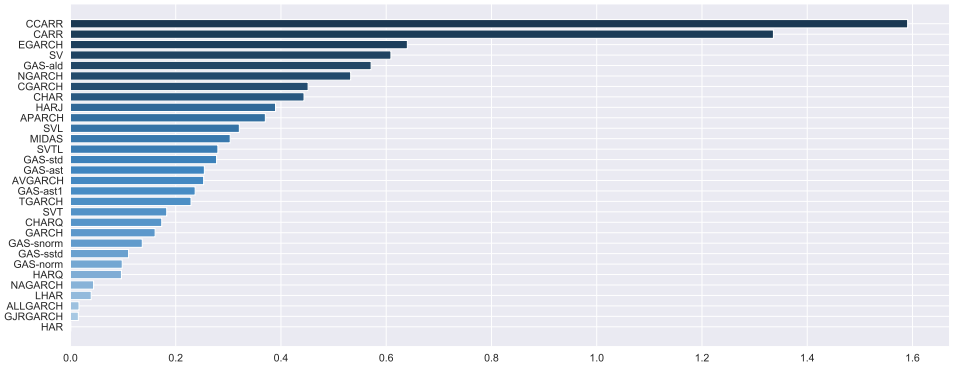

APPENDIX C

CHAPTER 3

C.1 TABLES

Table C.1.1
Summary statistics of daily log returns
This table presents summary statistics of daily log returns of TRY for the period January 2005 to October 2022, including mean (Mean), standard deviation (Sd), minimum (Min), maximum (Max), skewness (Skew), and kurtosis (Kurt), JB is Jarque-Bera statistic. ADF and PP are Augmented Dickey-Fuller and Phillips–Perron unit root tests, respectively.

	Mean	Sd	Min	Max	Skew	Kurt	J.B.	ADF	PP
TL	0.06	1.1	-20.9	20.54	0.41	66.32	817706***	-15.647***	-3905.7***
BIST	0.06	1.64	-11.06	12.13	-0.48	4.26	3537.7***	-15.206***	-4418.2***

***Significant at 1% level.

Table C.1.2
IMF statistics for TL returns
This table presents IMF statistics of daily log returns of TRY for the period January 2005 to October 2022.

	Mean period (days)	Pearson correlation	Kendall correlation	Variance as % of observed	Variance as % of (∑ IMFs + residual)
IMF1	2.71	0.66***	0.54***	51.13	56.34
IMF2	4.18	0.48***	0.33***	11.97	13.19
IMF3	5.51	0.47***	0.31***	10.77	11.87
IMF4	9.15	0.36***	0.25***	6.65	7.33
IMF5	17.21	0.25***	0.18***	4.1	4.52
IMF6	31.39	0.18***	0.12***	1.95	2.15
IMF7	57.88	0.15***	0.09***	1.85	2.04
IMF8	117.29	0.1***	0.08***	1.17	1.29
IMF9	247.61	0.05***	0.02**	0.51	0.56
IMF10	495.22	0.04**	0.03***	0.35	0.38
IMF11	891.4	0.02	0.02	0.15	0.17
Residual		0.03*	0.02**	0.14	0.15
Sum				90.74	100

***, **, *Signficant at 1%, 5%, and 10% levels, respectively.

Table C.1.3
IMF statistics for BIST returns
This table presents IMF statistics of daily log returns of BIST for the period January 2005 to October 2022.

	Mean period (days)	Pearson correlation	Kendall correlation	Variance as % of observed	Variance as % of (∑ IMFs + residual)
IMF1	2.74	0.73***	0.55***	53.44	63.09
IMF2	4.37	0.44***	0.31***	6.38	7.53
IMF3	5.91	0.45***	0.3***	7.36	8.68
IMF4	9.82	0.39***	0.25***	6.93	8.18
IMF5	18.12	0.27***	0.17***	4.12	4.87
IMF6	33.51	0.2***	0.12***	2.64	3.12
IMF7	65.54	0.15***	0.09***	1.94	2.29
IMF8	135.06	0.1***	0.06***	1.01	1.19
IMF9	278.56	0.09***	0.06***	0.59	0.7
IMF10	557.12	0.06***	0.04***	0.13	0.16
IMF11	1485.67	0.04***	0.03***	0.03	0.03
Residual		0.04***	0.03***	0.12	0.14
Sum				84.69	100

***Signficant at 1% level.

Table C.1.4
Reconstruction results
This table presents estimates for the Jarque-Bera (JB) normality test and Wilcoxon Rank Sum test (WRS) of TL and BIST returns. These values are used to reconstruct time series into short-term and long-term components.

	TL		BIST	
	JB	WRS	JB	WRS
IMF1	56601***	4908358	235.3***	4934614
IMF2	213397***	4911613	1092.2***	4942127
IMF3	369735***	4865335	1597.2***	4951016
IMF4	469496***	4872272	2228.5***	4977141
IMF5	553915***	4818902*	2861***	5012193
IMF6	628932***	4783081**	3308.3***	5082068
IMF7	720730***	4745892***	3434.4***	5111140*
IMF8	765083***	4756035**	3618.3***	5121411*
IMF9	784430***	4644915***	3669.9***	5188583**
IMF10	805114***	4647780***	3669.3***	5197518***
IMF11	811537***	4620697***	3649.8***	5181104**

***, **, *Signficant at 1%, 5%, and 10% levels, respectively.

C.2 PLOTS

Figure C.2.1
Correlation between TL and BIST
This figure graphs the correlation between TL returns and BIST returns for the period January 2005 to October 2022.

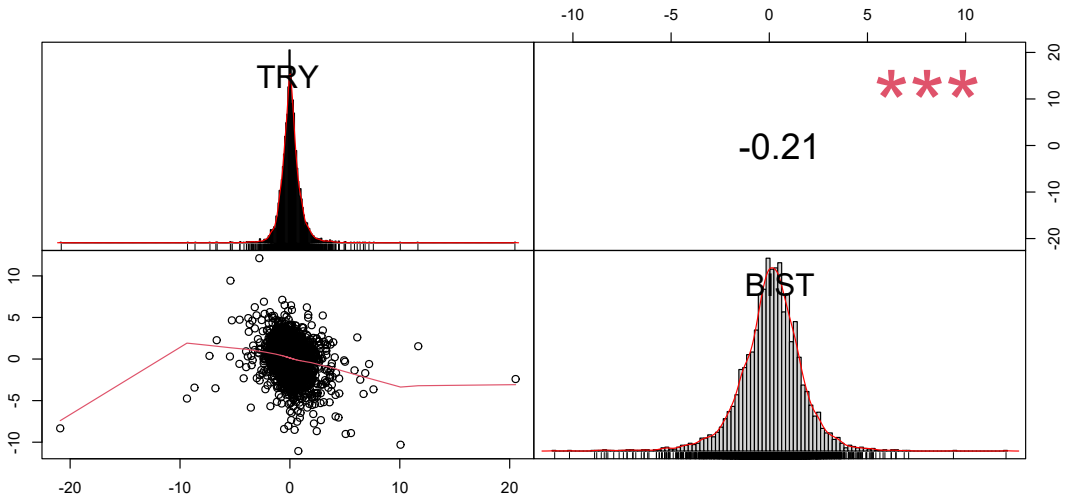

Figure C.2.2
Decomposition of TL
This figure plots the TL returns decomposition with CEEMDAN for the period January 2005 to October 2022. Estimation is done by using an ensemble size of 100 and 0.3 standard deviation.

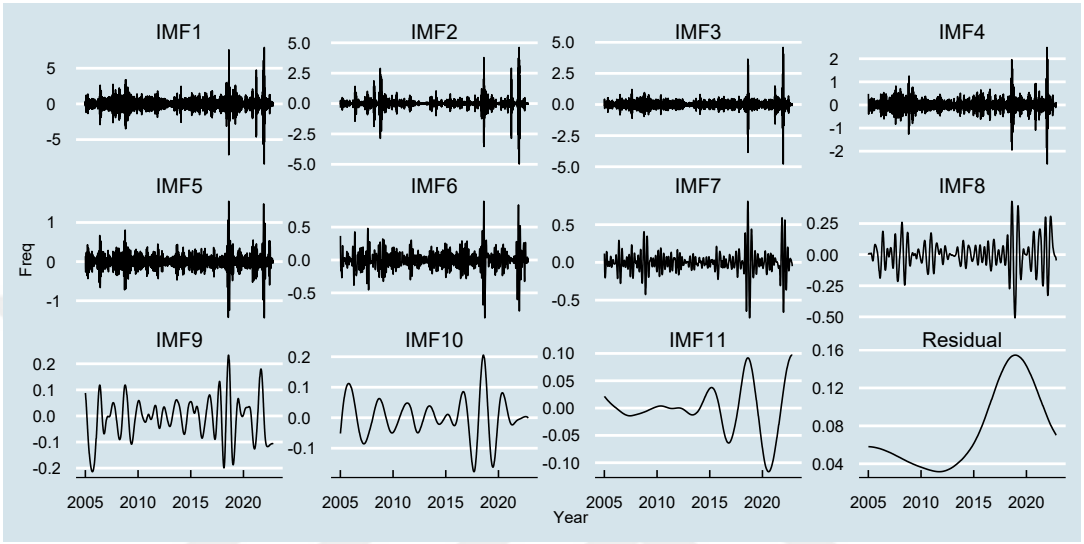

Figure C.2.3
Decomposition of BIST
This figure plots the BIST returns decomposition with CEEMDAN for the period January 2005 to October 2022. Estimation is done by using an ensemble size of 100 and 0.3 standard deviation.

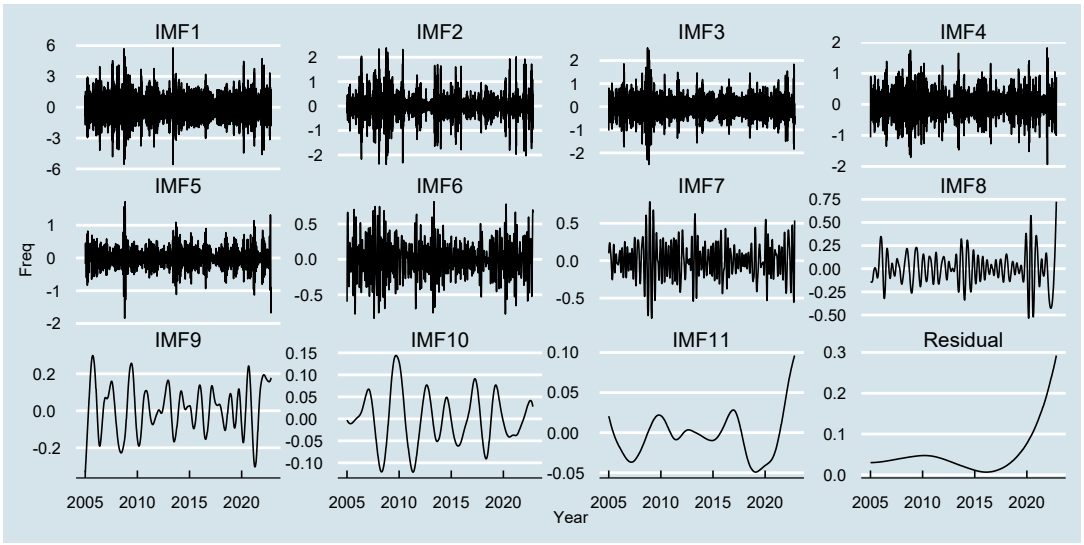

Figure C.2.4
Return and components of TL
This figure graphs the TL return and components obtained after the reconstruction of IMFs. This plot contains only the last year of the complete data to provide a 'zoomed in' version of the total sample.

Figure C.2.5
Return and components of BIST
This figure graphs the BIST return and components obtained after the reconstruction of IMFs. This plot contains only the last year of the complete data to provide a 'zoomed in' version of the total sample.

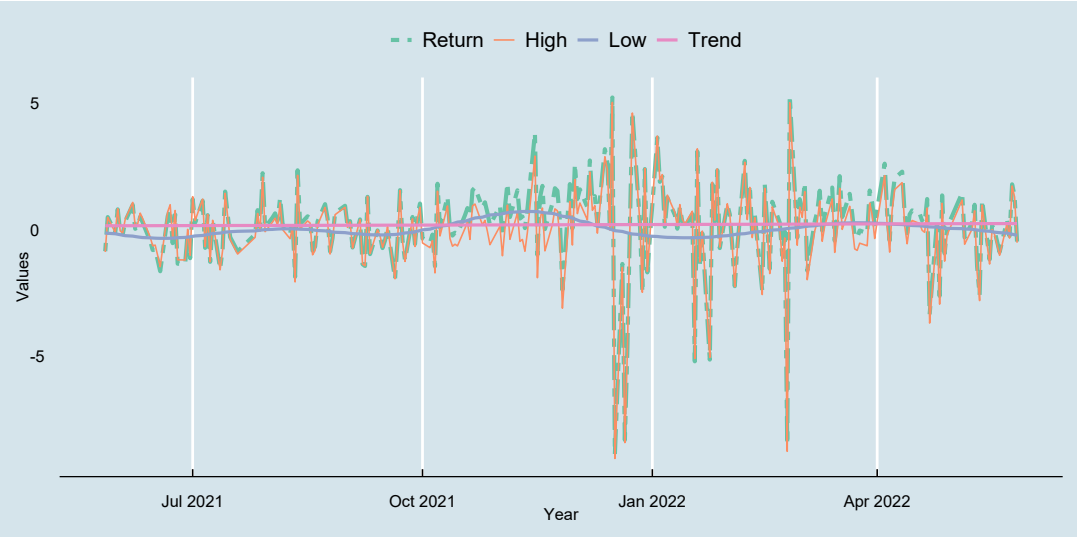

Figure C.2.6 (a)
Directional predictability from TL to BIST when $\hat{\rho}_\beta(k)$ for $\beta_2 = 0.1$
This subfigure presents the directional predictability from TL returns to BIST returns when $\hat{\rho}_\beta(k)$ for $\beta_2 = 0.1$. In the first row plots, bars are sample cross quantilogram whereas $\hat{Q}_\beta^p$ values are in the second row. Red lines are bootstrap values with a 95% confidence interval centered at zero.

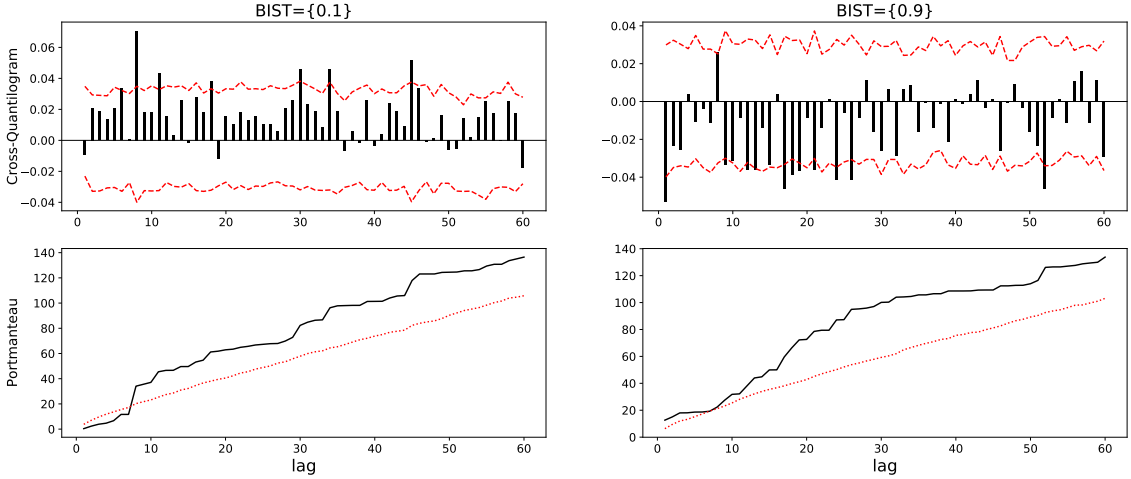

Figure C.2.6 (b)
Directional predictability from TL to BIST when $\hat{\rho}_\beta(k)$ for $\beta_2 = 0.9$
This subfigure presents the directional predictability from TL returns to BIST returns when $\hat{\rho}_\beta(k)$ for $\beta_2 = 0.9$. In the first row plots, bars are sample cross quantilogram whereas $\hat{Q}_\beta^p$ values are in the second row. Red lines are bootstrap values with a 95% confidence interval centered at zero.

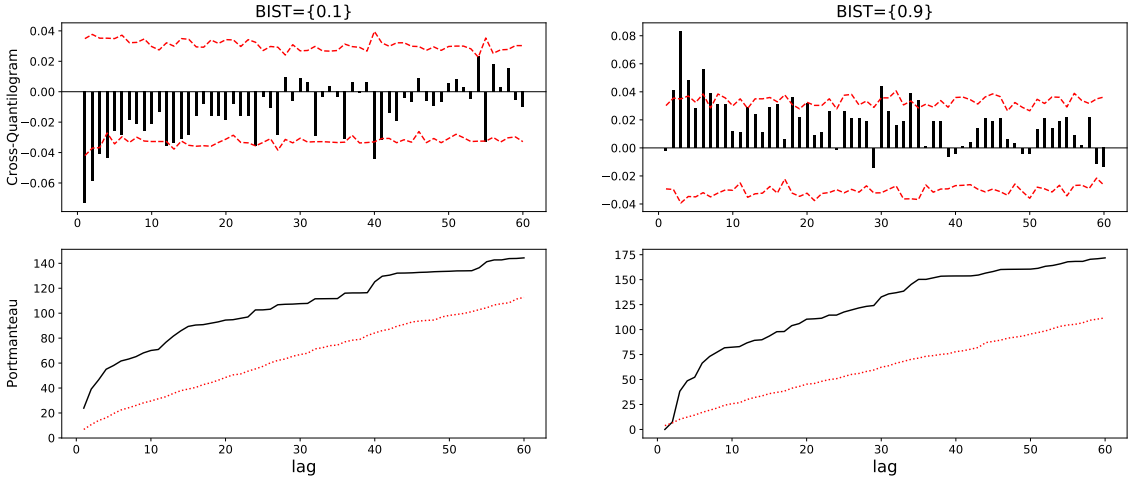

Figure C.2.6 (c)
Heatmap of spillover from TL to BIST
This subfigure presents the heatmap for sample cross quantilogram at $(\beta_2, \beta_1)|(\beta_2, \beta_1) \in 0.1, ..., 0.9$ and $k = 1$. It gives the magnitude of spillover from TL returns to BIST returns with lag 1. The star means significance in the test. Quantiles for BIST and TL are given on the x-axis and y-axis, respectively.

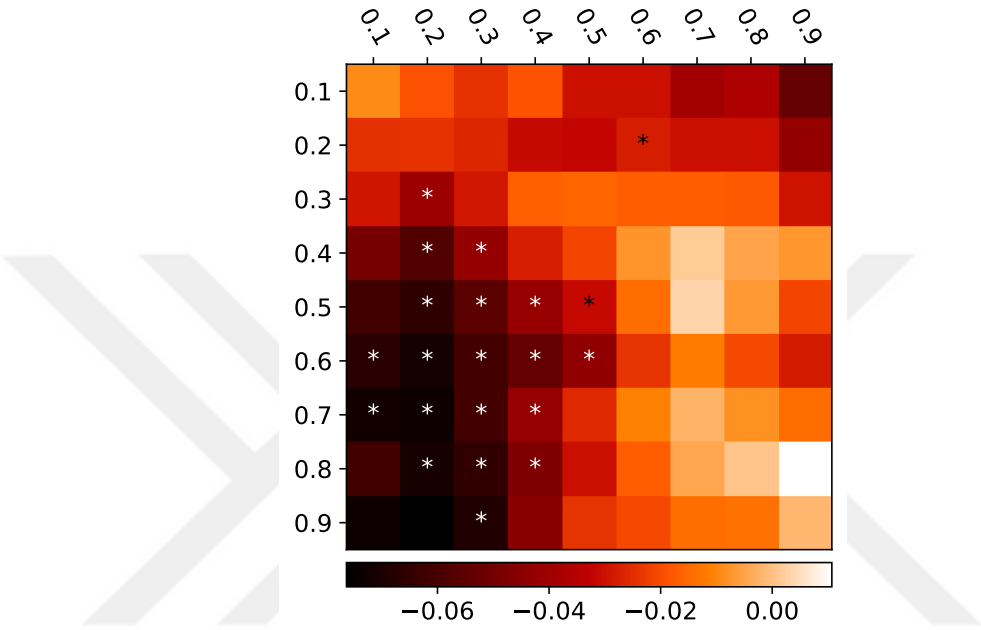

Figure C.2.7 (a)
Directional predictability from TL (high-frequency) to BIST (high-frequency) when $\hat{\rho}_\beta(k)$ for $\beta_2 = 0.1$
This subfigure presents the directional predictability from high-frequency TL returns to high-frequency BIST returns when $\hat{\rho}_\beta(k)$ for $\beta_2 = 0.1$. In the first row plots, bars are sample cross quantilogram whereas $\hat{Q}_\beta^p$ values are in the second row. Red lines are bootstrap values with a 95% confidence interval centered at zero.

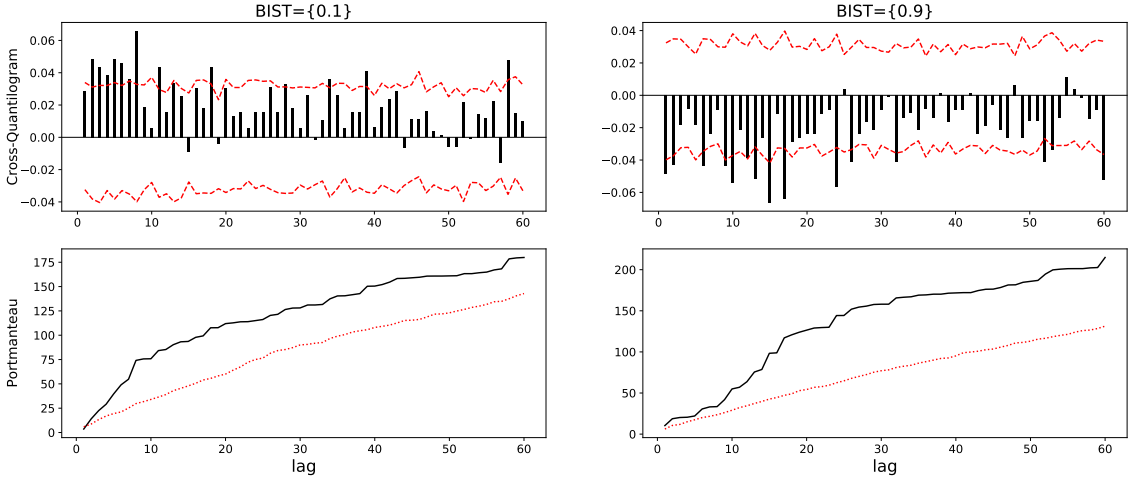

Figure C.2.7 (b)
Directional predictability from TL (high-frequency) to BIST (high-frequency) when $\hat{\rho}_\beta(k)$ for β_2 = 0.9

This subfigure presents the directional predictability from high-frequency TL returns to high-frequency BIST returns when $\hat{\rho}_\beta(k)$ for $\beta_2 = 0.9$. In the first row plots, bars are sample cross quantilogram whereas $\hat{Q}^p_\beta$ values are in the second row. Red lines are bootstrap values with 95% confidence interval centered at zero.

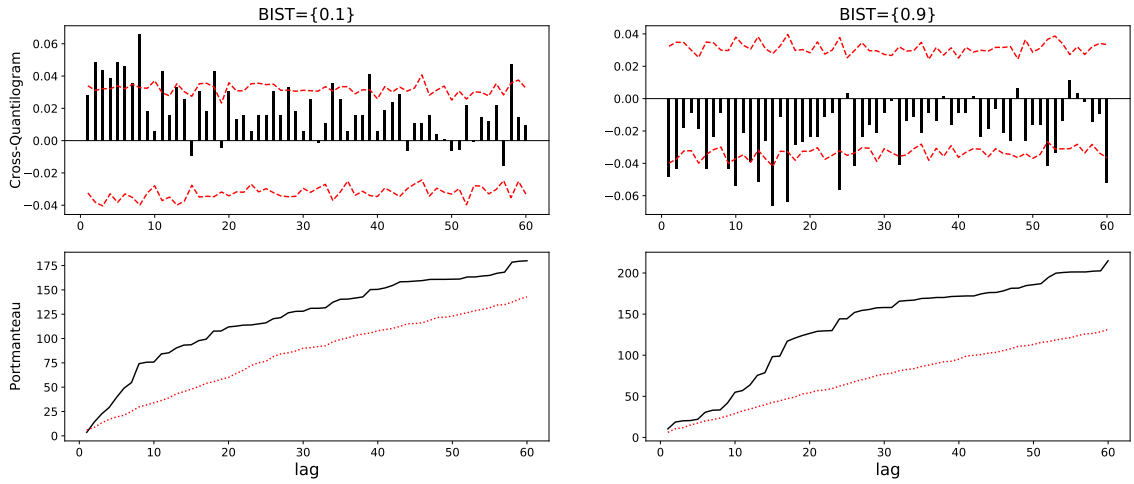

Figure C.2.7 (c)
Heatmap of spillover from TL (high-frequency) to BIST (high-frequency)

This subfigure presents the heatmap for sample cross quantilogram at $(\beta_2, \beta_1)|(\beta_2, \beta_1) \in 0.1, ..., 0.9$ and $k = 1$. It gives the magnitude of spillover from high-frequency TL returns to high-frequency BIST returns with lag 1. The star means significance in the test. Quantiles for BIST and TL are given on the x-axis and y-axis, respectively.

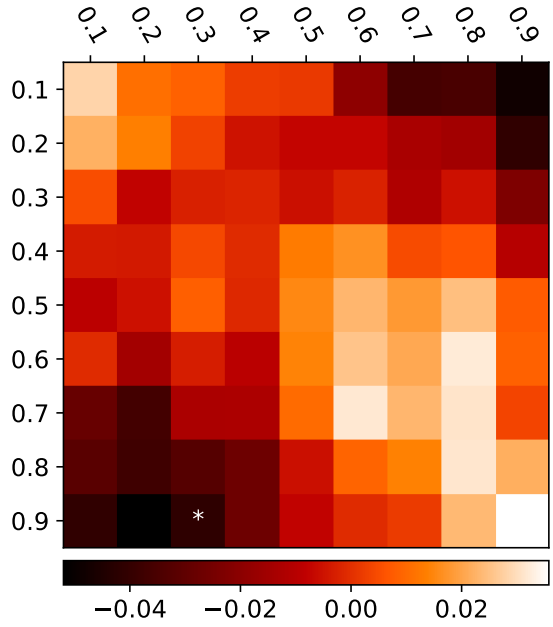

Figure C.2.8 (a)
Directional predictability from TL (low-frequency) to BIST (low-frequency) when $\hat{\rho}_\beta(k)$ for β_2 = 0.1
This subfigure presents the directional predictability from low-frequency TL returns to low-frequency BIST returns when $\hat{\rho}_\beta(k)$ for $\beta_2 = 0.1$. In the first row plots, bars are sample cross quantilogram whereas $\hat{Q}^p_\beta$ values are in the second row. Red lines are bootstrap values with a 95% confidence interval centered at zero.

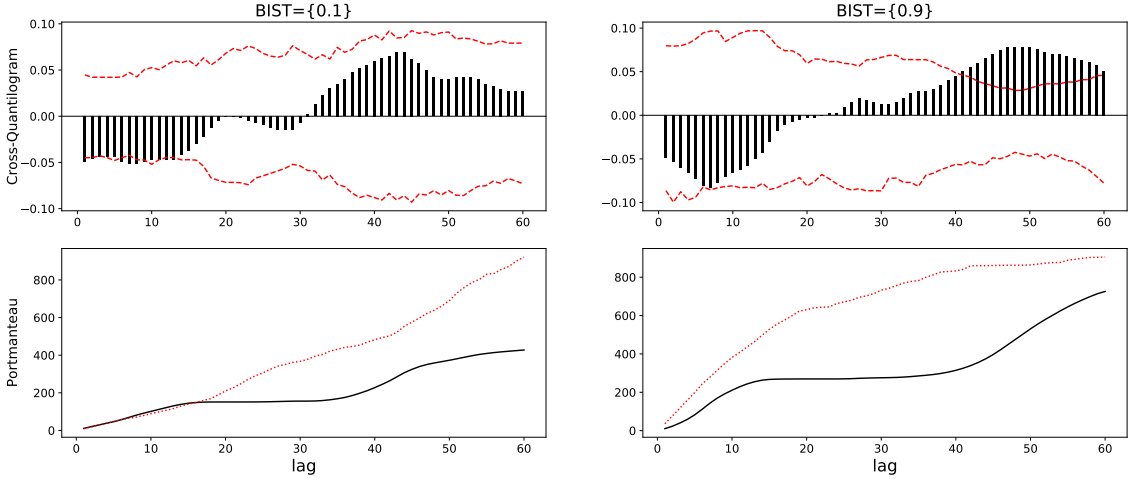

Figure C.2.8 (b)
Directional predictability from TL (low-frequency) to BIST (low-frequency) when $\hat{\rho}_\beta(k)$ for β_2 = 0.9
This subfigure presents the directional predictability from low-frequency TL returns to low-frequency BIST returns when $\hat{\rho}_\beta(k)$ for $\beta_2 = 0.9$. In the first row plots, bars are sample cross quantilogram whereas $\hat{Q}^p_\beta$ values are in the second row. Red lines are bootstrap values with a 95% confidence interval centered at zero.

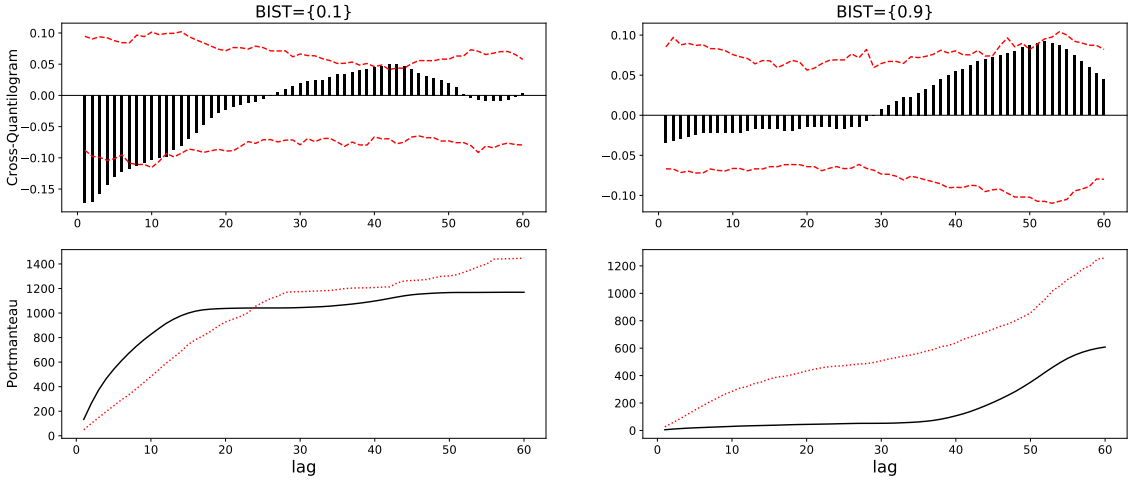

Figure C.2.8 (c)
Heatmap of spillover from TL (low-frequency) to BIST (low-frequency)
This subfigure presents the heatmap for sample cross quantilogram at $(\beta_2, \beta_1)|(\beta_2, \beta_1) \in 0.1, ..., 0.9$ and $k = 1$. It gives the magnitude of spillover from low-frequency TL returns to low-frequency BIST returns with lag 1. The star means significance in the test. Quantiles for BIST and TL are given on the x-axis and y-axis, respectively.

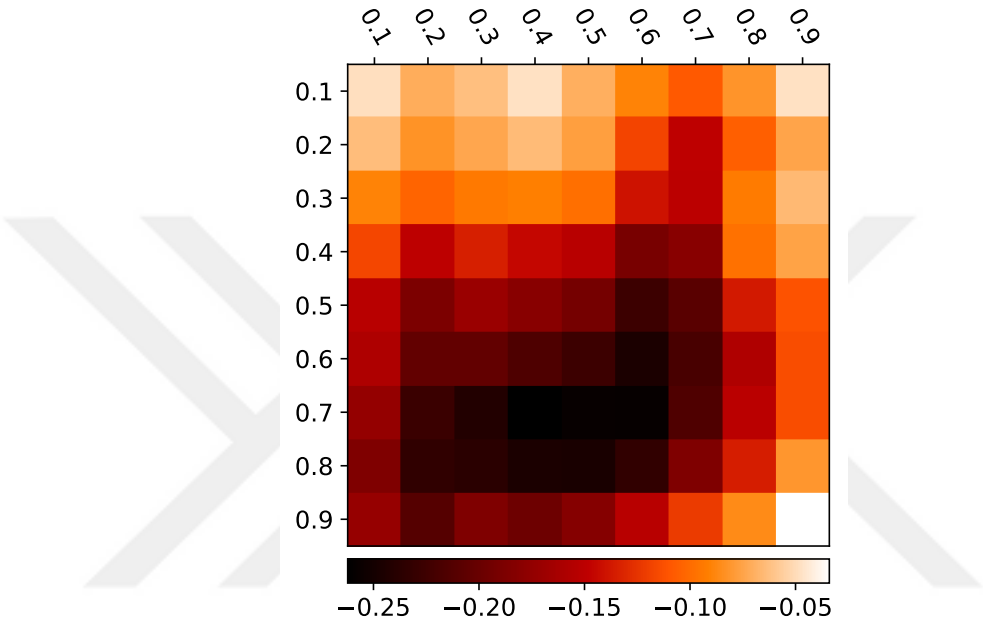

Figure C.2.9 (a)
Directional predictability from BIST to TL when $\hat{\rho}_\beta(k)$ for $\beta_1 = 0.1$
This subfigure presents the directional predictability from BIST returns to TL returns when $\hat{\rho}_\beta(k)$ for $\beta_1 = 0.1$. In the first row plots, bars are sample cross quantilogram whereas $\hat{Q}^p_\beta$ values are in the second row. Red lines are bootstrap values with a 95% confidence interval centered at zero.

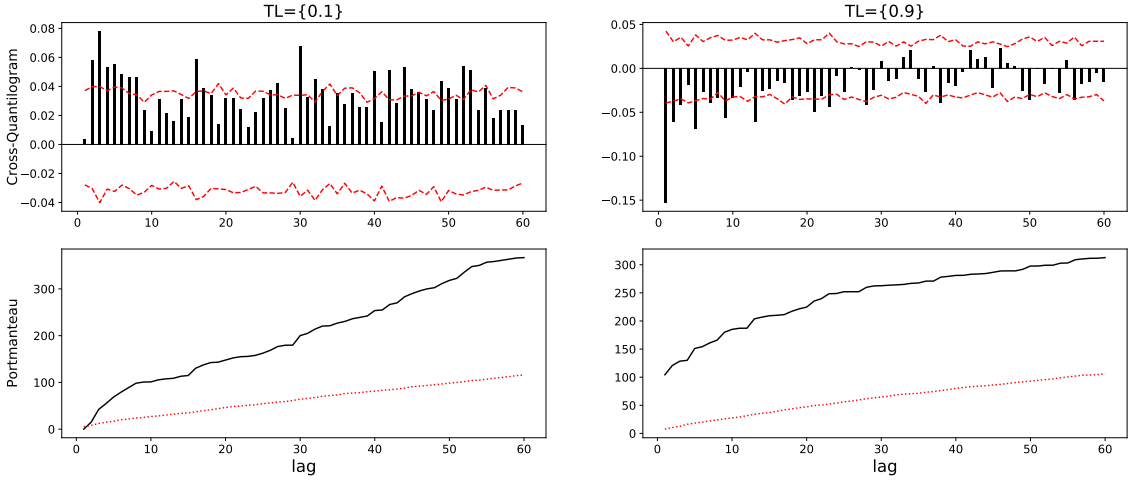

Figure C.2.9 (b)
Directional predictability from BIST to TL when $\hat{\rho}_\beta(k)$ for β_1 = 0.9
This subfigure presents the directional predictability from BIST returns to TL returns when $\hat{\rho}_\beta(k)$ for $\beta_1 = 0.9$. In the first row plots, bars are sample cross quantilogram whereas $\hat{Q}^p_\beta$ values are in the second row. Red lines are bootstrap values with a 95% confidence interval centered at zero.

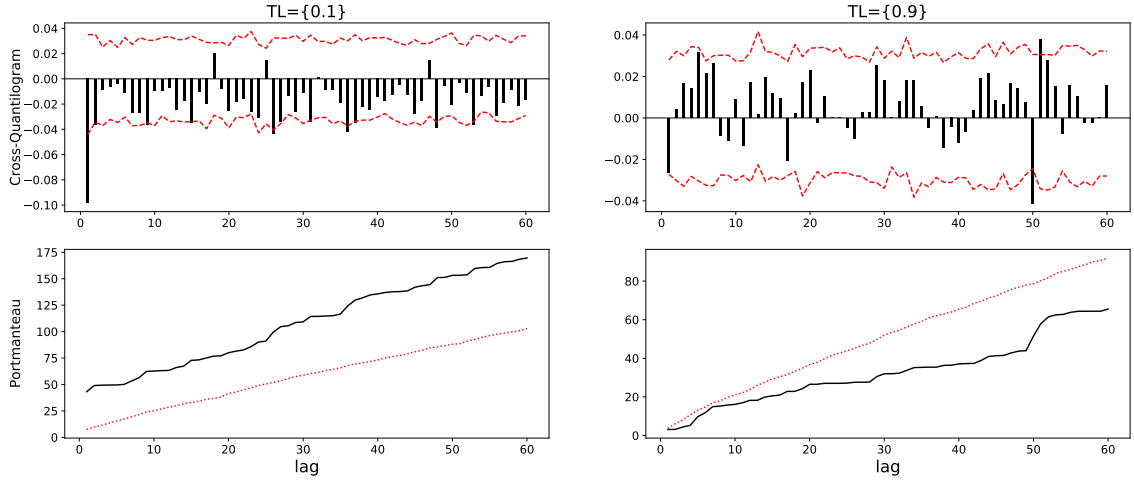

Figure C.2.9 (c)
Heatmap of spillover from BIST to TL
This subfigure presents the heatmap for sample cross quantilogram at $(\beta_2, \beta_1)|(\beta_2, \beta_1) \in 0.1, ..., 0.9$ and $k = 1$. It gives the magnitude of spillover from BIST returns to TL returns with lag 1. The star means significance in the test. Quantiles for TL and BIST are given on the x-axis and y-axis, respectively.

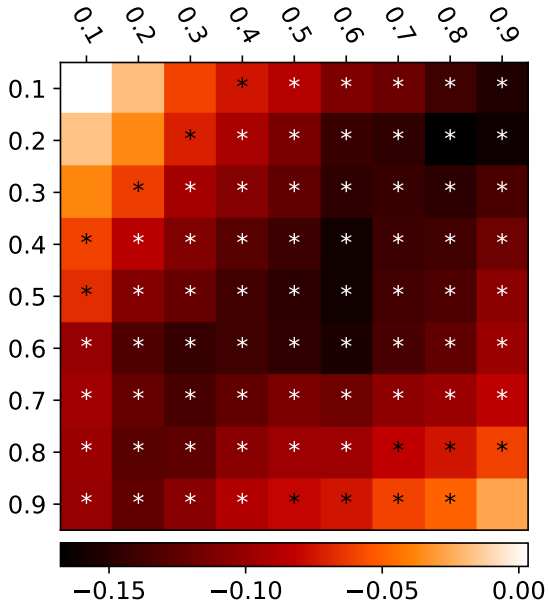

Figure C.2.10 (a)
Directional predictability from BIST (high-frequency) to TL (high-frequency) when $\hat{\rho}_\beta(k)$ for β_1 = 0.1
This subfigure presents the directional predictability from high-frequency BIST returns to high-frequency TL returns when $\hat{\rho}_\beta(k)$ for $\beta_1 = 0.1$. In the first row plots, bars are sample cross quantilogram whereas $\hat{Q}_\beta^p$ values are in the second row. Red lines are bootstrap values with a 95% confidence interval centered at zero.

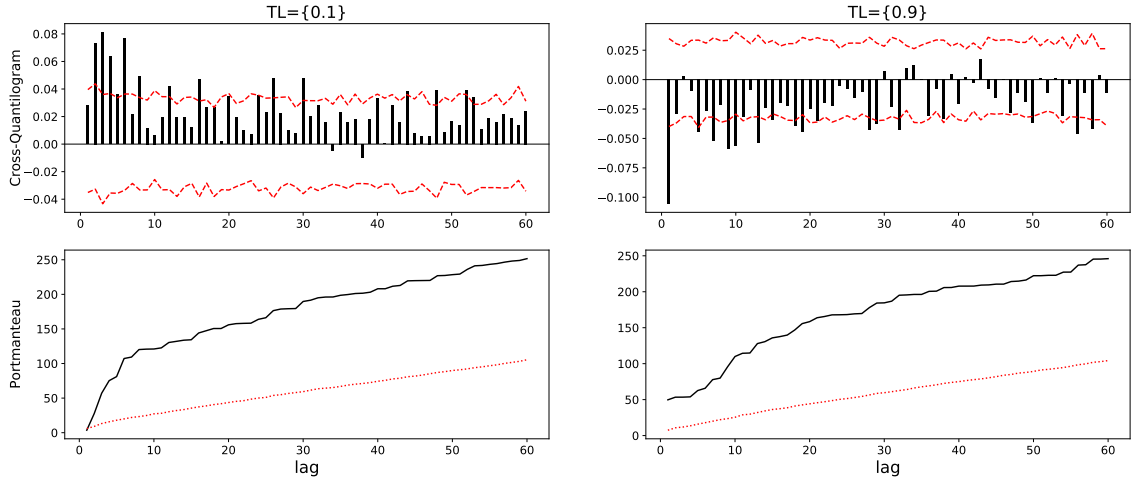

Figure C.2.10 (b)
Directional redictability from BIST (high-frequency) to TL (high-frequency) when $\hat{\rho}_\beta(k)$ for β_1 = 0.9
This subfigure presents the directional predictability from high-frequency BIST returns to high-frequency TL returns when $\hat{\rho}_\beta(k)$ for $\beta_1 = 0.9$. In the first row plots, bars are sample cross quantilogram whereas $\hat{Q}_\beta^p$ values are in the second row. Red lines are bootstrap values with a 95% confidence interval centered at zero.

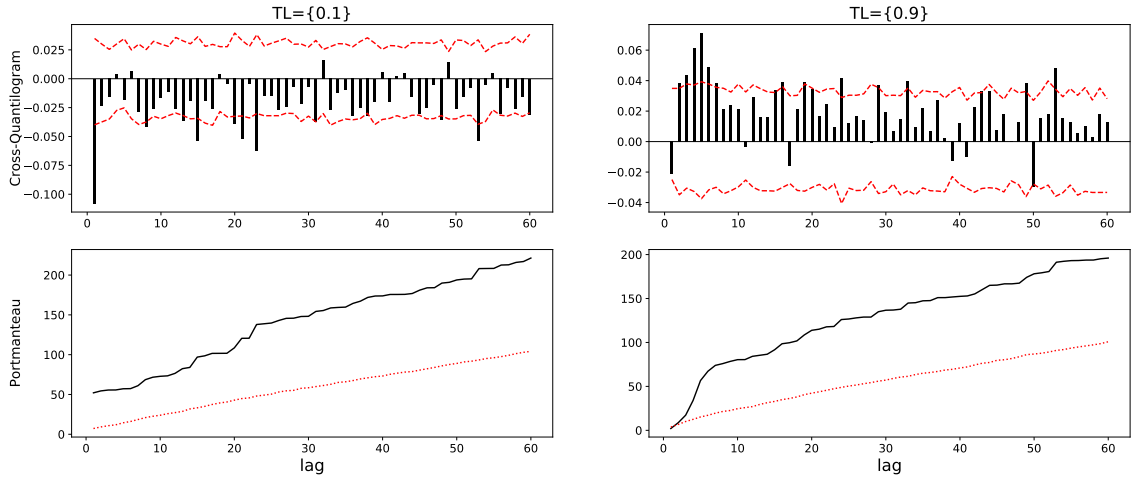

Figure C.2.10 (c)
Heatmap of spillover from BIST (high-frequency) to TL (high-frequency)
This subfigure presents the heatmap for sample cross quantilogram at $(\beta_2, \beta_1)|(\beta_2, \beta_1) \in 0.1, ..., 0.9$ and $k = 1$. It gives the magnitude of spillover from high-frequency BIST returns to high-frequency TL returns with lag 1. The star means significance in the test. Quantiles for TL and BIST are given on the x-axis and y-axis, respectively.

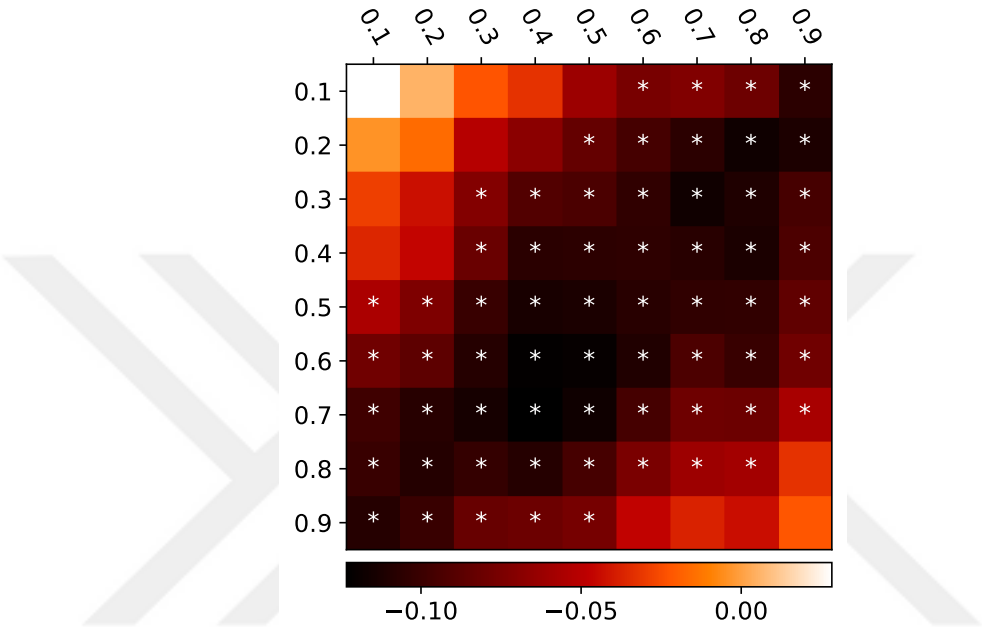

Figure C.2.11 (a)
Directional predictability from BIST (low frequency) to TL (low frequency) when $\hat{\rho}_\beta(k)$ for β_1 = 0.1
This subfigure presents the directional predictability from low-frequency BIST returns to low-frequency TL returns when $\hat{\rho}_\beta(k)$ for $\beta_1 = 0.1$. In the first row plots, bars are sample cross quantilogram whereas $\hat{Q}^p_\beta$ values are in the second row. Red lines are bootstrap values with a 95% confidence interval centered at zero.

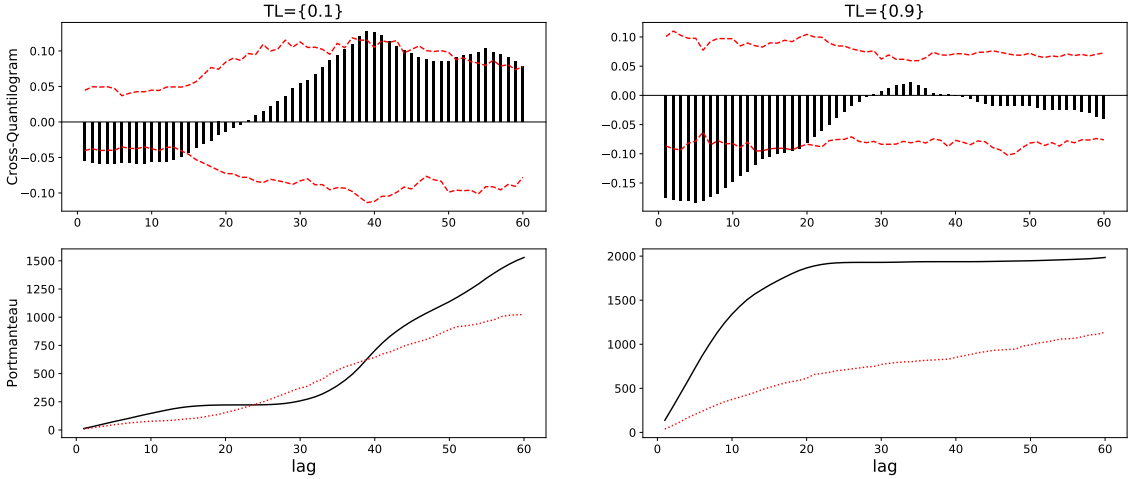

Figure C.2.11 (b)
Directional predictability from BIST (low-frequency) to TL (low-frequency) when $\hat{\rho}_\beta(k)$ for β_1 = 0.9
This subfigure presents the directional predictability from low-frequency BIST returns to low-frequency TL returns when $\hat{\rho}_\beta(k)$ for $\beta_1 = 0.9$. In the first row plots, bars are sample cross quantilogram whereas $\hat{Q}^p_\beta$ values are in the second row. Red lines are bootstrap values with a 95% confidence interval centered at zero.

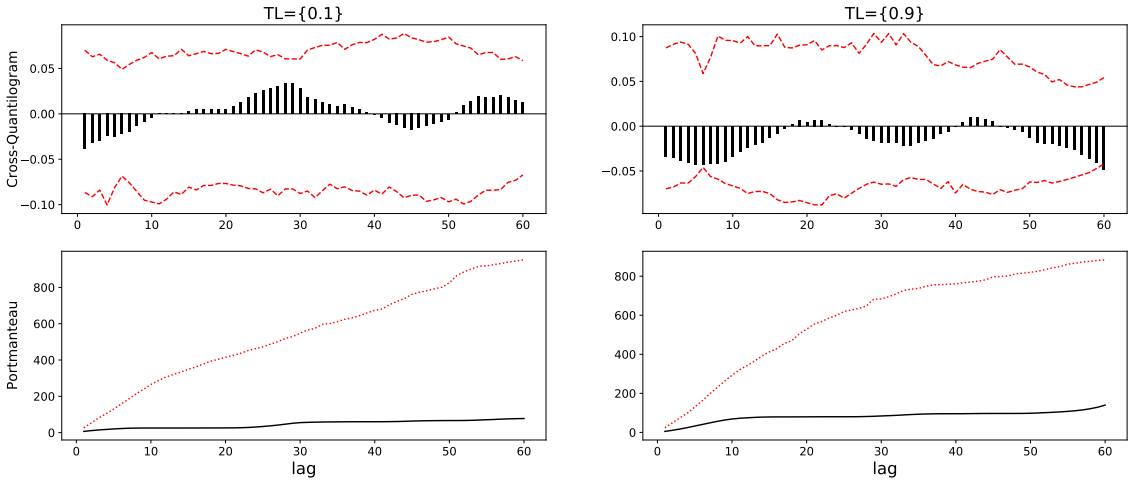

Figure C.2.11 (c)
Heatmap of spillover from BIST (low-frequency) to TL (low-frequency)
This subfigure presents the heatmap for sample cross quantilogram at $(\beta_2, \beta_1)|(\beta_2, \beta_1) \in 0.1, ..., 0.9$ and $k = 1$. It gives the magnitude of spillover from low-frequency TL returns to low-frequency BIST returns with lag 1. The star means significance in the test. Quantiles for BIST and TL are given on the x-axis and y-axis, respectively.

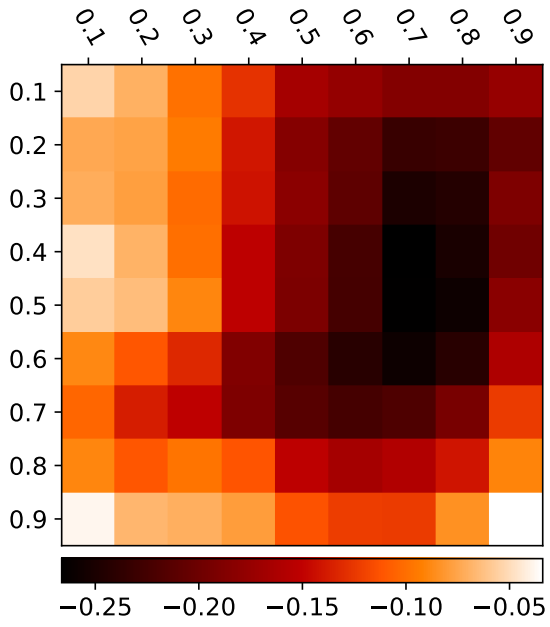

Figure C.2.12
Rolling window from BIST to TL
This figure plots rolling window analysis for the effect from BIST returns to TL returns. In the first row plots, the black line is a sample cross quantilogram over one year window with $k = 1$ whereas $\hat{Q}_{\beta}^{p}$ values are given in the second row. Red lines are bootstrap values with a 95% confidence interval centered at zero.

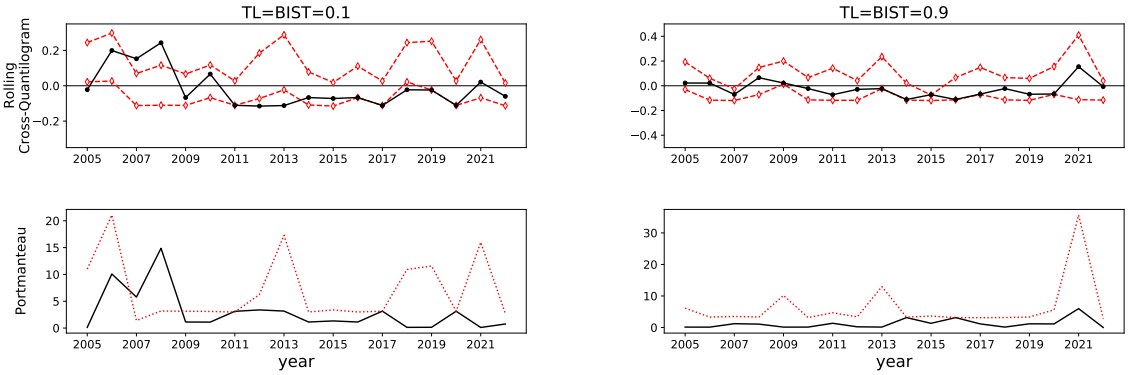

Figure C.2.13
Rolling window from BIST (high-frequency) to TL (high-frequency)
This figure plots rolling window analysis for the effect from high-frequency BIST returns to high-frequency TL returns. In the first row plots, the black line is a sample cross quantilogram over one year window with $k = 1$ whereas $\hat{Q}_{\beta}^{p}$ values are given in the second row. Red lines are bootstrap values with a 95% confidence interval centered at zero.